Max-Planck-Institut für Molekulare Pflanzenphysiologie
Pflanzen-Mikroben Interaktionen

Phosphate homeostasis and novel microRNAs are involved in the regulation of the arbuscular mycorrhizal symbiosis in *Medicago truncatula*

Dissertation

**zur Erlangung des akademischen Grades
"doctor rerum naturalium"
(Dr. rer. nat.)
in der Wissenschaftsdisziplin "Biochemie"**

**eingereicht an der
Mathematisch-Naturwissenschaftlichen Fakultät
der Universität Potsdam**

**von
Emanuel Devers
geb. am 04.01.1982 in Berlin**

Potsdam, June 2011

Published online at the
Institutional Repository of the University of Potsdam:
URL http://opus.kobv.de/ubp/volltexte/2011/5557/
URN urn:nbn:de:kobv:517-opus-55572
http://nbn-resolving.de/urn:nbn:de:kobv:517-opus-55572

CONTENTS

The following parts of this work were published:

Chapter 1.2. – 1.3., 2.2.4.9. – 2.2.4.11., 3.3.1. – 3.3.4. (including figures) and 4.3. in:

Stars and symbiosis: microRNA- and microRNA*-mediated transcript cleavage involved in arbuscular mycorrhizal symbiosis
Devers EA, Branscheid A, May P, Krajinski F.
Plant Physiology. 2011. doi:10.1104/pp.111.172627

Chapter 3.1.1.1. in:

Expression pattern suggests a role of MiR399 in the regulation of the cellular response to local Pi increase during arbuscular mycorrhizal symbiosis
Branscheid A, Sieh D, Pant BD, May P, Devers EA, Elkrog A, Schauser L, Scheible WR, Krajinski F.
Molecular Plant Microbe Interaction. 2010 Jul;23(7):915-26.

Other publications:

A processive glycosyltransferase involved in glycolipid synthesis during phosphate deprivation in *Mesorhizobium loti*
Devers EA, Wewer V, Dombrink I, Dörmann P, Hölzl G.
Journal of Bacteriology. 2011 Mar;193(6):1377-84. Epub 2011 Jan 14.

ABBREVIATIONS

AM	arbuscular mycorrhizal
ATP	adenosine-5'-triphosphate
BCIP	5-bromo-4-chloro-3-indolyl phosphate
bp	base pairs
CDS	coding sequence
cDNA	complementary deoxyribonucleic acid
CIP	calf intestine phosphatase
cm	centimeter
Ct	threshold cycle
DCL	Dicer-like protein
ddH_2O	double distilled water
DEPC	diethylpyrocarbonate
DIG	digoxigenin
DNA	deoxyribonucleic acid
DNase	deoxyribonuclease
dNTPs	deoxyribonucleotides
dpi	days post inoculation
DPU	direct phosphate uptake system
dsRNA	double stranded ribonucleic acid
DTT	dithiothreitol
E. coli	*Escherichia coli*
EDC	1-ethyl-3-(3-dimethylaminopropyl) carbodiimide
EDTA	ethylenediaminetetraacetic acid
eGFP	enhanced green fluorescent protein
EST	expressed sequence tag
et al.	and others
EtBr	ethidium bromide
EtOH	ethanol
g	gram
gDNA	genomic deoxyribonucleic acid
h	hour

GdmCl	guanidinium chloride
kb	kilo base pairs
l	litre
LFC	log_2-fold change
LNA	locked nucleic acid
M	molar
MES	2-(N-morpholino)ethanesulfonic acid
MFS	major facilitator superfamily
mg	milligram
min	minutes
miRNA	micro ribonucleic acid
miR	mature micro ribonucleic acid
miR*	micro ribonucleic acid star strand
ml	milliliter
mM	millimolar
mRNA	messenger ribonucleic acid
myc	mycorrhizal
NBT	nitro blue tetrazolium
nt	nucleotides
nmyc	non-mycorrhizal
ORF	open reading frame
PBS	phosphate buffered saline
PCA	principal component analysis
PCR	polymerase chain reaction
P_i	inorganic phosphate
qRT-PCR	quantitative real time PCR
RISC	RNA-induced silencing complex
RLK	receptor-like kinase
RLM-RACE	RNA ligase mediated rapid amplification of cDNA-ends
RNA	ribonucleic acid
RNase	ribonuclease
rpm	rotations per minute (centrifuge)/ reads per million (small RNAs)
rRNA	ribosomal ribonucleic acid
RT	room temperature

RT-	reverse transcription (prefix)
SD	standard deviation
siRNA	small interfering ribonucleic acid
sr	small ribonucleic acids
TAE	Tris-acetate-EDTA
TAP	tobacco acid pyrophosphatase
TF	transcription factor
Tris	Tris(hydroxymethyl)aminomethane
Tnt1	transposon 1 of *Nicotiana tabacum*
UTR	untranslated region
W/V	weight/volume
wpi	weeks post inoculation
V/V	volume/volume
Vol	volume
µg	microgram
µl	microliter
λ	wavelength

1. INTRODUCTION

1.1. Phosphate and plants

Beside nitrogen, phosphorus (P) is the most limiting element for plant growth. The growing cells need P for the synthesis of nucleic acids and phospholipids and it plays a crucial role in the energy transfer (e.g. ATP), regulation of enzymatic reactions and signal transduction. Phosphorous is gathered up by plant roots in the oxidized form as phosphate (P_i) and is predominantly metabolized as such. Phosphate in turn is one of the least available nutrients in the soil, because of its ability to form insoluble complexes with positively charged ions (e.g. $Fe^{2+/3+}$, Ca^{2+} and Al^{3+}), the adsorption to soil particles and conversion to organic compounds by soilborne microorganisms (Marschner, 1995; Raghothama, 2000; Tiessen, 2008). The actively available concentration of P_i in most soils is about 0.1-10 µM (Bieleski, 1973) and the low availability is often enhanced by the depletion of the soluble P_i in the rhizosphere, known as the P_i-depletion zone (Bhat and Nye, 1973). Consequently, in natural environments plants constantly suffer from P_i limitation and have evolved several strategies to maintain P_i homeostasis. These cover efficient coordination of P_i allocation among different organs, remobilization of P_i from old to young tissue and enhanced P_i-acquisition (Poirier and Bucher, 2002; Ticconi and Abel, 2004). The latter involves an altered root morphology, exudation of organic acids, phosphatases and nucleases in order to release P_i from organic resources, which can contribute up to 50% of the P_i-content of soils (Ozanne, 1980).

One additional strategy is the formation of a symbiosis with arbuscular mycorrhizal (AM) fungi, which in turn can enhance the phosphate uptake and growth of the plant (Harrison, 1999; Hause and Fester, 2005). Additionally, the fungal hyphae can grow beyond the phosphate depletion zone of the plant, hence increasing the accessibility of phosphate sources (Rhodes and Gerdemann, 1975; Smith and Read, 1997).

Pi fertilizers are broadly used in agriculture world wide to ensure plant growth and crop yield. However, because P_i resources are limited (Mengel, 1997) and extensive P_i fertilization influences the environment, this becomes an economic and ecologic concern (Bennett *et al.*, 2001). Therefore it is of great interest to further investigate the molecular mechanisms how plants cope with P_i-limitations.

1.2. Arbuscular mycorrhizal symbiosis

Arbuscular mycorrhizal (AM) symbiosis is an ancient (~450 million years) mutualistic symbiosis formed by most flowering plants in association with glomeromycotian fungi (Smith and Read, 2008). The establishment of an AM symbiosis requires an on-going molecular dialogue between AM fungus and host plants leading to reprogramming of plant root cells for endosymbiosis (Kosuta *et al.*, 2003; Akiyama *et al.*, 2005; Kosuta *et al.*, 2008). At later stages, the fungus forms the so-called arbuscules in cortical cells (figure 1). The arbuscules are supposed to be the place of nutrient transfer from fungus to plant. Arbuscule-containing cells are the result of a complex reprogramming of non-colonized cortical cells. They show fundamental morphological and physiological changes. The fungal hyphae, which form tree-like hyphal branches inside the cortical cells, are surrounded by a novel membrane type, the periarbuscular membrane (PAM). The PAM can be regarded as an extension of the plasma membrane, but it shows striking changes in the composition of proteins (Pumplin and Harrison, 2009) especially with regard to transporter proteins (Javot *et al.*, 2007; Benedito *et al.*, 2008). In the last years, several studies analyzed transcriptome changes in plant roots after colonization by AM fungi (Liu *et al.*, 2003; Wulf *et al.*, 2003; Frenzel *et al.*, 2005; Hohnjec *et*

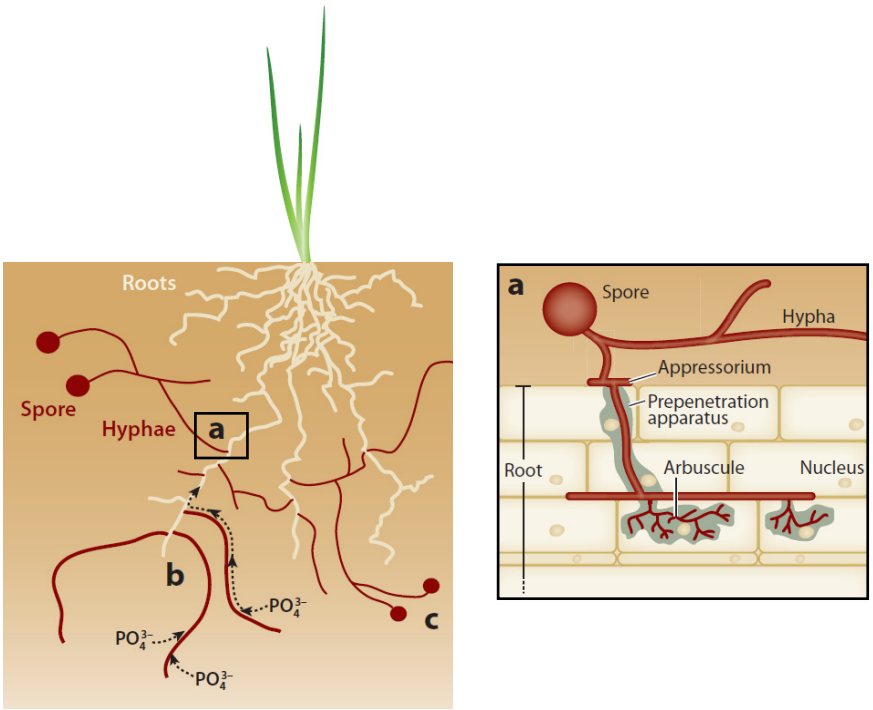

Figure 1: Arbuscular mycorrhizal symbiosis. (a) Fungal spores germinate in the soil. Caused by exchange of signaling compounds, the hyphae grow towards the root. After formation of an appressorium, the fungus penetrates the root epidermis and colonizes the root cortex. The fungus develops arbuscules, which are the major site of nutrient transfer. (b) Uptake of P_i by outgrowing hyphae beyond the P_i depletion zone. (c) Formation of fungal spores after receiving sufficient carbon by the plant. Picture adopted and modified from (Sanders and Croll, 2010).

al., 2005; Fiorilli *et al.*, 2009; Gomez *et al.*, 2009), demonstrating a massive reprogramming of the host cells in response to AM colonization, yet there is little information available about how these changes in gene expression are mediated (Krajinski and Frenzel, 2007).

1.2.1. Systemic phosphate homeostasis signaling and AM symbiosis

The rate of fungal root colonization inversely correlates with the P_i-content in the soil. Although local effects of the latter on AM fungal development have been described (deMiranda and Harris, 1994), the decreased formation of AM is primarily due to high P_i concentrations in the plant shoot. This was demonstrated in split root cultures or by foliar application of P_i (Sanders, 1975; Menge *et al.*, 1978) and implies that a systemic P_i signaling pathway in plants is involved in the adaptation of AM symbiosis to different P_i conditions.
A recently identified systemic P_i starvation signaling pathway in *Arabidopsis thaliana* (figure 2) involves the MYB transcription factor PHR1, the micro RNA (miRNA) 399 family and the E2 ubiquitin conjugase PHO2 (Bari *et al.*, 2006; Chiou *et al.*, 2006). Upon Pi starvation, transcription of miRNA 399 (miR399) is induced by the action of PHR1. The miRNA

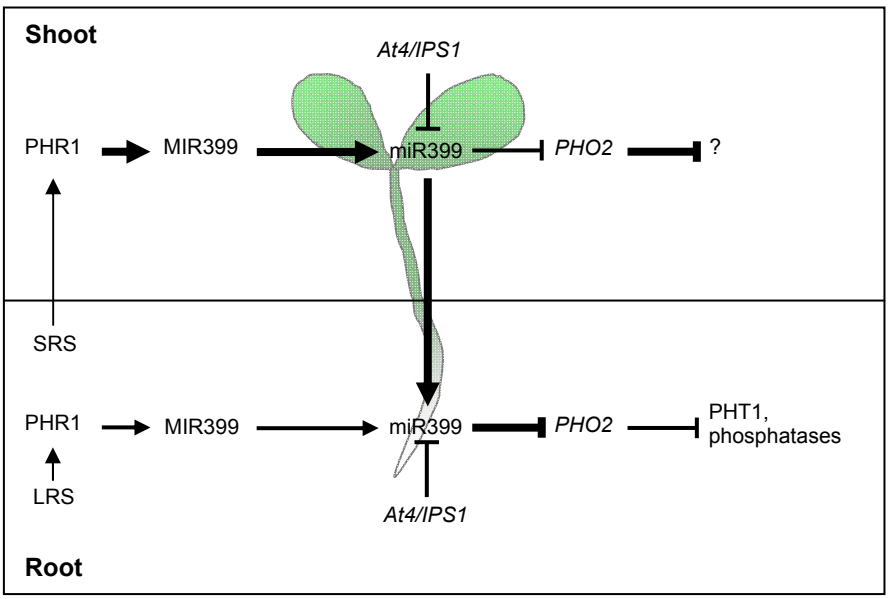

Figure 2: Model of the systemic P_i-starvation signaling pathway in plants. MIR399 is transcribed upon phosphate starvation by PHR1 after receiving a local root-borne signal (LRS) or systemic root-borne signal (SRS) in the roots or shoots, respectively. Mature miR399 is transported from the shoot to the root via the phloem and post-transcriptionally represses *PHO2* which leads to induced expression of phosphate transporters of the PHT1 family and excreted phosphatases. Model according to (Lin *et al.*, 2008).

negatively regulates the mRNA of PHO2, preventing its inhibition of a subset of other P_i starvation induced genes, e.g. phosphate transporters (Aung *et al.*, 2006; Bari *et al.*, 2006). The expression of miR399 occurs first in the shoot and later in roots and it has been shown to act as a long distance shoot-to-root signal through phloem transport (Buhtz *et al.*, 2008; Pant *et al.*, 2008). Additionally, it has been demonstrated that the non-coding RNA *At4/IPS1* sequesters the phosphate starvation induced miR399 by a mechanism called target mimicry (Franco-Zorrilla *et al.*, 2007), indicating a complex regulation in response to Pi deficiency.
During arbuscular mycorrhizal symbiosis, the phosphate partitioning within the plant and the expression levels of some components of the P_i-starvation response are altered. One striking example is the specific downregulation of the *At4/IPS1* orthologue *Mt4* in *Medicago truncatula* by AM symbiosis (Burleigh and Harrison, 1997). Additionally, transcription of several MIR399 genes is induced in mycorrhizal plants and mature miR399 accumulates in mycorrhizal roots to higher levels than in non-mycorrhizal roots of *M. truncatula* and *Nicotiana tabacum* (Branscheid *et al.*, 2010). These findings indicate that the mentioned systemic signal pathway is involved in the regulation of AM symbiosis. However, the function of PHO2 in AM symbiosis remains to be elucidated.

1.3. Micro RNAs

Small silencing RNAs are a complex group of short RNAs with sizes in the range of ~20-25 nucleotides (nt) in length which can regulate gene expression on transcriptional and post-transcriptional levels (Bartel, 2004; He and Hannon, 2004). Over the recent years it has become evident that two main classes of small silencing RNAs, short interfering RNAs (siRNAs) and miRNAs, are of great importance in plants. Small RNAs are involved in developmental processes, hormonal signaling, organ polarity, RNA metabolism, abiotic and biotic stress answers (Rhoades *et al.*, 2002; Borsani *et al.*, 2005; Kidner and Martienssen, 2005; Nogueira *et al.*, 2006; Laporte *et al.*, 2007; Liu *et al.*, 2007; Phillips *et al.*, 2007; Sunkar *et al.*, 2007; Willmann and Poethig, 2007; Zhou *et al.*, 2007; Chen, 2008; Chinnusamy *et al.*, 2008; Lu *et al.*, 2008; Lu and Huang, 2008; Navarro *et al.*, 2008; Zhao *et al.*, 2009). SiRNAs and miRNAs in plants are both generated by double stranded RNA and have a similar size. Both groups of small RNAs have different origins and they possess distinct biogenesis pathways (Carthew and Sontheimer, 2009; Ghildiyal and Zamore, 2009; Voinnet, 2009).

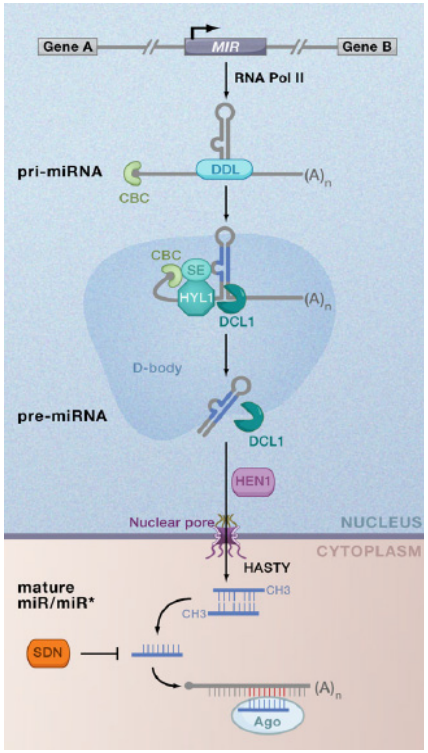

Figure 3: Biogenesis of plant miRNAs. The primary transcript of miRNAs (pri-miRNA) is often transcribed from intergenic regions by RNA polymerase II (Pol II) and subsequently processed to precursor miRNA (pre-miRNA) and mature miRNA by DCL1 and additional factors. The miRNA/miRNA* duplex is exported from the nucleus into the cytosol and the mature strand is incorporated into AGO and specifically suppresses destined target mRNAs. Picture from Voinnet O., 2009.

MiRNAs in plants are mostly transcribed from intergenic located *MIR* genes through RNA polymerase II activity (figure 3), resulting in a 5' capped and 3' polyA tailed primary transcript (Cai *et al.*, 2004; Lee *et al.*, 2004). A region within the primary transcript folds into an imperfect stem-loop structure, which is cut by DICER-like (DCL) proteins resulting in a miRNA precursor. This precursor is subsequently processed by the same DCL protein to yield the miRNA/miRNA* duplex with a 2 nt overhang at the 3' ends (Papp *et al.*, 2003; Vazquez *et al.*, 2004; Xie *et al.*, 2004). In contrast to animal miRNAs, both duplex strands of plant miRNAs are 2'-O-methylated at their 3' ends by HEN1 to prevent them against degradation (Yu *et al.*, 2005; Yang *et al.*, 2006). The duplex is then exported to the cytosol presumably by HASTY (Park *et al.*, 2005). An AGO protein then incorporates one of the duplex strands, which is then referred to as mature miRNA (Liu *et al.*, 2004; Meister *et al.*, 2004). Its counterpart from the duplex is called miRNA* and will often be degraded after release of the mature strand (Khvorova *et al.*, 2003; Schwarz *et al.*, 2003). The miRNA within the AGO protein then guides the RNA induced silencing complex (RISC) to the target mRNA (Bartel, 2009). This is achieved by pairing of the miRNA with a specific binding site within the target transcript (Wang *et al.*, 2008a; Wang *et al.*, 2008b). The RISC then suppresses expression of this transcript by inhibiting translation or transcript cleavage of the miRNA/target duplex, normally between the 10th and 11th nucleotide position from the miRNA 5'-end (Elbashir *et al.*, 2001a; Elbashir *et al.*, 2001b).

In contrast to animals where miRNAs often post-transcriptionally regulate gene expression via translational inhibition, it was speculated that plant miRNAs often lead to target cleavage due to a high degree of complementarity between target mRNA and miRNA (Rhoades *et al.*, 2002). But it was demonstrated that both mechanisms are involved in plant miRNA function

(Brodersen *et al.*, 2008). MiRNA auto-regulate their own biogenesis through targeting of *DCL1* and *AGO1* by miR162 and miR168 (Xie *et al.*, 2003; Vaucheret *et al.*, 2004).

1.3.1. Micro RNAs in plant-microbe interactions

There are now several lines of evidence that miRNAs play a significant role during the interaction of plants with symbiotic organisms. As mentioned in chapter 1.2.1., miR399 is involved in AM symbiosis. Additionally, miRNAs are also known to be key players in the response to parasitic organisms. For instance, flagellin, which is a major pathogen-associated molecular pattern (PAMP) of *Pseudomonas syringae,* enhances the transcription of miR393, which targets the transcript of the F-box auxin receptor transporter response protein and a number of related proteins (Navarro *et al.*, 2006; Fahlgren *et al.*, 2007). Arabidopsis mutants defective in miRNA biogenesis indicate an even more widespread role of miRNAs; these mutants are able to sustain disease from normally non-virulent bacteria strains (Navarro *et al.*, 2008). A successful development of tumors caused by *Agrobacterium tumefaciens* also requires an intact miRNA pathway, as Arabidopsis *dcl1 (Dicer-like 1)* mutants are immune to crown gall formation (Dunoyer *et al.*, 2006). Hence, there is increasing evidence that miRNAs are integral components of plant responses to adverse environmental conditions including biotic interactions (Voinnet, 2008), in addition to their established functions during normal growth and development, such as hormone responses and meristem regulation (Kidner and Martienssen, 2005; Wang *et al.*, 2011). Moreover, in *M. truncatula* miR169 is important for the spatial and temporal restriction of the CCAAT-binding family transcription factor *MtHAP2-1* during symbiotic nodule development (Combier *et al.*, 2006). Additionally, miR166 is expressed in developing root and nodule tips and overexpression in *M. truncatula* leads to a reduced number of lateral roots and symbiotic nodules (Boualem *et al.*, 2008). Two recent miRNA profiling studies in soybean and *M. truncatula* led to the discovery of a number of new miRNAs regulated during nodule symbiosis (Subramanian *et al.*, 2008; Lelandais-Briere *et al.*, 2009).

1.4. Aim of the work

During arbuscular mycorrhizal symbiosis, the *At4/IPS1* orthologue *Mt4* is specifically downregulated in *Medicago truncatula*. Additionally, transcription of several miR399 genes is induced in mycorrhizal plants and mature miR399 accumulates in mycorrhizal roots to higher levels than in non-mycorrhizal roots of *M. truncatula* and *Tobacco*. These findings indicate that the systemic miR399/PHO2 signaling pathway is involved in the regulation of AM symbiosis. However, the function of PHO2 in AM symbiosis remains to be elucidated and is a central aspect of this work. Consequently, a targeted approach is used to identify the functional orthologue of AtPho2, MtPho2, in the model legume *M. truncatula* followed by a characterization of its putative role during AM symbiosis. Using the now available knowledge of the P_i-starvation signaling pathway in plants, *M. truncatula* will be transformed with constructs leading to modulated expression of MtPho2. The subsequent detailed analysis of the molecular and mycorrhizal phenotype of these plants will indicate the putative role of this component in the connection between P_i-status and AM-development. Additionally, *M. truncatula* with modulated PHO2 expression can be used in the future as a tool for further analysis of legume plants with constitutive low or high P_i-signals.

It is known that the rate of fungal root colonization inversely correlates with the P_i-content in the soil. Compared to plants under P_i limiting conditions, plants with a high shoot P_i-status are much less colonized. However, the molecular mechanisms of the inhibition of root colonization are not understood. Hence, an untargeted large scale expression profiling using microarrays will be carried out to identify genes in *M. truncatula* roots and shoots, which respond to the adaptation of mycorrhizal colonization to different P_i-conditions using a split-root system as an experimental setup.

Since miRNAs have a major impact on the regulation of gene expression involved in nutrient homeostasis and stress response of plants, the influence of miRNAs in AM symbiosis is of great interest. Additionally, miRNAs have the capability to act as long distance signals mediating the systemic adaptation of AM symbiosis to different P_i levels. To get information about miRNAs involved in AM symbiosis, high-throughput sequencing of small RNAs isolated from mycorrhizal and non-mycorrhizal root tissue of *M. truncatula* will be used for genome wide identification of new and conserved miRNAs.

2. MATERIALS AND METHODS

2.1. Materials

2.1.1. Chemicals

2.1.1.1. Enzymes

All restriction enzymes used in this study were obtained from Fermentas (St. Leon-Rot, Germany) as Fast Digest® Restriction enzyme, if available. Non Fast Digest® restriction enzymes were obtained from NEB (Frankfurt a.M., Germany).

The following additional enzymes were used in this study:

Advantage® 2 DNA Polymerase	Clontech (Saint-Germain-en-Laye, France)
Anti-DIG-alkaline phosphatase	Roche (Mannheim, Germany)
BP-Clonase	Invitrogen (Darmstadt, Germany)
GoTaq® Flexi DNA Polymerase	Promega (Mannheim, Germany)
LR-Clonase	Invitrogen (Darmstadt, Germany)
Lysozym	Carl Roth (Karlsruhe, Germany)
MultiScribe™ Reverse Transcriptase	Applied Biosystems (Carlsbad, CA, USA)
Proteinase K	Invitrogen (Darmstadt, Germany)
RNase A	Fermentas (St. Leon-Rot, Germany)
RiboLock™ RNase Inhibitor	Fermentas (St. Leon-Rot, Germany)
SuperScript® II Reverse Transcriptase	Invitrogen (Darmstadt, Germany)
SuperScript® III Reverse Transcriptase	Invitrogen (Darmstadt, Germany)
TURBO DNase™	Ambion (Austin, TX, USA)

2.1.1.2. Reaction kits

Advantage® 2 DNA Polymerase Kit	Clontech (Saint-Germain-en-Laye, France)
FirstChoice® RLM-RACE Kit	Ambion (Austin, TX, USA)
Gateway® BP Clonase® II Enzyme Kit	Invitrogen (Darmstadt, Germany)
Gateway® LR Clonase® II Enzyme Kit	Invitrogen (Darmstadt, Germany)
GoTaq® Flexi DNA Polymerase Kit	Promega (Mannheim, Germany)

Maxima™ SYBR Green/ROX qPCR Master Mix (2x)	Fermentas (St. Leon-Rot, Germany)
pENTR™/D-TOPO® Cloning Kit	Invitrogen (Darmstadt, Germany)
Phire® Plant Direct PCR Kit	Finnzymes (Vantaa, Finland)
SuperScript® II Reverse Transcriptase Kit	Invitrogen (Darmstadt, Germany)
SuperScript® III Reverse Transcriptase Kit	Invitrogen (Darmstadt, Germany)
TOPO® TA Cloning® Cloning Kit for subcloning	Invitrogen (Darmstadt, Germany)
TURBO DNA-*free*™	Ambion (Austin, TX, USA)

2.1.1.3. Other Kits

DNA extraction Kit Plant mini	nexttec™ (Hilgertshausen, Germany)
InviTrap® Spin Plant RNA Mini Kit	STRATEC (Berlin, Germany)
*mir*Vana™ miRNA Isolation Kit	Ambion (Austin, TX, USA)
Plant RNA Isolation Aid	Ambion (Austin, TX, USA)
Wizard® SV Gel and PCR Clean-up System	Promega (Mannheim, Germany)
Small RNA Sample Prep Kit	Illumina® (Eindhoven, Netherlands)

2.1.1.4. Antibiotics

All antibiotics listed were purchased from Duchefa Biochemie B.V. (Netherlands).

Table 1: Antibiotics and their particular concentrations as well as target organisms used in this study

Antibiotic	Concentration	Target organism
Gentamycin	20 µg/ml	*E. coli*
Kanamycin	25 µg/ml	*M. truncatula*
	50 µg/ml	*E. coli*
Spectinomycin	50 µg/ml	*E. coli, A. rhizogenes*
Streptomycin	50 µg/ml	*E. coli*
	600 µg/ml	*A. rhizogenes*

2.1.1.5. Buffers and solutions

All buffers and solutions were prepared with bi-distillated H_2O (ddH_2O), if not mentioned otherwise.

Plasmid mini preparation

Solution 1	25 mM	Tris-HCl pH 8
	10 mM	EDTA
	5 mg/ml	Lysozym

Solution 2	0.2 mM 1 % [w/v]	Sodium hydroxide (NaOH) Sodium dodecylsulfate (SDS)
Solution 3	2 mM	Potassium acetate pH 4.8

Phosphate measurements

Color reagent	1 vol. 3 vol.	4.2 % [w/v] Ammonium molybdate ($[NH_4]_6Mo_7O_{24}\cdot H_2O$) in 5 M HCl 0.2 % [w/v] Malachite Green in H_2O
Phosphate Standard	0.5 mM	di-Potassium hydrogen phosphate (K_2HPO_4)
Total phosphate extraction buffer	10 mM 1 mM 100 mM 1 mM	Tris EDTA Sodium chloride (NaCl) β-Mercaptoethanol adjusted to pH 8

RNA isolation

RNA extraction buffer	6 M 20 mM 20 mM	Guanidinium chloride (GdmCl) EDTA MES adjusted to pH 7

Gel electrophoresis

50x TAE buffer	242 g 57.1 ml 100 ml	Tris base glacial acetic acid 0.5 M EDTA (pH 8) ad ddH_2O to 1 l
DEPC-H_2O	0.1 % [v/v]	in ddH_2O stirred over night 2x autoclaved
Ethidium bromide (EtBr) solution	0.01 % [w/v]	0.01 mg EtBr in 100ml 0.5xTAE
10x MOPS buffer	200 mM 50 mM 20 mM	MOPS sodium acetate EDTA (pH 7)
RNA sample buffer	100 µl 38 µl 20 µl 42 µl	formamide formaldehyde 10x MOPS buffer DEPC-H_2O
RNA loading buffer	99 µl 1 µl	6x loading dye 10 mg/ml EtBr

Staining of fungal structures

Trypan blue solution	0.1 % [w/v]	Trypan blue in lactophenol (25% [w/v] phenol in water/glycerol/ lactic acid in the ratio 1:1:1)

In-situ hybridization

1 M Tris-HCl	121.1 g	Tris-HCl, pH 8 adjust with HCl
Solution B1	0.1 M 0.15 M	Tris-HCl, pH 7.5 Sodium chloride (NaCl)
Solution B3	0.1 M 0.1 M 0.05 M	Tris-HCl, pH 9.5 NaCl $MgCl_2$, pH 9.5
1 x PBS	137 mM 2.7 mM 12 mM	Sodium chloride (NaCl) Potassium chloride (KCl) di-Sodium hydrogen phosphate (Na_2HPO_4) / Potassium di-hydrogen phosphate (KH_2PO_4)
PBST		1 x PBS with 0.1 % [w/v] Tween-20
1 x TBS	50 mM 150 mM	Tris-HCl Sodium chloride (NaCl) adjust to pH 7.5 with HCl
TBST		1 x TBS with 0.1 % [w/v] Tween-20
Fixative	10 ml 2.5 ml	10 % [w/v] para formaldehyde 10 x PBS add ddH_2O to 25 ml, adjust to pH 7
EDC buffer	1.6 ml 130 ml 450 µl 16 ml	130 mM 1-methylimidazol ddH_2O conc. HCl 3 M sodium chloride add ddH_2O to 160 ml
EDC solution	10 ml 176 µl 100 µl	EDC buffer EDC conc. HCl

Other Buffers

1 x TAE	40 mM 1 mM	Tris-acetate EDTA, pH 8
TE buffer	10 mM	Tris-HCl, 1 mM EDTA, pH 8

2.1.1.6. Synthetic oligonucleotides

Stem-loop RT-primer:

Stem-loop RT-Primer were HPLC purified and qRT-PCR primers were desalted. Both primers were synthesized by Eurofins MWG Operon (Ebersberg, Germany).

Mtr-miR5204
5’ GTCGTATCCAGTGCAGGGTCCGAGGTATTCGCACTGGATACGACGTTCCTA
Mtr-miR169d*/l*/m*/e.2*
5’ GTCGTATCCAGTGCAGGGTCCGAGGTATTCGCACTGGATACGACTATAGCC

Mtr-miR169d
5’ GTCGTATCCAGTGCAGGGTCCGAGGTATTCGCACTGGATACGACCCGGCAA
Mtr-miR160f*
5’ GTCGTATCCAGTGCAGGGTCCGAGGTATTCGCACTGGATACGACCCTGCT
Mtr-miR5229
5’ GTCGTATCCAGTGCAGGGTCCGAGGTATTCGCACTGGATACGACCATAGT
Mtr-miR167
5’ GTCGTATCCAGTGCAGGGTCCGAGGTATTCGCACTGGATACGACTAGATC
Mtr-miR160c
5’ GTCGTATCCAGTGCAGGGTCCGAGGTATTCGCACTGGATACGACTGGCAT
Mtr-miR1171h
5’ GTCGTATCCAGTGCAGGGTCCGAGGTATTCGCACTGGATACGACGAGTGA
Mtr-miR5204*
5’ GTCGTATCCAGTGCAGGGTCCGAGGTATTCGCACTGGATACGACATACTG

Stem-loop qRT-PCR:

Mtr-miR5204	5’ GATCGGCTGGAAGGTTTTG
Mtr-miR5204*	5’ CAGTCCCTCAAAGGCTTC
Mtr-miR169d*/l*/m*/e.2*	5’ ACTATGGCAGGTCATCCTTC
Mtr-miR169d	5’ TGAATGAGCCAAGGATGAC
Mtr-miR171h	5’ GGCCGAGCCGAATCAATA
Mtr-miR167	5’ GTCTGAAGCTGCCAGCAT
Mtr-miR160f*	5’ ATGGCGTGAAGGGAGT
Mtr-miR5229	5’ GCGGTTTAGCAGGAAGAG
Mtr-miR160c	5’ ATATGCCTGGCTCCCTGA
Stem-loop reverse	5’ CCAGTGCAGGGTCCGAGGT

Additional PCR primer:

All other PCR primers are listed in a supplemental file on the CD.

In-situ LNA probes:

LNA positioning is not shown. Probes were designed and synthesized by Exiqon A/S (Denmark).

Mtr-miR5229	5’/DIG/CATAGTCACTCTTCCTGCTAA
Mtr-miR169d*/l*/m*/e.2*	5’/DIG/TATAGCCGAAGGATGACCTGCC
Mtr-miR5204	5’/DIG/GTTCCTACAAAACCTTCCAGC
Mtr-miR160c	5’/DIG/TGGCATTCAGGGAGCCAGGCA
Mtr-miR169	5’/DIG/CCGGCAAGTCATCCTTGGCTT
Mtr-miR160f*	5’/DIG/CCTGCTTGACTCCCTTCACGC
Scramble-miR	5’/DIG/GTGTAACACGTCTATACGCCCA

2.1.1.7. Other chemicals

6x DNA Loading Dye	Fermentas (St. Leon-Rot, Germany)
Bacto™ Agar	Becton Dickinson (Heidelberg, Germany)
Bacto™ Trypton	Becton Dickinson (Heidelberg, Germany)
Biozyme LE Agarose	Biozym Scientific (Hess. Oldendorf, Germany)
Blocking Reagent for nucleic acid hybridization and detection	Roche (Mannheim, Germany)
CIP solution	Carl Roth (Karlsruhe, Germany)
DEPC	Carl Roth (Karlsruhe, Germany)
EDC	Sigma-Aldrich (Munich, Germany)
GeneRuler™ 100bp Plus DNA Ladder	Fermentas (St. Leon-Rot, Germany)
GeneRuler™ 1kb DNA Ladder	Fermentas (St. Leon-Rot, Germany)
In situ hybridization buffer	ENZO® life science (Lörrach, Germany)
IGEPAL® CA-630	Sigma-Aldrich (Munich, Germany)
MOPS	Sigma-Aldrich (Munich, Germany)
NBT/BCIP	Roche (Mannheim, Germany)
Nuclease free water (not DEPC-treated)	Ambion (Austin, TX, USA)
Phosphorous acid, ≥98.5%	Sigma-Aldrich (Munich, Germany)
Select Agar®	Invitrogen (Darmstadt, Germany)
Yeast extract	Duchefa Biochemie B.V. (Netherlands)

2.1.2. Growth media

2.1.2.1. Bacterial growth media

LB medium	10 g/l Bacto™ Tryptone, 5 g/l Yeast extract, 10 g/l NaCl, pH 7 (NaOH)
TY/Ca medium	5 g/l Bacto™ Tryptone, 3 g/l Yeast extract, pH 7.2 (NaOH), 4.5 mM $CaCl_2$ (addition after autoclaving)
YEB medium	5 g/l Bacto™ Beef extract, 5 g/l Bacto™ Peptone, 1 g/l Yeast extract, 5 g/l sucrose, 2 ml of 1 M Mg_2SO_4 added to 1 l medium, pH 7.2 (NaOH)
SOC medium	20 g/l Bacto™ Tryptone, 5 g/l Yeast extract, 0.5 g/l NaCl, 10 ml of 0.25 M KCl per 1 l medium (addition after dissolving the previous compounds), pH 7 (NaOH), addition of 5 ml sterile 2 M $MgCl_2$ solution after autoclaving, addition of 20 ml filter-sterilized 1 M glucose after autoclaving

For solid media 15 g/l Select Agar® (or Bacto™ Agar for TY medium) was added before autoclaving.

2.1.2.2. Plant growth media, solutions and substrates

Modified Fahraeus medium (Barker *et al.*, 2006)	0.8 mM	$Na_2HPO_4 \times H_2O$
	0.7 mM	KH_2PO_4
	0.5 mM	$MgSO_4 \times 7H_2O$
	0.5 mM	NH_4NO_3
	50 µM	$FeSO_4 \times 7H_2O$
	50 µM	$Na_2EDTA \times 2H_2O$
	0.1 mg/l	$CuSO_4$
	0.1 mg/l	H_3BO_3
	0.1 mg/l	$MnSO_4 \times H_2O$
	0.1 mg/l	$Na_2MoO_4 \times 2H_2O$
	0.1 mg/l	$ZnSO_4 \times H_2O$
	15 g/l	Bacto™ Agar
	1 mM	$CaCl_2$
		pH 6.5 (KOH)

For recovery of root transformed plants later grown under low phosphate condition 0.08 mM $Na_2HPO_4 \times H_2O$ and 0.07 mM KH_2PO_4 was used. Antibiotics for selection of transgenic plants and $CaCl_2$ were added after autoclaving and cooling down of the media.

Modified 0.5x Hoagland's solution (Hoagland and Arnon, 1950)	2.5 mM	$Ca(NO_3)_2 \times 4H_2O$
	2.5 mM	KNO_3
	1 mM	$MgSO_4 \times 7H_2O$
	50 µM	NaFeEDTA
	20 µM	KH_2PO_4/K_2HPO_4 pH 6.8
	10 µM	H_3BO_3
	2 µM	$MnCl_2 \times 4H_2O$
	1 µM	$ZnSO_4 \times 7H_2O$
	0.5 µM	$CuSO_4 \times 5H_2O$
	0.2 µM	$CoCl_2 \times 6H_2O$
	0.2 µM	$Na_2MoO_4 \times 2H_2O$
	0.2 µM	$NiSO_4 \times 6H_2O$
Quartz sand/vermiculite mixture	2 vol	0.6 – 1.2 mm quartz sand
	1 vol	0.3 – 0.8 mm quartz sand
	1 vol	vermiculite

2.1.4. Biological material

2.1.4.1. Bacterial strains

Escherichia coli DB3.1	Invitrogen (Darmstadt, Germany)
Escherichia coli DH5α	Invitrogen (Darmstadt, Germany)
Escherichia coli TOP10	Invitrogen (Darmstadt, Germany)
Agrobacterium rhizogenes Arqua-1	(Quandt *et al.*, 1993)
Sinorhizobium meliloti WT	Dr. Helge Küster (Hannover, Germany)

2.1.4.2. Fungal inoculum

Glomus intraradices BB-E	Agrauxine (Dijon, France)

2.1.4.3. Plasmids

pCR2.1	Invitrogen (Darmstadt, Germany)
pDONR207	Invitrogen (Darmstadt, Germany)
pENTR/D-TOPO	Invitrogen (Darmstadt, Germany)
pK7GW2D	(Karimi *et al.*, 2002)
pKDSR(I)	Dr. Igor Kryvoruchko (Ardmore, Oklahoma, USA)

2.1.4.4. Plant material

Medicago truncatula cv Jemalong genotype A17
Medicago truncatula R108

2.2. Methods

2.2.1. Cloning and preparation of plasmid constructs

2.2.1.1. Plasmid Miniprep

A liquid bacterial culture (5ml) was grown over night at the according culture condition for the used bacterial species and strain.

3 ml of the culture was successively centrifuged at 8000 rpm using a benchtop centrifuge to pellet the bacteria. After discarding the supernatant the bacterial pellet was carefully resuspended in 100 µl solution 1 and 5 µl RNase (10 mg/ml) was added prior to 5 min incubation at room temperature (RT).
Additional 200 µl of solution 2 were added and the solutions were mixed by inverting the tubes. The plasmid preparation was then incubated 5 min on ice. 150 µl of solution 3 was added. The solutions were again mixed by inverting and incubated 5 min on ice. The plasmid preparation was centrifuged twice for 5 min at full speed. The supernatant was collected and the plasmids were precipitated by adding 800 µl 96 % [v/v] ethanol, 40 µl 3 M sodium acetate pH 4.8 and incubated at -20 °C for 30 min. The plasmids were pelletized by 5 min centrifugation at full speed and the pellet was washed with 70 % [v/v] ethanol prior to drying. The plasmids were resuspended in 30 µl autoclaved ddH_2O or TE-buffer.

2.2.1.2. Cloning of overexpression, RNAi and target mimicry constructs

Overexpression and RNAi constructs for *MtPho2* were created via directional TOPO® cloning. For the overexpression construct a primer-pair was used to amplify the whole ORF of TC115486, which additionally eliminates the miRNA399 binding sites located in the 5'-UTR. The PCR was performed with Advantage® 2 Polymerase (Clontech) and cDNA derived from RNA of *M. truncatula* roots. PCR fragments were cloned into the pENTR™/D-TOPO vector and transformed into One Shot® TOP 10 *E. coli* cells using the pENTR™ Directional TOPO® Cloning Kit (Invitrogen) according to the manual, resulting in the entry vector pEpho2v2 for the ORF of *MtPho2*. White colonies were picked after a blue-white selection and positive constructs were confirmed via PCR and plasmid restriction. Positive constructs were sequenced by LGC Genomics (Berlin, Germany) using the Donr-F and T7-Promoter sequencing primer. Verified constructs were used for recombination with the destination vector pK7GW2D, using the LR-Recombinase Mix (Invitrogen) according to the manual. The vector pK7GW2D (Karimi *et al.*, 2002) containing eGFP as a visible marker was used for the overexpression construct resulting in the vector pKpho2v2D.
Using the same cloning and control procedures, RNAi constructs were generated from PCR amplified sequences with a length of 202 bp and 210 bp of the *MtPho2* 5'-UTR and 3'-UTR, respectively. Generated entry clones, pEpho2RNAi5' and pEpho2RNAi3', were used for LR recombination with the destination vector pKDSR(I).

The same cloning procedure was used for the overexpression and target mimicry constructs of the miRNAs. In short, predicted precursor sequences of miR5229a and miR5204 were amplified from cDNA using specific primer pairs and cloned into pK7GW2D as described above. The resulting vectors were named pKam09oexD and pKc1054oexD for miR5229a and miR5204, respectively. Target mimicry constructs (Franco-Zorrilla *et al.*, 2007) were based on the non-coding RNA Mt4. The miR399 binding site of Mt4 was exchanged via overlapping PCR against binding sites matching to miR5229a or miR5204 but retaining the 3 nt bulge between the 10^{th} and 11^{th} nt of the miRNA and the adjacent G-U pair to prevent cleavage of the target mimicry construct. The target mimicry constructs were cloned into pK7GW2D as described above.

2.2.2. Transformation of microorganisms

2.2.2.1. Transformation of *Escherichia coli*

50-80 µl chemically competent *E. coli* cells were thawed on ice and mixed with the appropriate vector. The cells were incubated on ice for at least 5 min. These were transformed with a heat shock for 30 s at 42 °C, subsequent chilling on ice and addition of 200 µl SOC medium. The transformed cell were incubated for 1 h at 37 °C. Positive clones were selected by plating 50 – 150 µl of the cells on solid LB medium containing an appropriate antibiotic.

2.2.2.2. Transformation of *Agrobacterium rhizogenes*

50 µl electrocompetent *A. rhizogenes* cells were thawed on ice and mixed with the appropriate vector in an electroporation cuvette (1 mm). The cells were incubated on ice for at least 5 min. These were transformed via electroporation (1.8 kV), subsequent chilling on ice and addition of 600 µl YEB medium. The transformed cells were incubated for 1 h at 28 °C. Positive clones were selected by plating 50 – 250 µl of the cells on solid YT/CaCl medium containing an appropriate antibiotic.

2.2.3. Plant growth and root transformation of *Medicago truncatula*

2.2.3.1. Surface sterilization and germination of *M. truncatula* seeds

Prior to germination all seeds were treated with concentrated H_2SO_4 for 8 minutes to break seed dormancy and were subsequently rinsed 3 times with sterile water and surface sterilized with a solution of 6% NaClO for 5 min. For germination seeds were put on 15% water agar and stored in the dark at 4 °C for 2 days and were then transferred to 25 °C for at least another 2 days.

2.2.3.2. Inoculation of plants with *Glomus intraradices*

G. intraradices-containing substrate included 10 % (v/v) of commercially available inoculum and was propagated in pots containing *Allium porrum* for at least 4 month. Plants were grown in the green house. Twice a week the substrate was soaked with ample amount of half-strength Hoagland's solution (20 µM P_i). For inoculation of *Medicago truncatula*, growth substrate was mixed (1:10 [v/v]) with the substrate of mycorrhizal *Allium porrum*.

2.2.3.3. Split-root experiment

For the split-root experiment seeds from *M. truncatula cv*. Jemalong genotype A17 were used and treated prior to germination as mentioned above. The root tip from 1 week old seedlings was cut off to induce lateral root growth and the seedlings were planted for 2 weeks in pots (Ø 6 cm) containing quartz sand (0.6-1.2 mm) and vermiculite at a volume ratio of 4:1. The plants were fertilized with half strength Hoagland's solution containing 20 µM phosphate. After 2 weeks the root system of the plants was transferred into two separate square pots (6 cm x 6 cm) designated as fertilized (F-) compartment or mycorrhizal/mock (M-) compartment. The pots of the F-compartment contained 2:1:1 quartz sand 0.3-0.8 mm/0.6-1.2 mm/vermiculite as a substrate and the pots of the M-compartment contained 10% (v/v) *G. intraradices* inoculum or the same substrate as the F-compartment as a control. The plants were fertilized in the F-compartment with a half strength Hoagland's solution containing 20 µM phosphate for low phosphate conditions or 2 mM phosphate for high phosphate

conditions. The M-compartment was fertilized with half strength Hoagland's solution containing 20 µM phosphate in all experimental conditions. Both halves of the pot were put in different trays or were put on lids of Petri dishes to avoid cross-contamination or -fertilization. The shoots and the roots from both compartments were harvested separately 3 weeks after inoculation. The tissue was shock-frozen with liquid nitrogen and stored at -80 °C.

2.2.3.4. Plant growth conditions

Growth conditions greenhouse

Plants were grown at 21 °C during the day and 17 °C during the night. A 16 h light period was used in the greenhouse. Relative humidity was 60 %.

Growth conditions phytotron

Root transformed plants were grown in a phytotron at 200 µE m^{-2} s^{-1} for 16 h, dark period 8 h, 22°C day/night, 65 % humidity.

2.2.3.5. Nodulation of *M. truncatula* plants

For nodulation assays of *M. truncatula* plants using *Sinorhizobium meliloti* plants were kept under nitrogen starvation for the whole treatment by equimolar replacement NO_3^- with Cl^- in the Hoagland's solution. *S. meliloti* WT was grown in liquid culture containing TY media until an optical density of 0.5 (λ = 600 nm) was reached and diluted 1:10 (v/v) with ddH_2O prior to inoculation by watering the plants with the bacterial suspension.

2.2.3.6. Root transformation mediated by *A. rhizogenes*

For the root transformations, seeds were surface sterilized and germinated as mentioned above (2.2.3.1.). The following protocol is based on axenic transformation developed by (Boisson-Dernier *et al.*, 2001).

The complete root from the seedlings was cut off with a sterile razor blade and discarded. The fresh wound from the shoot of the seedling was dipped on a 2 day old culture of *A. rhizogenes* strain Arqua-1 cultivated on YT-media and containing the appropriate destination vector.

The seedlings were then transferred on Fahräus-media containing 25 µg/ml kanamycin for 3 weeks. Plants expressing the visible marker were then transferred onto a quartz sand 0.3-0.8 mm/0.6-1.2 mm/vermiculite mixture (2:1:1) with or without *G. intraradices* inoculum and treated according to the experimental condition.

2.2.4. Molecular analysis of plants

2.2.4.1. Determination of soluble phosphate

Soluble phosphate was measured in a modified way according to (Itaya and Ui, 1966).
A determined amount (~20 mg) of frozen and grinded plant material was extracted with 200 µl 0.25 M NaOH and incubated at 96 °C under constant and vigorous shaking. Additional 200 µl of 0.25 M HCl and 100 µl 0.5 M Tris-HCl pH8 in 0.25 % [v/v] IPEGAL CA-630 were then added and the extract was incubated 2 min at 96 °C. After centrifugation for 4 min at 8000 rpm using a bench top centrifuge the supernatant was collected and kept frozen at -20 °C until further analysis. The soluble phosphate concentration was determined calorimetrically at OD 630 nm and an incubation of 30 min (RT, dark) using a 96 well micro titer plate containing 15 µl H_2O + 100 µl 1 M HCl in each well, a determined volume from the extract (2-20 µl) and 100 µl color reagent. The soluble phosphate concentration was calculated via standard curve using a phosphate standard.

2.2.4.2. Determination of the total phosphate concentration of plant material

All glass wares used for total phosphate measurements were boiled for 15 min in 0.2 M HCl and rinsed several times with ddH_2O.
10-50 mg of frozen fresh tissue was homogenized with total phosphate extraction buffer at a ratio of 1 mg of sample to 10 µl of extraction buffer. 100 µl of homogenized sample was mixed with 900 µl of 1 % glacial acetic acid and incubated at 42 °C for 30 min. An aliquot of 100 µl of the mixture was transferred to a glass tube for total phosphate determination. 30 µl of 10 % $Mg(NO_3)_2$ in 95 % ethanol was added to the aliquot.
The sample was then dried in an oven for 30 min at 180 °C and flamed to ash using a Bunsen burner under the fume hood. After cooling, 300 µl of 0.5 M HCl was added to dissolve the

sample at 60 °C for 30 min. For colorimetric determination an aliquot of 50 µl was mixed with 100 µl of color reagent and measured at OD 630 nm. Total phosphate concentration was calculated via standard curve using a phosphate standard. A blank sample without plant material was used as negative control.

2.2.4.3. RNA isolation methods

For small RNA library preparation and stem-loop qRT-PCR total RNA was isolated from plant tissue using *mir*Vana™ miRNA Isolation Kit (Ambion) together with the Plant RNA Isolation Aid (Ambion) according to the manufacturers description.
For cDNA synthesis used for normal qRT-PCR total RNA (>200nt) was isolated from plant tissue using either Invisorb® Spin Plant RNA Mini Kit (Invitek) according to the manual using Lysis Buffer RP or an organic extraction method using GdmCl. Therefore 50 to 100 mg grinded tissue was extracted with 400 µl RNA extraction buffer by vortexing thoroughly. After 10 min centrifugation at full speed (4°C) the supernatant was taken into a new tube and 300 µl of CIP solution (Roth) was added vortexed for 1 min. For phase separation the extract was centrifuged at full speed for 10 min (4°C). The upper phase was carefully collected (≡1 vol). After addition of 0.1 vol 1 M acetic acid and 0.7 vol 100 % ethanol, the mixture was incubated 30 min at RT. The nucleic acid was pelletized by centrifugation for 30 min at full speed (RT). The pellet was successively washed with 3 M sodium acetate and 70 % [v/v] ethanol, then dried and resuspended in 42 µl nuclease free water

2.2.4.4. Northern blot analysis

20 µg of total RNA were run on a formamide Gel and blotted onto a nitrocellulose membrane. Two different MtPho2 PCR products were amplified and used as a detection probe after hot-PCR radio labeled dATP or after radioisotope end-labeling. Gel electrophoresis and Northern Blot was carried out according to standard protocols (Sambrook and Russell, 2001).

2.2.4.5. cDNA synthesis for real-time quantification of mRNAs

Superscript™ III Reverse transcription kit (Invitrogen) and oligo $(dT)_{18}$ primer (Fermentas) was used for the cDNA synthesis. First strand synthesis was performed with ~1 µg of total RNA (in a maximum volume of 11 µl) according to the manufacturers.

2.2.4.6. cDNA synthesis for real-time quantification of small RNAs

Small RNAs were reverse transcribed according to (Chen *et al.*, 2005; Pant *et al.*, 2008) using sequence specific stem-loop primer. The protocol was modified to allow simultaneous relative quantification of mRNAs and subsequent normalization against Housekeeping genes. An amount of 1 µg total RNA including small RNA fraction (<200 nt) was added to reaction mix of 1 µl of 10 mM dNTPs, 1 µl per 2.5 mM stem-loop primer (maximum of 6 individual primers), 1 µl oligo $(dT)_{18}$ primer in a total volume of 36.5 µl. The mixture was incubated for 5 min at 65 °C and chilled on ice. 10 µl 5x First strand buffer, 2 µl of 100 mM DTT, 0.5 µl RNase inhibitor and 1 µl MultiScribe™ Reverse Transcriptase were added. CDNA was synthesized using the following program: 30 min at 16 °C, 1 h at 42 °C, 5 min 85 °C, kept on 4 °C until storage at -20 °C

2.2.4.7. Quantitative real-time PCR (qRT-PCR)

QRT-PCRs were performed in a 10 µl approach with 1 µl 1:10 diluted cDNA, 4 µl of 2 mM primer-pair mix and 5 µl Maxima™ SYBR Green/ROX qPCR Master Mix (Fermentas). The qRT-PCR machine, ABI Prism 7900 HT' (Applied Biosystems) was used and the reaction set up was: one cycle 95 °C for 10 min, 40 cycles 95 °C for 15 sec and 60 °C for 60 sec. An additional dissociation stage for analyzing melting curves was included. The data was analyzed using SDS 2.3 (Applied Biosystems) and MS Excel 2003 (Microsoft). The Ct-threshold was set to 0.2 and an automatic baseline correction was chosen for all experiments. The average from the Ct-values of *MtEF1-α*, *MtPDF2* was used as a housekeeping gene-index (HK-index) to normalize transcript abundance. The formula for calculating the relative expression is given below.

$$\text{Relative expression} = P_{eff}^{-\Delta Ct}$$

The primer efficiency (P_{eff}) was calculated using LinRegPCR (Ramakers *et al.*, 2003) and ΔCt was calculated by subtracting the Ct-value of the HK-index from the Ct-values of the measured transcripts. P_{eff}-values below 1.6 and over 2 were set as 2 in order to minimize distortion of the Dataset.

2.2.4.8. Modified 5'- RLM-RACE to determine miRNA target cleavage

MiRNA mediated cleavage products of target mRNAs were identified using a modified RLM-RACE protocol. Adapter ligation and cDNA synthesis was performed according to the manual, but without prior CIP and TAP treatment. Afterwards the cDNA was amplified using specific nested primers downstream of the predicted target cleavage site. Resulting bands of appropriate size were excised from the agarose gel and cloned into pCR®2.1 vector using the TOPO® TA cloning® Kit (Invitrogen) for subsequent sequencing and cleavage position confirmation.

2.2.4.9. Small RNA library preparation

Small RNA libraries from 10 µg total RNA were generated using the Digital Gene Expression Small RNA Sample Prep Kit (Illumina®) according to manual. User supplied materials were bought from companies suggested by Illumina®.
In short, the small RNA fraction was isolated from total RNA via denaturing polyacrylamid gel electrophoresis, 5'- as well as 3'- ligated to specific Illumina® sequencing adapters and reverse transcribed into cDNA.

2.2.4.10. Deep sequencing of the small RNA libraries and data analysis

To perform a quality check prior to sequencing, an aliquot of the blunt ended cDNA from the small RNA libraries was adenylated, using dATP and a Taq Polymerase which produces A overhangs, for 10 min at 72 °C and was TOPO TA cloned for subsequent sequencing of 48 colonies per library. After bioinformatic confirmation of the library qualities (nature and size of the insert), the libraries were sent to FASTERIS (Switzerland) for Illumina® sequencing.

The resulting data was pre-processed, filtered and subjected to bioinformatic prediction by Dr. Patrick May as described in Devers *et al.*, 2011.
Resulting candidates were manually inspected using the RNAfold with annotation tool from the UEA Plant sRNA toolkit (http://srna-tools.cmp.uea.ac.uk/plant/cgi-bin/srna-tools.cgi), using sequence information of mature, star strands as well as the most abundant reads to filter false positive candidates according to criteria from Meyers *et al.*, 2008 and Sam Griffith-Jones (personal communication). Sequence distribution of all small RNA reads mapping to a candidate locus were manually inspected using a Medicago genome browser with the genome version 3.0.

2.2.4.11. In-situ hybridization for miRNA localization

After fixation of roots, paraffin embedding and cutting (10 µm cross sections), root sections were deparaffinized (100% xylene, 50% xylene in Ethanol, 100%EtOH, 50% Ethanol in DEPC-H_2O, DEPC-H_2O; 5 min each step), deproteinated (proteinase K 1 µg/ml in TE buffer, 5 min at 37 °C) and fixed in 4 % PFA (10 min at room temperature). To avoid the loss of miRNA molecules, an additional step for the irreversibly immobilization of miRNAs was included. An EDC fixation using 1-ethyl-3-(3-dimethylaminopropyl) carbodiimide was done as described in (Pena *et al.*, 2009). Afterwards the sections were acetylated (triethanol amine, conc. HCl, acetic anhydride) and dehydrated by an ethanol series (25%, 50%, 70%, 85%, 90%, 100%; 30 sec each step). The sections were dried at room temperature and subsequently hybridized in ENZO hybridization buffer containing 0.4 pmol/µl of the appropriate 5'DIG-labelled LNA detection probe. As negative control a 5'DIG-labelled scramble probe was used, which is a random 21 nt LNA enhanced DNA oligonucleotide (5´gtgtaacacgtctatacgccca 3´) not able to bind any known plant transcript. The scramble probe was directly ordered at Exiqon, Denmark. The whole procedure of hybridization, stringency washes and the immunological detection using NBT/BCIP was carried out according to (Nuovo, 2010). This method is also published in Devers *et al.*, 2011.

2.2.4.12. Microarray hybridizations and data analysis

1 µg RNA was isolated from plant root and shoot material separately, using the total RNA procedure of the *mir*Vana™ miRNA Isolation Kit in addition with the Plant RNA Isolation

Aid. The RNA was sent to ImaGenes (Berlin, Germany) for further processing and hybridization. Medicago 4x44k microarrays were purchased from Agilent (Böblingen, Germany). Data analysis was carried out using Robin v1.8 (http://mapman.gabipd.org/web/guest/robin) (Lohse *et al.*, 2010) for quality control, data normalization and statistical evaluation. In short, the raw median values were background corrected using the half-minimum method and were quantile normalized. Statistic was carried out using the LIMMA (Smyth, 2005) package with a Benjamini-Hochberg p-value correction and a p-value cut-off of 0.05. The microarray probes were assigned to the corresponding gene annotation using an Mt3.5 annotation file provided from J*CVI* (http://j*cv*i.org/cgi-bin/medicago/gene_expression.cgi) and MtGI9 annotations (provided by Agilent). The processed data was used for further statistical analysis or visualization using the MeV: MultiExperiment Viewer tool (http://www.tm4.org/mev/). For visualization of functional annotated and classified genes in metabolic and signaling pathways MapMan v3.5.1 (http://mapman.gabipd.org/web/guest/mapman) (Thimm *et al.*, 2004) using a mapping for the Medicago genome release Mt3.5 (Marc Lohse, pers. communication).

3. RESULTS

3.1. Analysis of the mycorrhizal phenotypic response to constitutive low or high phosphate signals

The transcription of miRNA399 primary transcripts is induced upon mycorrhization and leads to high abundances of mature miR399 in mycorrhizal roots (Branscheid *et al.*, 2010) indicating that *Pho2* transcript levels are regulated during AM symbiosis. Plants with a modified expression level of *Pho2* would be a useful tool for the investigation of AM symbiosis at constitutive high and low Pi signaling levels.

3.1.1. Identification and cloning of the *AtPho2* homologue *MtPho2*

So far no functional homologue of AtPho2 has been identified in *M. truncatula*. However, a study of AtPho2 in Arabidopsis indicated the presence of a homologous sequence in the *M. truncatula* genome (Bari *et al.*, 2006). Therefore an EST Database [The Medicago Gene Index 9.0 (DFCI)] and the Medicago genome release Mt2.0 (IMGAG) were investigated for the presence of a putative *AtPho2* orthologue in *Medicago truncatula*. The tentative consensus sequence TC115486 showed the highest similarity to the full length *AtPho2* mRNA sequence (NCBI Reference Sequence: NM_179887.2) with an E-value of $1.6e^{-148}$. Only one full length hit was found in the Mt2.0 genome (chromosome 2; BAC clone mth2-154m16; GenBank AC159143.1) corresponding to a gene containing 8 introns (figure 4). The 5'UTR sequence contains 5 conserved sequence boxes with putative binding sites to miRNA399, which can be found in the AtPho2 5'UTR confirming the results of Bari *et al.* Due to sequence and structure similarity, the gene was named MtPho2.

Figure 4: Gene structure of *MtPho2*. The gene spans 6268 bp and is composed of 9 exons (green boxes) and 8 introns (white boxes). Exon 2 contains 5 putative miRNA 399 binding sites (orange boxes).

To confirm an AtPho2-similiar function of this homologous gene before investigation of its role during AM symbiosis, a preliminary experiment was conducted. It is known that the loss of function of AtPho2 in the Arabidopsis *pho2* mutant leads to an over accumulation of phosphate in the shoot, when grown under phosphate replete conditions (Delhaize and Randall, 1995), but not in the roots (Dong *et al.*, 1998). Therefore constructs for downregulation of *MtPho2* via RNAi were generated (see section 2.2.1.2.), to investigate whether the downregulation phenocopies the *pho2* mutant.

Downregulation of *MtPho2* in *M. truncatula* roots via root transformation led to high accumulation of soluble phosphate in the shoot (figure 5), when the plants were treated with 2 mM phosphate, but higher shoot phosphate levels were detected using 20 µM phosphate, too. Most of the plants with transgenic roots expressing either of the two RNAi constructs died at 2 mM phosphate concentrations, presumably suffering of toxic shoot phosphate levels compared to the empty vector control plants (figure 6). These findings correspond to the Arabidopsis *pho2* mutant and together with the high homology of TC115486 to *AtPho2* and the conservation of its miRNA binding sites and their distribution in the 5'UTR confirmed this gene as a functional homologue of *AtPho2*.

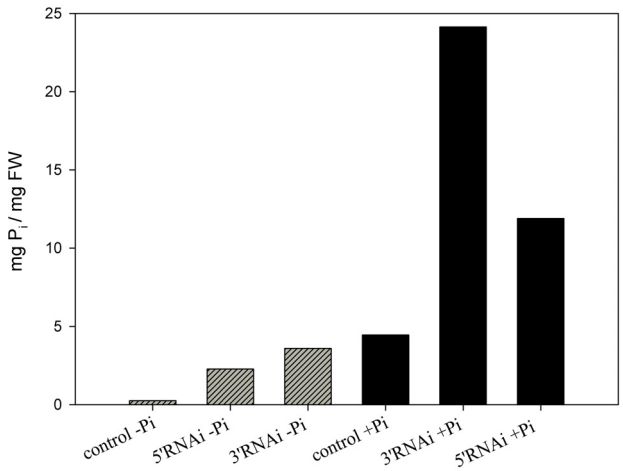

Figure 5: Soluble phosphate concentration of single root-transformed plants expressing RNAi constructs with fragments of the 3' or 5' UTR of *MtPho2* or a control RNAi construct containing a fragment of GFP. Plants were fertilized with 20 µM P_i (grey bars) or 2 mM P_i (black bars) containing half strength Hoagland's solution.

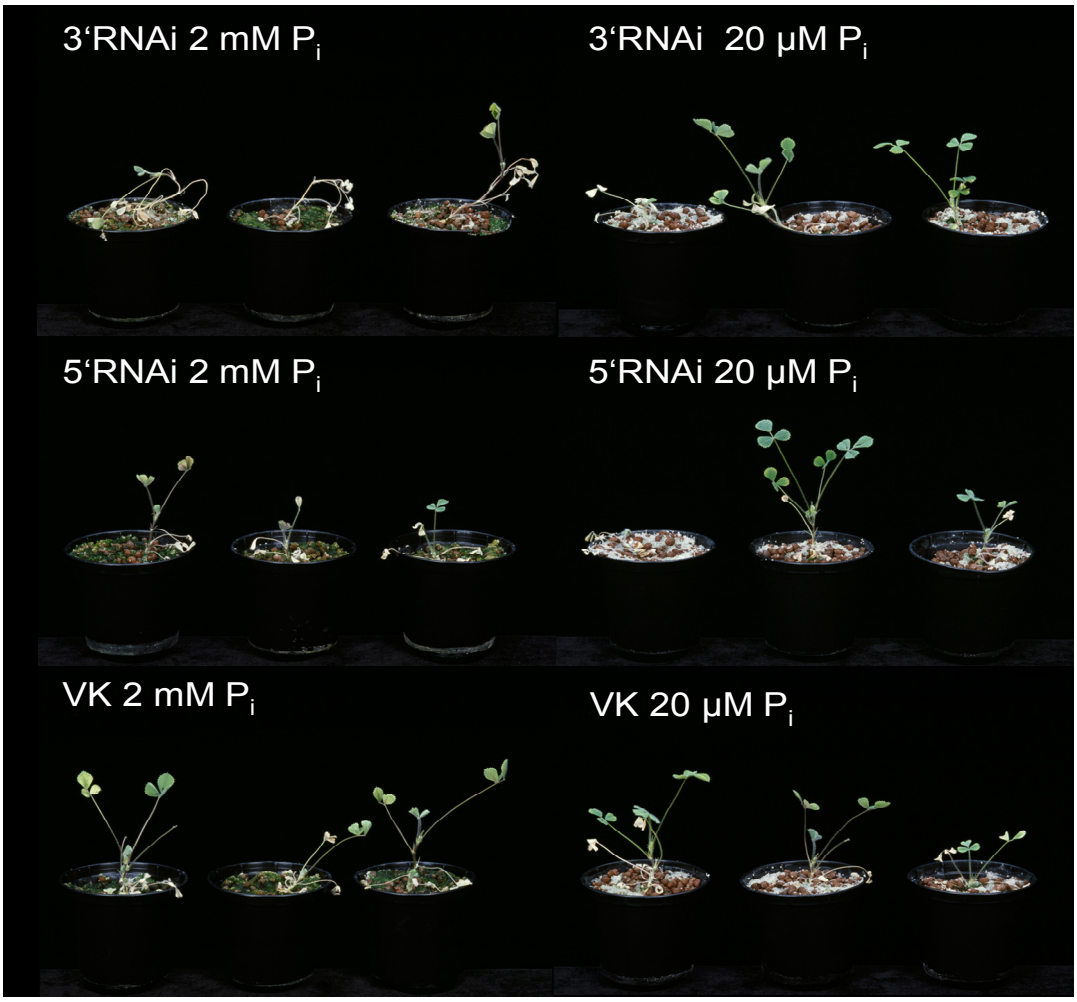

Figure 6: Phenotype of representative root-transformed plants expressing RNAi constructs containing either fragments of the 3’ or 5’ UTR of TC115486 or a control RNAi construct containing a fragment of GFP. Plants were fertilized with 2 mM phosphate (left side) or 20 µM phosphate containing half strength Hoagland’s solution.

3.1.1.1. *MtPho2* is cleaved by miR399

As mentioned above, *MtPho2* possesses 5 putative binding sites of miR399 in the 5’ UTR (figure 7a). To confirm the posttranscriptional regulation of *MtPho2* by miR399 a modified RLM-5’RACE experiment was carried out to investigate if the *MtPho2* transcript is also degraded by miRNA399-mediated cleavage in roots and which binding site is used. After designing a specific reverse primer, one or more bands with the size range of 400 – 600 bp were expected, depending on which 399-binding site is preferred in the *MtPho2* transcript. One band within the expected size range was visible after a nested PCR, when using RNA from phosphate starved plant roots (figure 7b) but not from RNA of roots from plants grown at 1 mM P_i. Cloning of the whole PCR product and subsequent sequencing of 5 plasmids from randomly picked colonies revealed a *MtPho2* transcript cleavage at the second miR399-

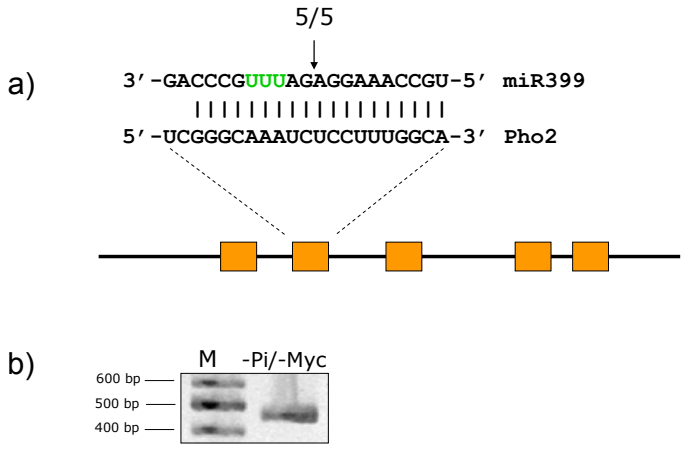

Figure 7: Modified RLM-5'RACE experiment for the target validation of miR399-mediated *MtPho2* transcript degradation. a) Alignment miR399 with the second binding site (orange boxes) of the *MtPho2* 5'UTR. Numbers above the alignment represent sequenced clones and position of the cleavage. b) Shows a section from the agarose gel after the nested PCR of the modified RLM-5'RACE before cloning. Gel picture was also published in Branscheid *et al.*, 2010. –P: plants were fertilized with 20 µM P_i.

binding site between 10th and 11th nt of the miR399 5'-end (figure 7a). Under the conditions tested, no other miR399 binding site was involved in *MtPho2* cleavage.

This binding site might have a prevalence binding affinity to the miR399 fraction containing a UUU motif at position 13-15 relative to the 5'end of the miRNA in contrast to the miR399 fraction containing an GCU or GUU motif at this site.

3.1.1.2. Search for additional miR399 targets

Bioinformatic target prediction of several *M. truncatula* miR399s which contain a GCU motif instead of a UUU motif, suggested TC103436 as an additional putative target (figure 8) (Leif Schauser, pers. comm.). Blast searches (http://blast.ncbi.nlm.nih.gov/Blast.cgi) of TC103436 against several databases revealed weak homologies to a TFIIb basal transcription factor in the N-terminal region of the putative CDS. The predicted binding site lies within the longest ORF of the tentative consensus sequence. RT-PCR with specific primers to TC103436 revealed that this transcript is present in all tested experimental conditions (+/-P and +/- myc), therefore quantitative real-time (qRT) PCR analysis was performed to investigate whether TC103436 is regulated during high or low phosphate fertilization and AM symbiosis. The relative expression was not altered comparing all four treatments and an additional modified RLM-5'RACE analysis with plant material from all treatments failed to detect miRNA399

```
5′-AGGGGCAGCUCUUCUUUGGAA-3′  TC103436
     |||||||||||||||| |
3′-GUCCCGUCGAGAGGAAACCGU-5′   miR399b
```

Figure 8: Predicted target-binding site of miRNA399b to TC103436. The GCU motif is depicted in green letters.

mediated degradation products of TC103436, indicating that this gene product is not regulated via miR399, different phosphate availability and AM symbiosis.

3.1.2. Functional analysis of *MtPho2* during AM symbiosis

After confirming a function of *MtPho2* in P_i homeostasis, *MtPho2* expression was modified to investigate a putative role of Pho2 in arbuscular mycorrhizal symbiosis. A constitutive high phosphate signal can be simulated by over-expressing a miR399 resistant *MtPho2* transcript. In contrast, plants with reduced *MtPho2* expression display a constitutive low phosphate signal.

3.1.2.1. Overexpression of *MtPho2* in transgenic roots of *Medicago truncatula*

It can be hypothesized that overexpression of *MtPho2* under low phosphate conditions would lead to a reduction or lack of AM symbiosis through a block of the *MtPho2* downstream acting phosphate starvation signals, simulating the plant to be in a high phosphate state.
The coding sequence (CDS) of *MtPho2*, which lacks the miR399 binding site, was cloned into the 35S driven destination vector pK7GW2D (Karimi *et al.*, 2002) resulting in vector pKpho2v2D for constitutive expression in root transformed *M. truncatula* plants. As vector control, the CDS of mRFP was cloned into the same destination vector. To distinguish transformed from non transformed roots for subsequent removal of non transformed roots prior to inoculation, pK7GW2D contains a constitutive expressed eGFP gene as a visible marker.

After root transformation, all plants were inoculated with *G. intraradices* and planted into a sand/vermiculite mix. The plants were grown for 21 days at low phosphate fertilization (20 µM P_i) allowing optimal colonization conditions until harvesting. The soluble phosphate concentration was measured, as well as the mycorrhizal phenotype and the expression of P_i starvation marker genes was analyzed via qRT-PCR.

Expression of pKpho2v2D in transgenic roots led to strong overexpression (up to 545%) of the *MtPho2* CDS compared to its endogenous expression (figure 9 A). The measurement of the relative transcript abundance of the phosphate starvation gene markers *MtPlD*, *MtSPX*, and the non-coding RNA *Mt4* revealed no difference in their gene expression levels. Contrary to the hypothesis mentioned above, overexpression of *MtPho2* led to a significantly increased expression of the AM symbiosis marker gene *MtPt4* and *G. intraradices* rRNA, compared to the vector control (figure 9 A and B), indicating a stronger colonization. However, correlation analysis using Spearman-Rank order correlation demonstrated, that the degree of the expression of the *MtPho2* CDS did not correlate with any of the measured AM symbiosis marker genes ($p > 0.05$) (figure 10). In contrast, the relative transcript abundance of all AM symbiosis marker genes strongly correlated with each other. The soluble P_i contents of the root transformed plants varied greatly (figure 9 C) but this variation didn't correlate with *MtPho2* overexpression, too ($p > 0.05$).

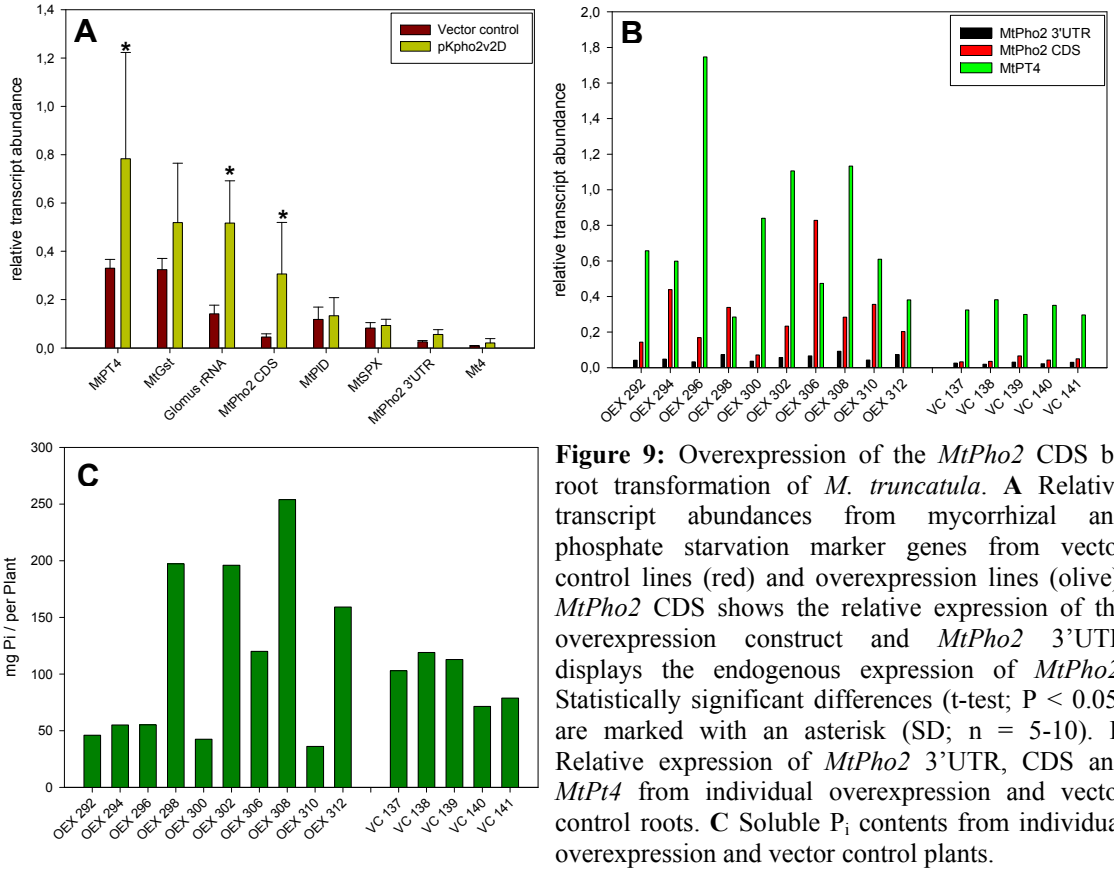

Figure 9: Overexpression of the *MtPho2* CDS by root transformation of *M. truncatula*. **A** Relative transcript abundances from mycorrhizal and phosphate starvation marker genes from vector control lines (red) and overexpression lines (olive). *MtPho2* CDS shows the relative expression of the overexpression construct and *MtPho2* 3'UTR displays the endogenous expression of *MtPho2*. Statistically significant differences (t-test; $P < 0.05$) are marked with an asterisk (SD; n = 5-10). **B** Relative expression of *MtPho2* 3'UTR, CDS and *MtPt4* from individual overexpression and vector control roots. **C** Soluble P_i contents from individual overexpression and vector control plants.

Spearman Rank Order Correlation

Cell contents given below gene name:
Correlation coefficient
p-value
Number of samples

	MtPt4	***MtGst1***	**Glomus rRNA**
MtPho2 CDS	0.325	0.082	0.496
	0.230	0.763	0.058
	15	15	15
MtPt4		0.818	0.818
		$2*10^{-7}$	$2*10^{-7}$
		15	15
MtGst1			0.682
			0.005
			15

Figure 10: Correlation analysis with Spearman rank order using all individual root transformed vector control and overexpression plants.

3.1.2.2. Functional knock-out of MtPho2 using the insertion mutant *mtpho2*

The identification of an insertion mutant line of *MtPho2* from a *M. truncatula* Tnt1 transposon insertion library (Igor Kryvoruchko, PhD thesis) gave the opportunity to further characterize the function of *MtPho2* during AM symbiosis. The mutant NF6180 has an insertion of the *Tnt1* transposon in exon 3 of the MtPho2 gene in the coding sequence.

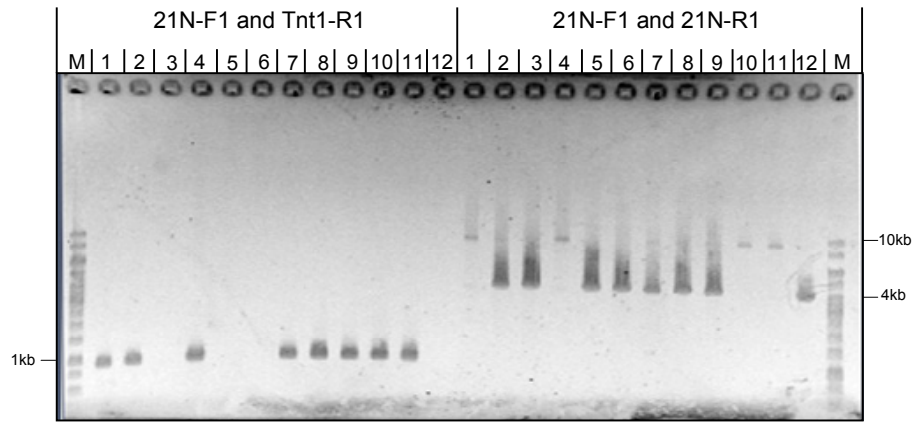

Figure 11: Gel analysis from a PCR screening of 12 *Tnt1*-insertional mutant plants concerning Tnt1-insertion in the *MtPho2* locus. The primers 21N-F1 and 21N-R1 are flanking the insertion site and Tnt1-R1 binds inside the transposon. If a transposon is present in the exon 3 of *MtPho2*, a PCR with the primer 21N-F1 and Tnt1-R1 results in a fragment of approximately 1kb (left side of the gel). The combination of the primer 21N-F1 and 21N-R1 results in fragment of ~4kb if the wild type gene and ~9kb fragment if a Tnt1-insertion is present. (M = 1kb-marker)

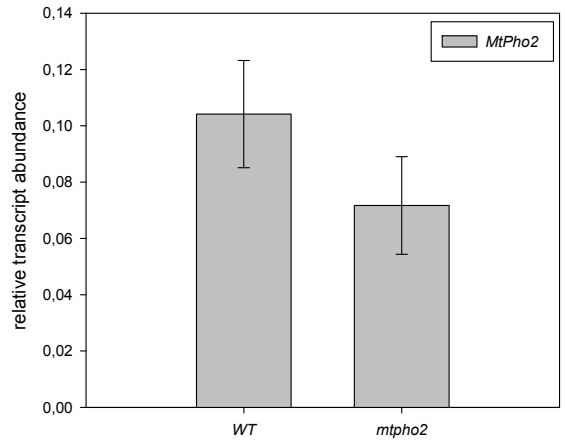

Figure 12: Relative transcript abundance of *MtPho2* in *M. truncatula* WT (with Tnt1 background) and *mtpho2*. Primers for qRT-PCR were positioned in the 3' UTR of the MtPho2 mRNA (SD, n=4).

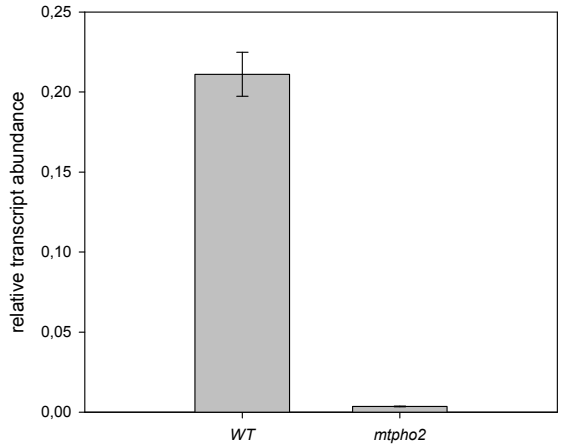

Figure 13: Relative transcript abundance of *MtPho2* in *M. truncatula* WT (with Tnt1 background) and *mtpho2*. Primers for qRT-PCR were positioned flanking the transposon insertion site (SD, n=3).

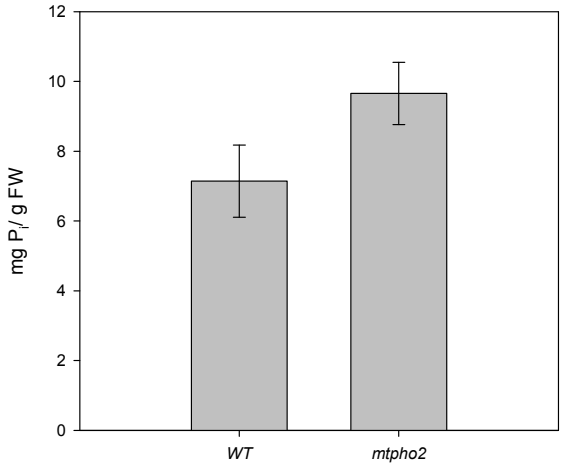

Figure 14: Total P_i concentrations from shoots of Tnt1 WT and *mtpho2* plants fertilized with 2 mM P_i. Statistical significant change demonstrated by Student's t-test ($p \leq 0.01$); (SD; n=5).

The plants were screened for homozygous progenies using low phosphate conditions to prevent toxic effects phosphate and subsequent discrimination of *mtpho2* mutant plants due to P_i over-accumulation.

The Tnt1 insertion line was screened for homozygous plants via PCR using genomic DNA (gDNA) and specific primer pairs binding to the inverted repeat region of the transposon or genomic regions flanking the insertion site. Four homozygous plants concerning the insertion in the *MtPho2*-gene could be confirmed (figure 11). Additional four plants with a homozygous MtPho2 wild type (WT) gene and Tnt1 insertion background could be confirmed as well and were used as control plants.

To analyze if the Tnt1 insertion leads to loss of transcription, qRT-PCR analysis was carried out. However, using primers binding to the 3'UTR of *MtPho2* revealed no significant difference in the relative transcript abundance between *mtpho2* plants and plants carrying the WT gene (figure 12). However, a slight reduction in the transcript abundance was detectable. Northern blot analysis was used to investigate whether the transcript is present in a longer aberrant form including the transposon, but due to the low transcript abundance of *MtPho2*, no signal of the *mtpho2* and WT transcript could be detected.

Because no antibody against MtPHO2 is available to check for the presence on the

protein level, the insertion was monitored via qRT-PCR after designing a primer pair flanking the Tnt1 insertion site. Given that the amplification step in the qRT-PCR program is optimized for small amplicons ~50-250 bp in size, insertion of the transposon would result in a drastically increase in amplicons at a size of ~5 kb and hence, a loss or reduction in amplification products. Indeed, using the flanking primers, a drastic reduction in the measurable relative transcript abundance between *mtpho2* and the control plants could be seen (figure 13). This suggests that *mtpho2* is transcribed in a longer aberrant form. The nucleotide sequence of the Tnt1 transposon contains several stop codons in the nucleic acid sequence. Therefore it is assumed that this mutation leads to a loss of function of the MtPHO2 gene product. To proof this assumption, the total phosphate content of *mtpho2* and control plant shoots was measured and compared after growing the plants for 3 weeks at 2 mM P_i. Plants carrying the *mtpho2* gene accumulated P_i to significantly higher levels than the control plants (figure 14), indicating a loss of MtPHO2 function.

Over accumulation of P_i in the plant shoots is the result of the activation of a subset of phosphate starvation genes. If the miR399-Pho2 Pi-homeostasis signaling pathway is involved in the down regulation of AM symbiosis during high phosphate levels, it can be hypothesized that the constitutive activation of this signaling pathway leads to higher arbuscule development at high phosphate levels. To test this hypothesis, Tnt1 WT and *mtpho2* plants were grown at low (20 µM) and high (2 mM) phosphate levels and arbuscule abundance was analyzed 28 days post inoculation (dpi). The expression of *MtPt4* was used as

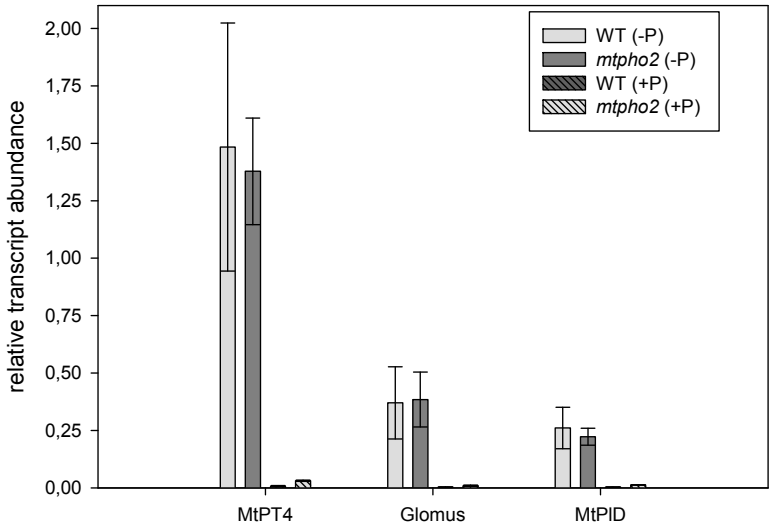

Figure 15: Analysis of the molecular AM symbiosis phenotype of *M. truncatula* Tnt1 WT and *mtpho2* plants 28 days post inoculation with *G. intraradices*. At –P conditions 20 µM P_i and at +P conditions 2 mM P_i was used for fertilization. *MtPt4* corresponds to arbuscule frequency and Glomus (*G. intraradices* rRNA) corresponds to fungal biomass. *MtPlD*, a phosphate starvation marker gene, was measured as a control for the different P_i conditions.

a molecular marker due to its correlation with arbuscule frequency in the root system (Harrison *et al.*, 2002), additionally the relative abundance of *G. intraradices* rRNA (Glomus) was monitored, which correlates to fungal biomass and hence, the colonization of the root system (Isayenkov *et al.*, 2004). No difference between the *mtpho2* and control plants could be detected at low and high phosphate concentrations showing a high or drastically reduced relative *MtPt4* and *G. intraradices* rRNA expression in both lines, respectively (figure 15).

Alternatively, a time-course experiment was carried out and monitored over a 21 days, to investigate if *MtPho2* plays a role in the establishment of the arbuscular mycorrhizal symbiosis at different phosphate levels. First, the expression of AM symbiosis marker genes was monitored after 7, 14 and 21 dpi in seedlings treated with low (20 µM) phosphate levels. As a control, the transcript levels of *MtPho2* were measured in WT and *mtpho2* seedlings. In agreement with the previous results the aberrant transcript of *mtpho2* led to a significant reduction of its measured expression level (figure 16). In the wild type plants, the highest expression of *MtPho2* could be seen at 7 dpi with a sharp drop at 14 dpi and a slight rise after 21 dpi. In contrast, the mutant shows a constant increase in the abundance of the aberrant transcript but still at very low expression levels.

The expression of *MtPt4* and *G. intraradices* rRNA was barely detectable after 7 dpi,

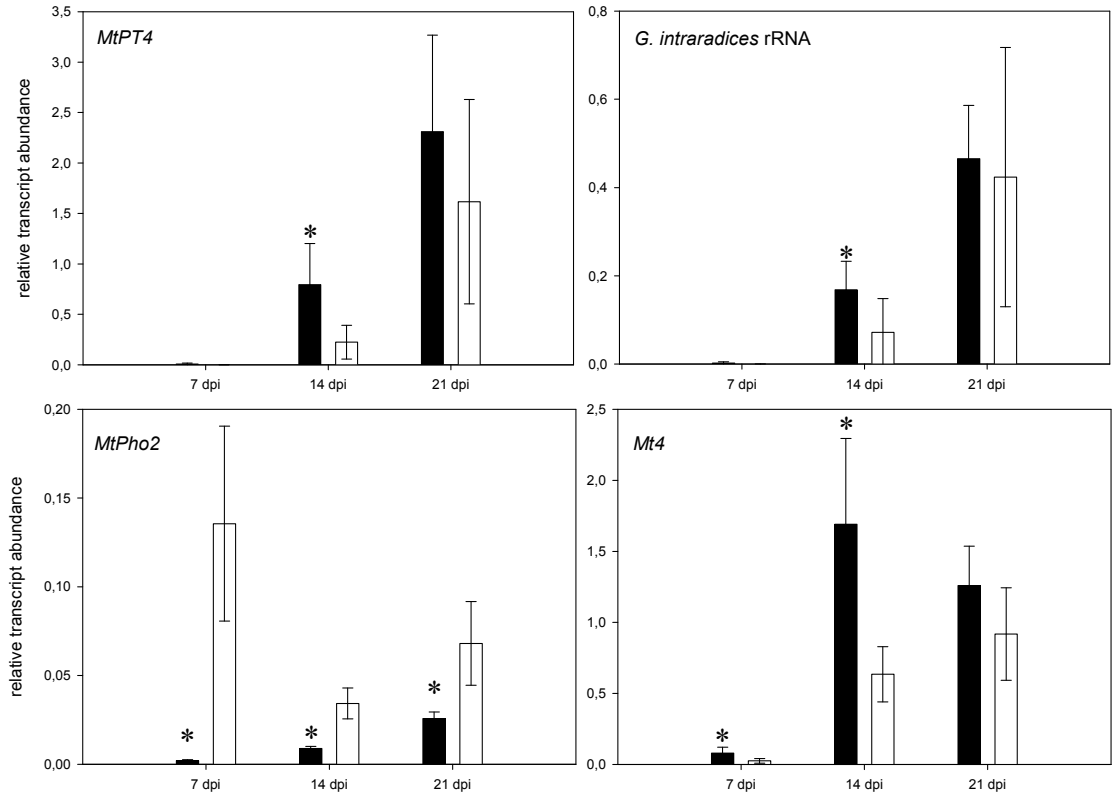

Figure 16: Relative transcript abundance of marker genes in seedlings grown under low phosphate conditions (20 µM). WT (white bars) and *mtpho2* plants (black bars) were harvested at three different time points (7 dpi, 14 dpi and 21 dpi). An asterisk marks statistically significant changes between *mtpho2* and WT plants (Student's t-test; $p \leq 0.05$) (SD_{14dpi}, n = 7; $SD_{7,21dpi}$, n = 3).

indicating that the fungus begins intraradical growth and colonization of the plant root system, but AM symbiosis is not fully established yet. Interestingly, significant higher levels of *MtPt4* and *G. intraradices* rRNA transcripts were detectable after 14 days post inoculation (Student's t-test, $p \leq 0.05$) showing a stronger colonization of *mtpho2* seedlings compared to wild type plants (figure 16) at 14 dpi. However, no significant difference could be measured at 21 dpi and the expression values are comparable with the 28 dpi time point from the previous experiment (figure 15), suggesting that colonization reaches a maximum. Another interesting observation is that *Mt4* showed a significant higher expression at 7 and 14 dpi, with its maximum at 14 dpi, in the mutant compared to WT. As mentioned in the introduction, the *AtIPS1* homologue *Mt4* negatively regulates levels of mature miR399.

The time course was repeated with high (2 mM) phosphate fertilization, to test whether the same phenotype is visible at AM symbiosis suppressible conditions. Comparing the relative expression levels of *MtPt4* and *G. intraradices* rRNA, a significant higher relative expression of *MtPt4,* but not *G. intraradices* rRNA, could be detected again after 14 dpi, even though the expression is at a very low level due to the dominant repression of the symbiosis by high levels of phosphate in WT as well as *mtpho2* plants (figure 17). No difference in the

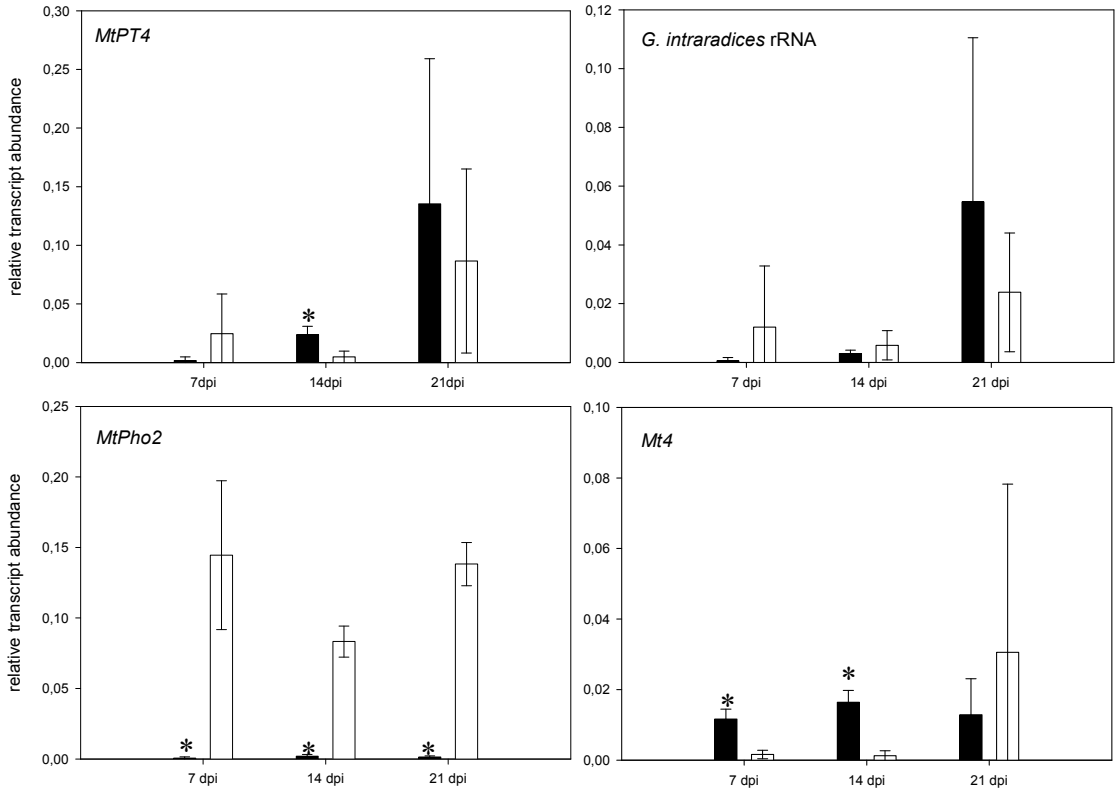

Figure 17: Relative transcript abundance of marker genes in seedlings grown under high phosphate conditions (2 mM). WT (white bars) and *mtpho2* plants (black bars) were harvested at three different time points (7 dpi, 14 dpi and 21 dpi). An asterisk marks statistically significant changes between *mtpho2* and WT plants (Student's t-test; $p \leq 0.05$) ($SD_{7,14,21dpi}$, n = 3-5).

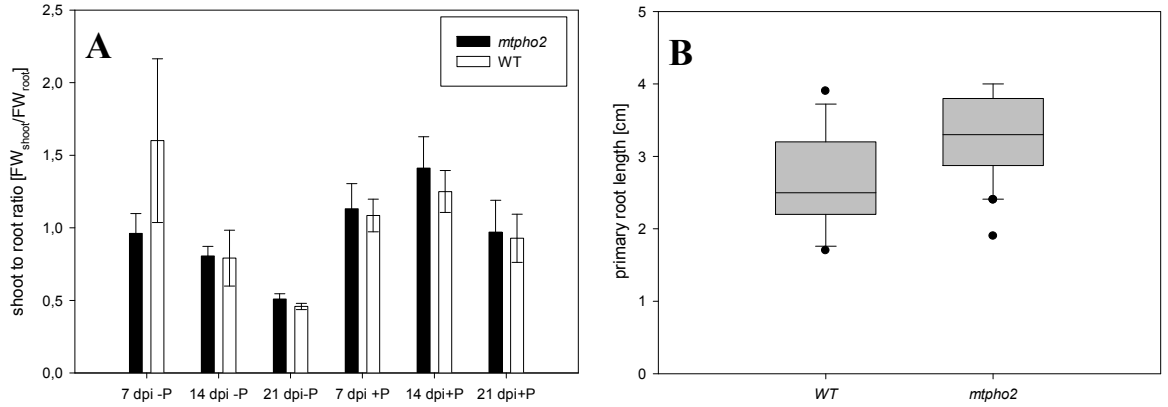

Figure 18: A Shoot to root mass ratios of *mtpho2* and WT calculated using the fresh weight (FW) from shoots and roots of each condition and time point (SD; n = 3-7). **B** Box-Plot of the primary root length from WT and *mtpho2* seedlings one week post germination (SD; n = 15-30).

expression of *MtPt4* could be observed at 21 dpi and the expression is strongly repressed by high levels of phosphate, which goes in line with previous results (figure 15).

Additionally, significant higher relative expression levels of *Mt4* could be detected at 7 and 14 dpi.

Faster colonization of the *mtpho2* root system by *G. intraradices*, indicated by the higher expression of AM symbiosis marker genes at 14 dpi, might be the result of a faster root growth or altered morphology.

To test this hypothesis, the shoot-to-root mass ratios of each genotype, condition and time point were compared. For seedlings grown under low phosphate conditions, the shoot-to-root ratio at 7 dpi is decreased in the mutant, *mtpho2,* compared to the Tnt1 WT, suggesting a longer primary root or a smaller shoot (figure 18 A). However, this phenotype was not observed if the seedlings were grown at high phosphate conditions. The length of the primary root from the *mtpho2* and WT seedlings was measured 7 days after germination. There was a small but statistical significant difference in primary root growth detectable (Student's t-test, $p \leq 0.05$). Seedlings of mtpho2 have a ~0.5 cm longer primary root as demonstrated by box-plots in figure 18 B.

3.1.3. Identification of a second *AtPho2* homologue, *MtPho2-2*, in the *M. truncatula* genome release Mt3.0

The genomic sequence of the *Medicago truncatula* genome release Mt2.0 includes a single homologue to the gene *AtPho2* from *Arabidopsis thaliana*, which was named *MtPho2* (see

Table 2: Percentage of the amino acid sequence similarities of the translated nucleotide sequences of *MtPho2-2* compared to *MtPho2-1*, *AtPho2* and *AtUBC23* calculated using ClustalW.

	AtUBC23	AtPHO2	MtPHO2-2	MtPHO2
AtUBC23		39.7%	36.8%	39.2%
AtPHO2			47.3%	50.8%
MtPHO2-2				88.8%

chapter 3.1.1.). However, the release of the genome version Mt3.0 and Mt3.5 revealed a second homologue of *AtPho2*, consecutively named *MtPho2-2*. The homologue was found on the pseudo-chromosome 4 (Mt3.0: Medtr4g018250-Medtr4g018270; Mt3.5: Medtr4g020620). In contrast, *MtPho2* is positioned on pseudo-chromosome 2 (Mt3.5: Medtr2g017250; Mt3.5: Medtr2g013650). However, no EST sequences which map fully or partially with a high similarity to *MtPho2-2* were found at the DFCI Medicago Gene Index release 9, in contrast to *MtPho2* (see chapter 3.1.1.).

After prediction of the *MtPho2-2* gene structure with FGENESH+ (http://linux1.softberry.com) the nucleotide sequence was aligned with *MtPho2* using the ClustalW method. Both sequences show a high sequence similarity to each other (95%). The translated nucleotide sequences were than compared with the protein sequence of AtPHO2 and AtUBC23, another E2 ubiquitin conjugase, which were used as reference and outlier, respectively. As presented in table 2, MtPHO2 and *MtPHO2-2* are highly similar (89%) but *MtPHO2-2* show a weaker similarity to AtPHO2 (~47% instead of ~51%) and the weakest similarity to AtUBC23 (~37%). Interestingly, the putative 5'UTR region of *MtPho2-2* contains five miRNA399 binding sites equivalent to the *MtPho2* 5'UTR, although with slightly different nucleotide sequences. These findings indicate that *MtPho2-2* is a paralogue

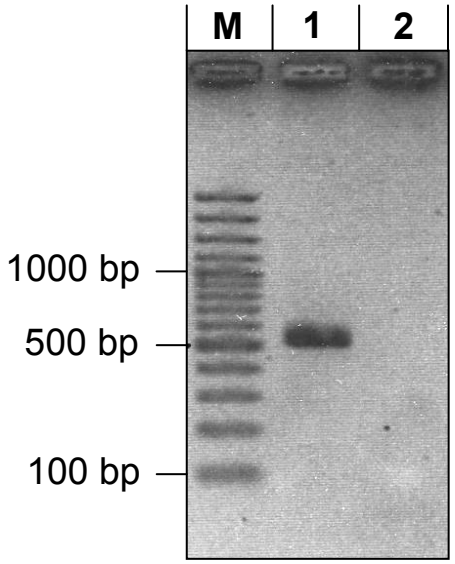

Figure 19: RT-PCR with gene specific primers results in a 513 bp long amplicon of *MtPho2* (1). Gene specific primers spanning 130 bp of the *MtPho2-2* gene (2) using cDNA from *M. truncatula* A17 roots fertilized with 2 mM phosphate. M = 100 bp Ladder.

of *MtPho2*.

RT-PCR using a primer set binding in the ORF of *MtPho2* and subsequent cloning and sequencing of the PCR product from 10 plasmids showed no presence of *MtPho2-2*. To specifically detect *MtPho2-2* transcripts, RT-PCR primers for MtPho2-2 were designed spanning a gap in the sequence compared to *MtPho2*. Using RNA from plants fertilized with 1 mM phosphate containing half strength Hoagland's solution, no RT-PCR product for *MtPho2-2* was visible in contrast to a specific band using primers designed to bind to the *MtPho2* transcript (figure 19), explaining its absence from the EST libraries. Therefore, taken the missing EST sequences and the result of the RT-PCR analysis into account, the results showed that *MtPho2-2* is not expressed in *M. truncatula* roots under the tested conditions.

3.1.4. Triggering high P_i signals with the phosphate structure analogue phosphite

Because phosphite is a structure analogue of phosphate and capable of repressing the PHR1-399-Pho2 signaling pathway including *At4/IPS1* in *A. thaliana* (Ticconi *et al.*, 2001; Stefanovic *et al.*, 2007; Ribot *et al.*, 2008), a phosphate and phosphite (Ph_i) re-supply experiment was carried out.

The plants were inoculated with *G. intraradices* and starved of phosphate for 2 weeks (20 µM P_i) and were then re-supplied 1 mM P_i, 980 µM Ph_i + 20 µM P_i or 20 µM P_i (control). The plants were harvested at two time points, t_{0d} (14 dpi) and t_{14d} (28 dpi). The impact of the phosphite treatment on the AM symbiosis was characterized by measuring the relative expression of AM symbiosis and phosphate starvation marker genes and normalization to the time point t_{0d}.

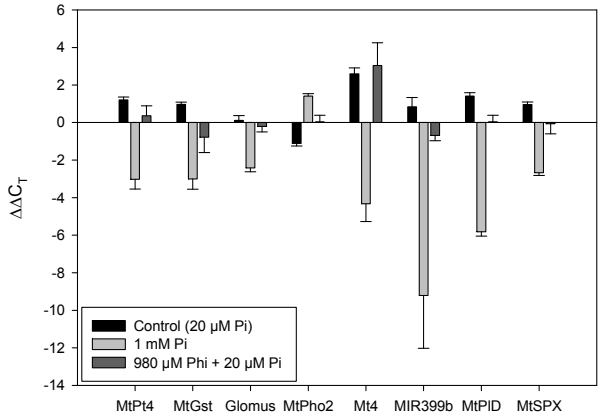

Figure 20: Phosphite and phosphate re-supply of *M .truncatula* A17 WT plants inoculated with *G. intraradices*. Plants were starved of phosphate for 14 days with fertilizer containing 20 µM P_i. At 14 dpi (t_{0d}) the plants were fertilized for the next 14 days with 1 mM P_i or 980 µM phosphite (Ph_i) + 20 µM P_i and a control group was fertilized with 20 µM P_i. At 28 dpi (t_{14d}) the plants were harvested, analyzed via qRT-PCR and the expression of t_{14d} was normalized to t_{0d}. Changes in the expression values are as $\Delta\Delta C_T$ (SD: $n_{control,Pi} = 3$; $n_{Phi} = 5$).

Prolongation of the phosphate starvation (control) led to a further increase in the relative expression of AM symbiosis marker genes at t_{14d} (figure 20), indicating

an increased colonization of the root system between t_{0d} and t_{14d}. As expected, there is also an increase in the relative expression of P_i-starvation marker genes. Re-supply of phosphate led to the suppression of AM symbiosis, visible by downregulation of *MtPt4*, *MtGst1* and *G. intraradices* rRNA relative transcript abundance. All P_i-starvation marker genes are strongly repressed by 1 mM phosphate, except *MtPho2*, whose relative expression is induced due to downregulation of miR399 (indicated by the downregulation of the primary transcript MIR399b). The increase in AM symbiosis and Pi-starvation gene expression is completely blocked by phosphite. Interestingly, *Mt4* is not affected by addition of phosphite, showing the same induction intensity in Ph_i treated plants compared to the control plants. However, re-supply of Ph_i instead of phosphate is not sufficient to completely downregulate AM symbiosis and P_i-starvation marker gene expression to the same extend as 1 mM P_i.

3.2. Analysis of the systemic adaptation of mycorrhizal plants to different phosphate concentrations

As mentioned in the introduction the rate of fungal root colonization inversely correlates with the P_i-content in the soil. The decreased formation of AM is primarily due to high P_i concentrations in the plant shoot. The molecular mechanisms behind this systemic regulation are not fully understood and therefore a transcriptional analysis was carried out.

3.2.1. Systemic suppression of arbuscular mycorrhizal symbiosis by phosphate using split root cultures

The split-root system permits the alteration of the internal P_i-status of the plant. Simultaneously, this also avoids direct effects of phosphate on the AM fungus (deMiranda and Harris, 1994; Nagahashi *et al.*, 1996). Under these conditions, the interaction between the systemic P_i status and the mycorrhizal colonization can be studied in a relatively simple system.

3.2.1.1. Establishment of a functional split-root system to study systemic interactions between *M. truncatula* and *G. intraradices*

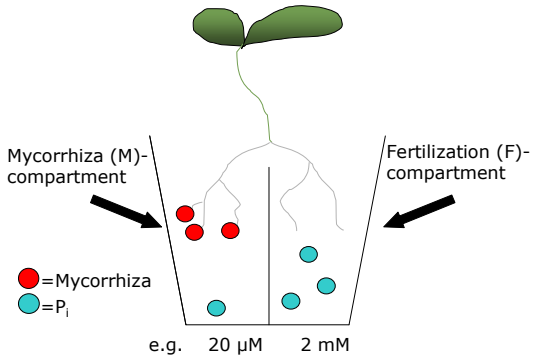

Figure 21: Simple sketch of the split-root design. The root system of the plant was divided and planted into two separated compartments. The fertilization (F)-compartment is used to alter the plants phosphate status by external application of nutrient solution containing a defined concentration of phosphate. The mycorrhizal (M)-compartment, containing an inoculum of AM-fungi, is fertilized with a basal phosphate concentration of 20 µM at all experimental conditions.

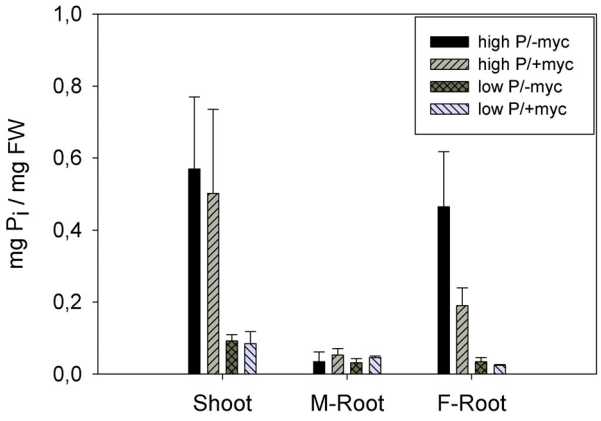

Figure 22: Soluble phosphate concentration of plants grown in the split-root system. The soluble phosphate concentration of the shoot and the root-system in either side of the compartment was determined. High P = 1 mM P_i in the F-compartment; low P = 20 µM in the F-compartment. (SD;n = 4)

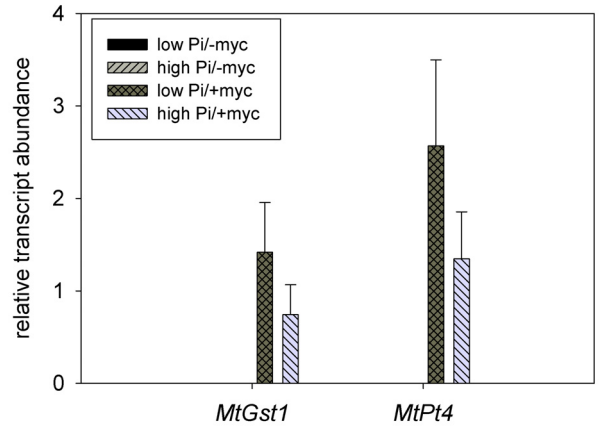

Figure 23: Systemic downregulation of *MtGst1* and *MtPt4* at high phosphate conditions. Expression was measured using RNA of roots from the M-compartment. (SD; n = 4).

The plants were grown in two-compartment pots at four different conditions (see material and methods). They were fertilized in the fertilization (F)-compartment and in inoculated with *G. intraradices* or mock treated in the mycorrhizal (M)-compartment. The F-compartment was fertilized with either 1 mM or 20 µM P_i representing high or low phosphate conditions. All M-compartments were fertilized with 20 µM at all conditions (figure 21). To test whether the system is functional, the shoot tissue and the root tissues from the M- and F-compartment was harvested separately and the soluble phosphate concentration was determined and mycorrhizal as well as phosphate marker genes were measured.

The soluble phosphate concentration of the plants grown at the four experimental conditions is presented in figure 22.

As expected, high P_i fertilization of the plants led to high levels of soluble phosphate in the shoot compared to plants treated with low P_i. When treated with high P_i, roots showed elevated soluble phosphate concentrations in the F-compartment but not in the M-compartment, indicating that soluble phosphate does not accumulate at high Pi conditions in roots with a low local Pi supply. At these conditions, AM symbiosis is not influencing the soluble phosphate concentration of the shoot and of the mycorrhizal roots in the M-compartment. However, mycorrhizal plants fertilized with

high levels of phosphate show a significant drop ($p \leq 0.05$; Student's t-test) of the soluble phosphate concentration in the non-colonized roots of the F-compartment to ~40% of the level from non-mycorrhizal plants. To analyze if the split-root system is capable of systemically suppress AM symbiosis at high phosphate conditions, the molecular marker genes *MtPt4* and *MtGst1* were measured by qRT-PCR (figure 23).
As assumed, high phosphate concentration in the shoot systemically downregulates the relative expression of *MtGst1* and *MtPt4* in mycorrhizal roots reaching only half the value of low P_i treated plants. Non-mycorrhizal control plants show no expression of *MtGst1* and *MtPt4*, as expected. This indicates that root colonization is systemically suppressed by a high P_i status provided by high P_i-fertilization in the F-compartment of the split-root system.

3.2.2. Transcriptomic profiling of *Medicago truncatula* roots and shoots in split root cultures

As mentioned in the introduction, numerous transcriptomic studies of AM symbiosis have been published over the years, but these were mainly focused on root colonization at AM symbiosis-promoting low P_i conditions. Two studies investigated systemic effects of AM symbiosis in the plant shoots of *M. truncatula* and *S. lycopersicum* (Liu *et al.*, 2007; Fiorilli *et al.*, 2009), however a transcriptomic study analyzing the suppression of AM symbiosis by phosphate is still missing. After establishing the split-root system (3.2.1.1.), it was used for a transcriptomic approach by microarray hybridization to get insights into the regulation of transcripts during systemic AM symbiosis suppression by high phosphate.

For the experiment, the plants were grown for 22 dpi in split-root pots as described above, but high phosphate treated plants were fertilized in the F-compartment with 2 mM phosphate, to reach a stronger repression of AM symbiosis. After harvesting, 4 plants were pooled and the shoots, roots from the M-compartment and roots from the F-compartment were separately frozen. Four independent pools of the respective plant tissue were harvested per condition [(high P_i/myc) (high P_i/nm) (low P_i/myc) (low P_i/nm)] and analyzed for marker gene expression as a quality control prior to microarray hybridization (appendix figure 42 A and B). Furthermore, the total shoot phosphate concentration was determined (appendix figure 43). Three RNA samples per condition and tissue were used for hybridization to Agilent

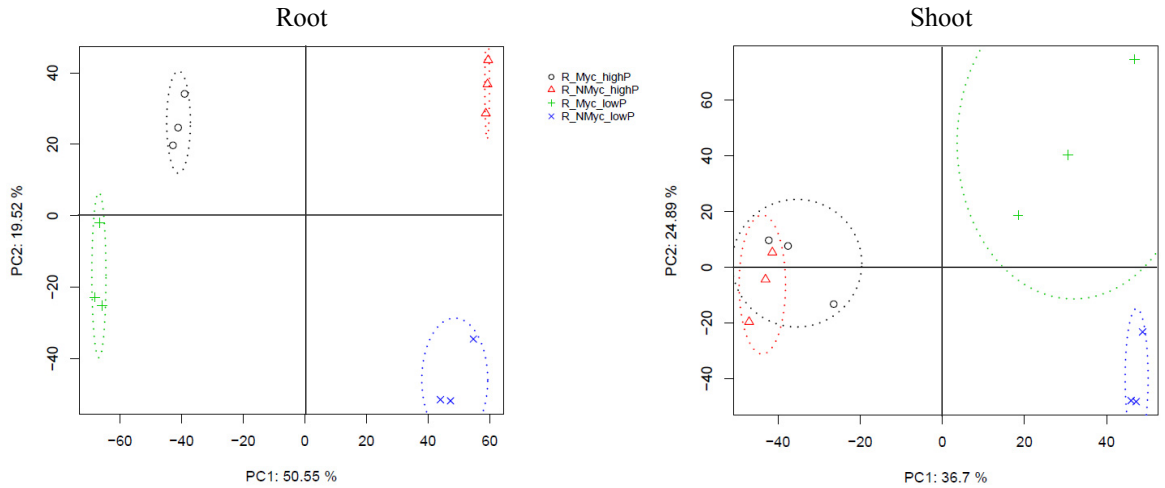

Figure 24: Principal component analysis of the *M. truncatula* root and shoot transcriptome.
Colors indicate the following conditions: high P_i/myc (black); high P_i/nmyc (red); low P_i/myc (green); low P_i/nmyc (blue) and are identical for the root and shoot tissue.

Medicago 4x44k microarrays. The root tissue from the F-compartment was not used for hybridization in this study, but was kept for future analysis.

After normalization of the data (see chapter 2.2.4.12.) a principal component analysis (PCA) for the root and shoot tissue was carried out to compare the status of the whole transcriptome of the plant during all tested conditions (figure 24). In case of the root tissue all four conditions could be clearly separated by the PCA, indicating that the root transcriptome exhibits distinct states. Interestingly, the status of mycorrhizal roots at low phosphate conditions is shifted towards the high phosphate status compared to the non-mycorrhizal low and high phosphate conditions. Moreover, the status of mycorrhizal roots at high phosphate conditions is shifted towards the non-mycorrhizal condition. This observation reflects the improved phosphate status of mycorrhizal roots at low phosphate availability and the reduced colonization of the root system of plants with a high content of phosphate in the shoot.

In contrast, the PCA of the shoot tissue was not able to separate all treatments. Especially at high phosphate availability, mycorrhizal and non-mycorrhizal shoot samples were grouped together. However, at low phosphate conditions the shoot transcriptomes could be clearly separated from each other, but the mycorrhizal shoot transcriptome at low P_i tends to be more variable.

Next, the transcript accumulation at all conditions was compared with each other ([low P: myc/nm]; [high P: myc/nm]; [myc: high P/low P]; [nm: high P/low P]) and differential transcript accumulation for roots and shoots was calculated using the program Robin (see chapter 2.2.4.12.) with a $\log_2$fold change cut-off = 1 and -1. After annotating the genes according to the recently updated Medicago genome version (mt3.5), the differentially expressed genes were then sorted into functional categories using MapMan v3.5.1 (Thimm *et*

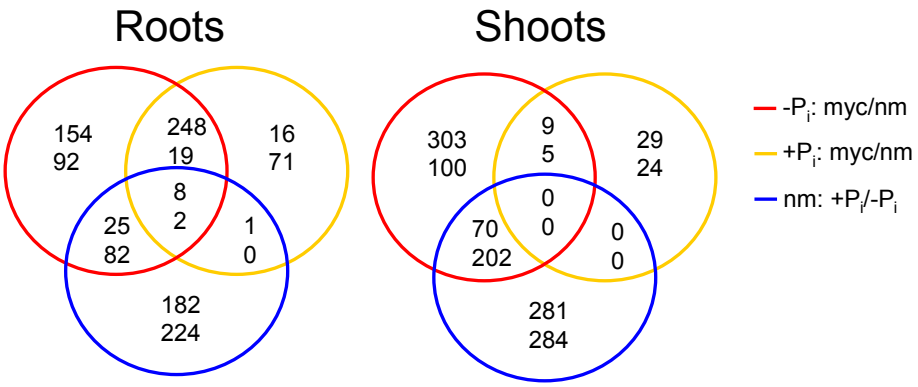

Figure 25: Venn diagrams of genes after mapping to MapMan which show differential regulation in response AM symbiosis at low phosphate conditions (red circle), high phosphate conditions (yellow circle) and to phosphate at non-mycorrhizal (nm) conditions from roots and shoots of the split-root experiment. Upper numbers indicate induced genes and lower numbers indicate repressed genes. The number of genes responsive to various conditions is shown in the overlapping portion. Note that responses to phosphate are systemic and +P corresponds to the fertilization compartment, whereas the genes indicated were measured from root tissue in the mycorrhizal compartment.

al., 2004). 42% of all annotated *M. truncatula* genes could be mapped to functional categories based on protein sequence information of *A. thaliana* (Marc Lohse, pers. communication). From the root tissue 1109 out of 1798 genes (62 %) and 1386 out of 1810 (77 %) of the differentially regulated genes from the shoot could be mapped to functional categories. Venn diagrams were constructed to display overlaps of differentially expressed transcripts in mycorrhizal tissue at low phosphate conditions or systemically at high phosphate conditions and upon high phosphate treatment without AM symbiosis as a control (figure 25). In roots the number of transcripts which are co-regulated by myc (low Pi) and also high phosphate (nm) is lower as compared to shoots. Interestingly, 248 transcripts were induced in mycorrhizal roots regardless of the phosphate condition and 21 transcripts were repressed at both conditions. At low phosphate conditions 246 transcripts were regulated by myc alone and 154 (63%) of them were induced by AM symbiosis. In contrast, 87 myc responsive transcripts were found to be regulated specifically at high phosphate conditions and only 16 (18%) of them were induced by AM symbiosis.

3.2.2.1. Differentially regulated transcripts of *M. truncatula* roots colonized by *G. intraradices* at low and high phosphate conditions

To analyze the data in concert with previously published transcriptional data, the dataset was verified by correlation of 100 randomly picked genes which are significantly regulated ($p \leq 0.05$; LFC cut-off = 1) by AM symbiosis in roots [low P: myc/nm] to the same set of genes

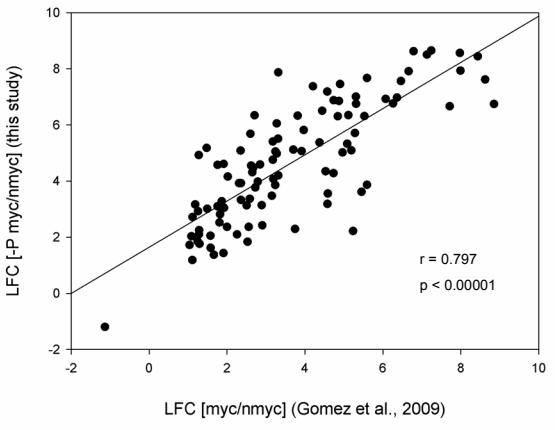

Figure 26: Correlation between the root dataset derived from this study and Gomez *et al.* (2009).
The LFCs of 100 randomly picked genes with significant differential expression comparing myc and nmyc at low P_i conditions were correlated using a Pearson-correlation.

from Gomez *et al.*,2009 (figure 26). Both datasets highly correlated with each other as indicated by the high correlation coefficient and the low p-value.

Furthermore, the expression of AM symbiosis specific genes, like *MtPt4* (Harrison *et al.*, 2002), *MtGst1* (Wulf *et al.*, 2003), *MtHa1* (Krajinski *et al.*, 2002), *MtGlp1* (Doll *et al.*, 2003), *MtDSX2* (Walter *et al.*, 2002) *MtBcp1* and a myc specific serine carboxypeptidase (Hohnjec *et al.*, 2005), was analyzed. These genes were found to be the highly upregulated when comparing myc versus nm at low P_i conditions (table 3). Interestingly, the LFC values for the highest expressed genes are nearly identical or even higher at high phosphate conditions compared to low P_i, although downregulation of *MtPt4* was clearly confirmed by qRT-PCR measurements from the same starting material (figure 42 A), indicating the higher dynamic range of the latter method and suggesting that these probes are saturated at both mycorrhizal conditions due to very high transcript abundance. Surprisingly, the two GRAS transcription factors (TFs) encoding genes *MtNsp1* and *MtNsp2* were found to be induced during AM symbiosis and *MtNsp2* is additionally systemically induced by phosphate. Both TFs are essential in nod factor signaling (Kalo *et al.*, 2005; Smit *et al.*, 2005) and *MtNsp2* has recently been shown to be involved in mycorrhizal signaling (Maillet *et al.*, 2011).

Table 3: Log_2fold expression values of arbuscular mycorrhizal and nodule symbiosis genes comparing different conditions in roots.

Gene	IMGA (mt3.5)	TIGR/Genbank	Comparison[a]			
			-Pi: m/nm	+Pi: m/nm	m: +Pi/-Pi	nm: +Pi/-Pi
MtPt4	contig_52795_1	TC112872	9.13	9.87	ns	ns
MtHa1	contig_74284_1	AJ499192	1.47	1.28	ns	ns
MtGlp1	contig_172043_1	TC124054	8.58	8.52	ns	ns
MtGst1	Medtr5g076900.1	TC135802	8.65	9.28	ns	ns
MtScp	Medtr3g079570.1	TC122974	7.45	ns	-1.31	ns
MtDSX2	Medtr8g068300.1	TC112682	1.64	2.06	ns	ns
MtBcp1	Medtr7g086140.1	TC132480	8.08	7.29	-1.31	ns
MtNsp1	Medtr8g020840.1	TC112834	1.21	ns	ns	ns
MtNsp2	Medtr3g072710.1	TC112920	2.34	1.09	ns	1.24

[a]-Pi: 20 µM P_i; +Pi: 2 mM P_i; m: mycorrhizal; nm: non-mycorrhizal; ns: non-significant ($p > 0.05$)

In summary, obtained microarray data from mycorrhizal roots corresponds to previously published data of this system.

Since, transcriptional responses in mycorrhizal roots at low phosphate conditions have been analyzed before (see above), the main focus will be laid on the high phosphate conditions. The genes showing differential transcript levels in mycorrhizal roots were sorted into functional categories (figure 27). A large portion of genes encoding for unknown proteins and was neglected in this study. Most of the genes with specific response to myc at high shoot phosphate conditions belong to three major functional groups, namely gene expression and RNA processing (1), protein modification and turnover (2) and signal transduction (3). Regulated genes belonging to the secondary metabolism are strongly overrepresented, specifically at high phosphate conditions. In contrast, the main functional categories of genes specifically regulated at low phosphate conditions and those showing regulated at both conditions belong to protein modification and turnover, transport and gene expression and RNA processing.

Interestingly, at high phosphate conditions 14 out of 15 transcription factors (TFs) were specifically downregulated and only one putative GRAS TF, which shows a weak homology

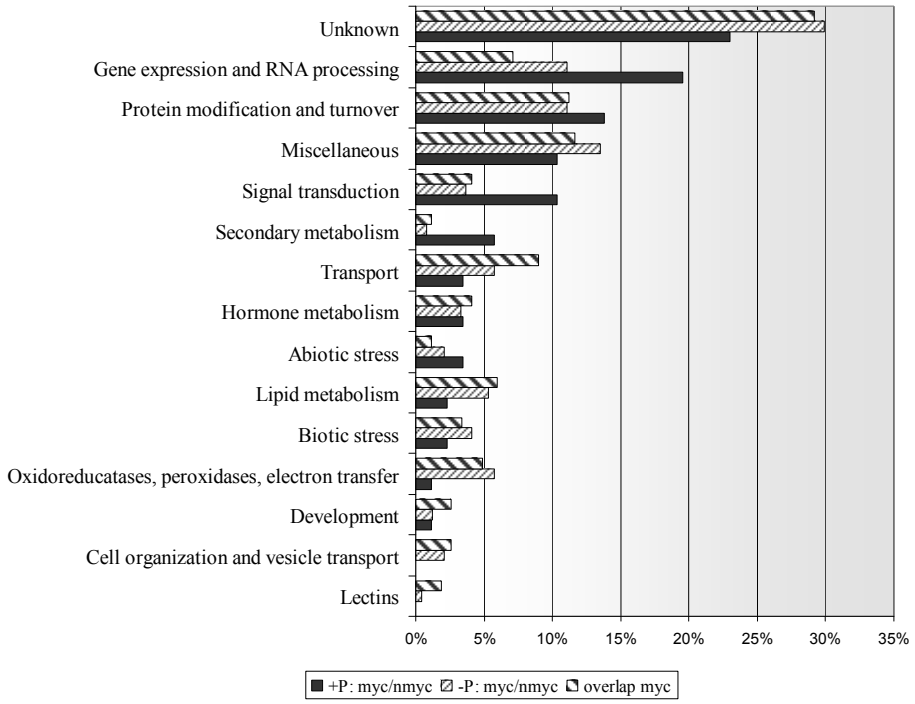

Figure 27: Molecular functional categories of mycorrhizal regulated genes in roots at low and high phosphate conditions and of co-regulated genes. Shown is the percentage of genes given in figure 26 A (red and yellow circles) grouped into the according functional categories by a protein sequence based MapMan annotation (Thimm *et al.*, 2004). Miscellaneous: all genes not sorted into one of the given category.

to *MtNsp2* is upregulated 3-fold (table 4). 10 out of 11 transcripts encoding several protein kinases and E3 ubiquitin ligases were downregulated. The same trend is visible for genes belonging to the signal transduction group, where 5 out of 7 transcripts, encoding mostly putative calmodulin-binding proteins, were downregulated.

Table 4: A subset of genes from *M. truncatula* which are specifically and significantly regulated in roots during AM symbiosis at high phosphate conditions. (full table is attached on CD)

Mt3.5 ID	Putative annotation	+P myc/nm	-P myc/nm	nm +P/-P
Gene expression and RNA processing				
medtr1g086530.1	MYB domain transcription factor family	-2.64	-0.79	1.94
medtr4g086220.1	AP2/EREBP transcription factor family	-2.14	-0.76	1.37
medtr8g098450.1	moderately similar to At3g44260	-2.06	-0.98	1.27
medtr3g090860.1	WRKY domain transcription factor family	-1.80	-0.53	1.13
medtr4g007060.1	WRKY domain transcription factor family	-1.56	-0.70	0.99
medtr5g014640.1	bHLH,Basic Helix-Loop-Helix family	-1.54	0.11	1.25
medtr5g010930.1	AP2/EREBP transcription factor family	-1.53	-0.32	1.20
medtr2g097390.1	GRAS transcription factor family	-1.40	-0.31	1.18
ac233680_9.1	WRKY domain transcription factor family	-1.31	-0.28	0.39
medtr2g039620.1	bHLH,Basic Helix-Loop-Helix family	-1.29	-0.08	1.52
medtr7g100080.1	C2H2 zinc finger family	-1.25	-0.02	0.79
medtr4g064150.1	GRAS transcription factor family	-1.14	-0.75	0.19
medtr1g101550.1	AP2/EREBP transcription factor family	-1.07	-0.20	0.93
medtr1g075140.1	moderately similar to At4g14660	-1.02	-0.20	0.77
medtr7g069740.1	GRAS transcription factor family	1.62	0.39	-1.81
Protein modification and turn over				
medtr5g023980.1	receptor like kinase	-2.65	-0.78	1.64
medtr8g067280.1	moderately similar to At1g32640	-1.57	0.06	1.84
medtr8g011780.1	Serine/threonine-protein kinase	-1.31	-0.79	0.32
medtr5g091130.1	aspartyl protease family	-1.20	-0.33	0.65
medtr1g102360.1	receptor like kinase	-1.19	-0.59	0.61
medtr2g030420.1	AAA-ATPase	-1.11	-0.26	0.31
medtr3g086540.1	MAP kinase	-1.11	-0.38	0.43
medtr2g097620.1	ubiquitin E3 ligase.RING	-1.09	-0.66	0.17
medtr7g113800.1	ubiquitin E3 ligase.RING	-1.08	-0.65	0.30
medtr4g091100.1	ubiquitin E3 ligase.RING	-1.08	0.78	1.51
medtr1g072380.1	aspartyl protease family	-1.05	-0.10	1.44
medtr7g089670.1	ubiquitin E3 ligase SCF.FBOX	1.76	0.72	-2.34
Signaling				
medtr8g107110.1	calmodulin-binding protein	-1.94	-0.44	1.31
medtr4g103650.1	calmodulin-binding protein	-1.93	-0.16	1.69
medtr2g039910.3	calmodulin-binding protein	-1.61	-0.51	0.79
medtr7g082310.1	leucine-rich repeat family protein	-1.56	-0.44	1.12
medtr5g017550.1	calmodulin-related protein	-1.05	-0.12	0.95
medtr4g098530.1	leucine-rich repeat family protein	1.03	0.63	-0.94
medtr3g070490.1	very weakly similar to At2g40080	1.24	0.54	-3.38

In summary, the abundance of transcripts specifically regulated in mycorrhizal roots at high phosphate conditions was much lower compared to low phosphate conditions and these were mostly downregulated.

3.2.2.2. Transcriptional response of *M. truncatula* shoots colonized by *G. intraradices* at low and high phosphate conditions

Since all transcriptional responses of mycorrhizal roots to P_i are mediated by the plant shoot phosphate status, the differentially regulated transcripts in the shoots were analyzed according to their functional classification and direction of regulation. To compare this with the general response to phosphate, genes showing overlapping responses to AM symbiosis and P_i were considered as well for the functional classification.

The distribution of genes between the different functional categories shows more variation in response to the treatments compared to the root tissue (figure 28). At low phosphate conditions myc-responsive genes were mainly grouped into the categories of gene expression

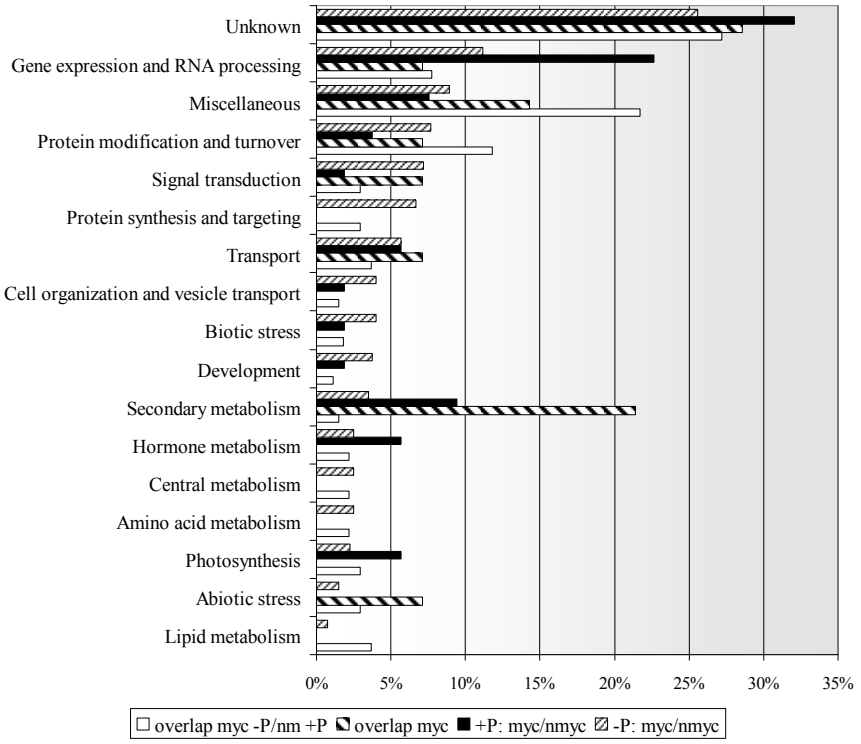

Figure 28: Molecular functional categories of mycorrhizal regulated genes in shoots at low and high phosphate conditions and of genes with overlapping regulation pattern between both myc treatments or low P_i myc and high P_i non-myc conditions. Shown is the percentage of genes given in figure 26 B (red, yellow circles and blue circle overlapping with red) grouped into the according functional categories by a protein sequence based MapMan annotation (Thimm *et al.*, 2004). Miscellaneous: all genes not sorted into one of the given functional category.

and RNA processing (1), protein modification and turnover (2) and signal transduction (3). Additionally, other transcripts regulated in mycorrhizal at low phosphate conditions belong to protein synthesis and targeting, transport, cell organization and vesicle transport, development, central metabolism, amino acid metabolism and photosynthesis, indicating an improved shoot metabolism and growth rate. The latter groups are shared with the high phosphate treatment of non-mycorrhizal plants. However, different sets of genes were specifically regulated at low P_i/myc and in case of the group of protein synthesis and targeting a higher abundance of different transcripts were regulated.

A subset of differentially regulated genes of mycorrhizal *M. truncatula* shoots at low phosphate conditions is given in table 5. The analysis revealed that 27 out 36 (75 %) of the transcripts encoding for putative transcription factors, were upregulated in mycorrhizal shoots. The putative TFs belong to different transcription factor families.

Table 5: A subset of ninety-three genes from *M. truncatula* which are specifically and significantly regulated in shoots during AM symbiosis at low phosphate conditions. (full table is attached on CD)

Mt3.5 ID	Putative annotation	-P myc/nm	+P myc/nm	nm +P/-P
Gene expression and RNA processing				
medtr4g074600.1	Zn-finger (DHHC)	2.28	0.41	-0.31
medtr5g055210.1	BAH domain-containing protein-like	2.17	-0.39	0.90
medtr5g007180.1	PHD finger family protein	2.09	0.44	-0.31
medtr4g007060.1	WRKY domain transcription factor family	1.97	0.60	0.64
medtr3g098420.1	Zn-finger(CCHC)	1.77	0.38	0.01
medtr2g087480.1	RNA polymerase beta' subunit-2	1.75	-0.34	0.71
medtr5g010020.1	MYB domain transcription factor family	1.72	0.28	0.74
medtr7g025010.1	Homeobox transcription factor family	1.66	-0.22	0.77
medtr2g008840.1	AtSR Transcription Factor family	1.55	0.06	0.04
medtr8g022820.1	AP2/EREBP transcription factor family	1.48	0.15	0.56
medtr4g051130.1	Chloroplast DNA-dependent RNA polymerase B subunit	1.46	0.18	0.38
medtr2g039620.1	Basic Helix-Loop-Helix family	1.42	0.83	-0.25
medtr3g117380.1	Zn-finger GATA transcription factor family	1.34	0.51	0.45
medtr4g034840.1	RNA polymerase beta' subunit-2	1.32	0.51	0.60
medtr5g017470.1	HSF,Heat-shock transcription factor family	1.31	0.52	-0.35
medtr5g029370.1	JUMONJI family	1.27	0.56	-0.05
medtr4g082580.1	WRKY domain transcription factor family	1.24	0.64	-0.36
medtr2g099500.1	Alfin-like	1.20	-0.01	0.33
medtr4g124260.1	Chromatin remodeling factor	1.16	0.07	0.24
medtr2g033880.1	Basic Helix-Loop-Helix family	1.14	0.15	0.44
medtr6g087590.1	CPP1-related transcription factor family	1.11	-0.08	0.11
medtr7g104320.1	zinc finger (AN1-like) family	1.10	-0.04	0.60
medtr4g116160.1	TIP1	1.10	0.34	0.50
medtr4g055440.1	Histone deacetylase 2a	1.10	0.08	0.43
medtr5g073480.1	moderately similar to At5g8430	1.10	0.14	0.35
medtr3g099180.1	CCAAT box binding factor family, HAP5	1.09	-0.20	0.64
medtr5g030130.2	zinc-binding family	1.02	0.52	0.23
medtr1g021520.1	G2-like transcription factor family, GARP	-1.04	-0.25	-0.96
medtr1g086590.1	MYB domain transcription factor family	-1.04	-0.83	0.45

Mt3.5 ID	Putative annotation	-P myc/nm	+P myc/nm	nm +P/-P
medtr3g108220.1	SWIM zinc finger family	-1.16	-0.33	-0.12
medtr8g013860.1	AP2/EREBP transcription factor family	-1.18	-0.32	-0.56
medtr4g063100.2	MYB domain transcription factor family	-1.19	-0.67	0.28
medtr2g096380.3	MYB domain transcription factor family	-1.20	-0.23	-0.36
medtr5g017290.1	Remorin family protein	-1.20	0.04	-0.11
medtr4g100450.1	AP2/EREBP transcription factor family	-1.27	-0.78	-0.03
medtr5g037080.1	MYB-related transcription factor family	-1.49	-0.80	-0.55
Protein synthesis and targeting				
medtr7g100720.1	ribosomal protein.eukaryotic.40S subunit.S23	2.62	0.16	0.99
medtr4g034730.1	ribosomal protein.prokaryotic.chloroplast.50S subunit.L2	2.44	-0.02	0.54
medtr4g074930.1	ribosomal RNA	2.23	0.35	0.41
medtr2g100410.1	ribosomal protein.eukaryotic.60S subunit.L28	2.20	0.14	0.80
medtr4g032660.1	ribosomal protein.prokaryotic.50S subunit.L18	2.20	-0.01	0.58
medtr4g014810.1	EF-1-alpha	2.09	0.08	0.58
medtr1g023590.1	ribosomal protein.eukaryotic.60S subunit.L13A	1.72	0.09	0.57
medtr7g059170.1	ribosomal protein.eukaryotic.60S subunit.L7	1.70	0.26	0.30
medtr4g062410.1	ribosomal protein.eukaryotic.60S subunit.L35	1.69	0.36	0.57
medtr1g040020.1	ribosomal protein.prokaryotic.chloroplast.50S subunit.L22	1.40	0.27	0.09
medtr5g097200.1	ribosomal protein.eukaryotic.40S subunit.S26	1.39	0.16	0.41
medtr2g086500.1	ribosomal protein.eukaryotic.60S subunit.L10A	1.37	-0.05	0.78
medtr3g035610.1	ribosomal protein.prokaryotic.chloroplast.30S subunit.S14	1.35	0.33	0.57
medtr5g006440.1	ribosomal protein.eukaryotic.40S subunit.S3A	1.29	0.25	0.47
medtr4g116410.1	ribosomal protein.eukaryotic.40S subunit.S11	1.27	-0.34	0.90
medtr4g034820.1	ribosomal protein.prokaryotic.chloroplast.50S subunit.L14	1.22	-0.18	0.50
ac235488_11.1	ribosomal protein.eukaryotic.40S subunit.SA	1.18	0.13	0.49
medtr7g108300.1	translation release factor	1.10	0.25	0.35
medtr7g078800.1	ribosomal protein.prokaryotic.chloroplast.50S subunit.L5	1.08	-0.15	0.77
medtr2g101550.1	ribosomal protein.prokaryotic.chloroplast.30S subunit.S11	1.08	0.12	0.97
medtr1g088450.1	ribosomal protein.eukaryotic.60S subunit.L22	1.06	-0.10	0.38
medtr4g034030.1	ribosomal protein.eukaryotic.40S subunit.S20	1.05	0.02	0.51
medtr7g055910.1	ribosomal protein.prokaryotic.chloroplast.30S subunit.S12	1.04	0.14	0.72
Amino acid metabolism				
medtr7g102120.1	Methionine adenosyltransferase	2.58	0.08	0.48
medtr2g009080.1	3-deoxy-7-phosphoheptulonate synthase	1.99	-0.14	0.44
medtr4g123810.1	Methionine adenosyltransferase	1.77	0.22	0.24
medtr4g079780.1	Ketol-acid reductoisomerase	1.46	-0.10	0.65
medtr7g087110.1	Cysteine synthase	1.15	0.38	0.34
medtr4g092620.1	L,L-diaminopimelate aminotransferase/ transaminase	1.08	-0.02	0.61
medtr5g075450.1	Trans-cinnamate 4-monooxygenase	1.05	-0.06	0.26
medtr4g124470.1	Lysine-ketoglutarate reductase	-1.01	-0.18	-0.13
medtr5g095470.1	Serine O-acetyltransferase	-1.10	-0.21	-0.95
Photosynthesis				
medtr5g080450.1	Rubisco activase	2.46	-0.18	0.42
medtr3g035600.1	PSI polypeptide subunit A2	1.82	0.16	0.68
medtr4g051150.1	PSI polypeptide subunit A2	1.79	-0.03	0.91
medtr4g034830.1	PSII polypeptide subunit K	1.67	-0.09	0.80
medtr4g034650.1	PSI polypeptide subunit A1	1.59	-0.05	0.78
medtr4g034660.1	PSII polypeptide subunit E	1.47	0.50	0.03
medtr7g117970.1	PS.lightreaction.unspecified.TEF	1.20	-0.10	0.57
medtr4g053840.1	NADH DH subunit J	1.15	0.22	0.51
medtr4g131180.1	Glyceraldehyde-3-phosphate dehydrogenase	-1.07	-0.39	0.41

Mt3.5 ID	Putative annotation	-P myc/nm	+P myc/nm	nm +P/-P
Biotic stress				
medtr2g042900.1	JAZ2	2.38	0.68	0.85
medtr2g037140.1	PR-protein	2.35	-0.24	0.26
medtr6g071550.1	PR-protein	1.70	-0.38	0.43
medtr6g074780.1	PR-protein	1.42	-0.24	0.04
medtr2g037150.1	PR-protein	1.36	-0.22	0.09
medtr7g055990.1	PR-protein	1.34	0.00	0.18
medtr6g072780.1	PR-protein	1.17	0.12	-0.31
medtr6g074810.1	PR-protein	1.12	-0.93	0.34
ac151738_32.1	PR-protein	1.09	-0.25	-0.08
medtr2g083830.1	PR-protein	1.04	-0.28	-0.50
medtr3g062140.1	PR-protein	1.03	-0.03	-0.45
medtr7g091190.1	PR-protein	1.02	0.22	0.24
medtr3g032340.1	PR-protein	1.01	0.02	-0.05
medtr3g027250.1	PR-protein	1.01	-0.10	-0.17
medtr5g013340.1	PR-protein	-1.00	-0.51	-0.62
medtr5g027910.1	PR-protein	-1.03	0.12	0.05

Surprisingly, a large amount of transcripts encoding various eukaryotic and prokaryotic ribosomal subunits, one elongation factor EF-1α and one translation release factor were upregulated 2-6 fold in shoots of phosphate starved plants upon colonization with *G. intraradices*. In contrast, only two eukaryotic and two prokaryotic ribosomal subunits were induced by P_i in non-mycorrhizal plants.

This expression pattern was also found for genes of the amino acid metabolism group. Interestingly, transcripts of four genes involved in the sulfur metabolism were regulated in this functional group. Of these transcripts, 3 were upregulated; two methionine adenosyltransferase encoding genes and a cysteine synthase encoding gene. The transcript encoding for the serine-O-acetyltransferase is downregulated. It is also worth to mention, that several genes involved in photosynthesis are responsive to AM symbiosis and do not exhibit overlapping expression patterns in response to phosphate alone.

A high number of PR protein encoding genes have been found to be upregulated by AM symbiosis at low phosphate and this induction was completely abolished by addition of phosphate. This indicates an enhanced plant pathogen resistance gained by the AM symbiosis specifically at low P_i. In comparison to the transcriptional changes in mycorrhizal shoots at low phosphate, very few myc responsive genes were regulated at high phosphate conditions. Most of the regulated transcripts encode genes involved in gene expression and RNA processing (1), secondary metabolism (2), hormone metabolism (3), transport (4) and photosynthesis (5) (table 6).

Table 6: A subset of genes from *M. truncatula* which are specifically and significantly regulated in shoots during AM symbiosis at high phosphate conditions. (full table is attached on CD)

Mt3.5 ID	Putative annotation	+P myc/nm	-P myc/nm	nm +P/-P
Gene expression and RNA processing				
medtr4g091490.1	MYB domain transcription factor family	1.52	-0.13	-0.59
medtr8g026960.1	Homeobox transcription factor family	1.2	-0.67	0.52
medtr4g070190.1	weakly similar to At2g21660	1.05	0.67	-0.88
medtr1g098460.1	AP2/EREBP transcription factor family	1	-1.38	-1.73
medtr5g021580.1	Constans-like zinc finger family	-1.07	-0.77	2.57
medtr5g014600.1	Basic Helix-Loop-Helix family	-1.11	0.11	1.03
medtr1g016170.1	GATA transcription factor family	-1.21	-0.2	1.26
medtr7g118260.1	ARR transcription factor family	-1.22	-0.96	2.36
medtr2g089310.1	Constans-like zinc finger family	-1.32	-0.22	2.99
medtr2g099010.1	Constans-like zinc finger family	-1.41	-0.77	4.11
medtr5g086350.1	PRLI-interacting factor K	-1.48	0.15	2.54
medtr7g118330.1	MYB-related transcription factor family	-1.54	-0.75	3
Secondary metabolism				
medtr7g010710.1	Terpene synthase	2.94	-1.09	-1.09
medtr7g014200.1	anthocyanin 5-aromatic acyltransferase	1.54	0.84	-0.43
medtr3g083130.1	NAD(P)H-dependent 6'-deoxychalcone synthase	1.13	0.92	-0.8
medtr7g046720.1	anthocyanidin 5,3-O-glucosyltransferase	1.03	-1.63	-2.47
ac235677_32.1	flavonol synthase/flavanone 3-hydroxylase	-1.5	-0.65	1.37
Hormone metabolism				
medtr4g133620.1	auxin-responsive protein	1.05	0.89	-1.48
medtr4g072890.1	auxin-responsive protein	-1.1	0.68	2.07
Transport				
medtr3g117090.1	phosphatidylinositol transporter	1.43	0.93	-0.05
medtr2g017590.1	Aquaporin	1.4	-0.69	-2.1
medtr1g108840.1	MATE efflux family protein	1.07	-0.05	-0.63
Photosynthesis				
medtr6g012080.1	LHC-II	-1.18	-0.05	4.04
medtr4g071880.3	fructose-bisphosphate aldolase	-1.42	-0.34	1.11

75 % of the transcripts encoding transcription factors were downregulated, in contrast to this most genes of the secondary metabolism were upregulated in response to AM symbiosis. A transcript encoding a terpene synthase was found to be the highest (7.7 fold) upregulated transcript in mycorrhizal shoots of *M. truncatula* at high phosphate conditions.

Interestingly, both regulated transcripts of the photosynthesis group, which were strongly induced by AM symbiosis at low phosphate, were downregulated in mycorrhizal shoots at high phosphate conditions.

3.2.2.3. Transcripts with overlapping differential regulation in roots and shoots of *M. truncatula* at high phosphate conditions

All detected responses to high phosphate nutrition in roots are systemically mediated by the shoot phosphate status, due to the used split-root system. To get further insights into the systemic plant responses to high phosphate conditions, it was investigated which genes show a general common response plant roots and shoots. Therefore, the differentially regulated transcripts at non-mycorrhizal conditions from roots and shoots were compared with each other and displayed in a Venn diagram (figure 29). 42 % and 27 % of the genes were regulated in roots and shots, respectively. This indicates that plant shoots exhibit a higher organ specific response to high phosphate nutrition. Among the genes with a common response to phosphate in both organs, 72 % were downregulated. A subset of genes encoding differentially regulated transcripts from the major functional groups or showing strong induction or repression is listed in table 7.

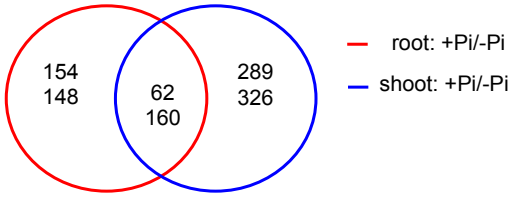

Figure 29: Venn diagram displaying differentially regulated genes of *M. truncatula* roots (red circle) and shoots (blue circle), which are responsive to high phosphate treatment. Venn diagram was created using MapMan.

A high number of transcripts, which were downregulated in both organs encode for several purple acid phosphatases, RNases, phosphate transporters, a SPX-containing protein as well as phospholipase D and genes involved in glycolipid synthesis (full table on CD), which are all known to be common molecular markers of P_i-starvation responses in plants (Wasaki *et al.*, 2003; Misson *et al.*, 2005; Hernandez *et al.*, 2007; Morcuende *et al.*, 2007).

Most other transcripts regulated in both organs encode transcription factors, transporters or are putatively involved in protein modification or turnover, e.g. MtPho2, which showed the same magnitude of induction in roots and shoots of non-mycorrhizal plants. Additionally, transcripts encoding proteins involved in the ubiquitin-proteasome pathway were highly induced. Several receptor-like kinases (RLKs) were downregulated by phosphate and one RLK, ac233661_3.1, was highly repressed, showing an 83-fold and 13-fold downregulation in *M. truncatula* roots and shoots, respectively. Notably, two RLKs with homology to MtSYMRK were systemically downregulated by addition of phosphate.

Table 7: A subset of significant differentially regulated genes from *M. truncatula* roots and shoots responsive to high phosphate nutrition showing a common response in both organs. (full table is attached on CD)

Mt3.5 ID	Putative annotation	root +P/-P	shoot +P/-P
Protein modification and turnover			
medtr5g016890.1	E3 ubiquitin ligase. F-Box	3.71	4.48
medtr4g119400.1	Protein kinase	2.15	2.00
medtr5g036360.1	Metalloprotease	1.88	1.90
medtr4g106690.1	E2 ubiquitin conjugating enzyme	1.64	1.70
medtr7g108820.1	E3 ubiquitin ligase. F-Box	1.42	1.44
medtr2g013650.1	MtPho2	1.22	1.40
medtr4g073240.1	E2 ubiquitin conjugating enzyme	1.16	1.78
medtr2g088570.1	E3 ubiquitin ligase. Ring-Box	1.15	1.39
medtr5g085300.1	Tyrosine protein phosphatase	-1.11	-2.92
medtr1g015020.1	moderately similar to MtSYMRK	-1.13	-2.14
medtr7g111060.1	Cysteine protease	-1.14	-1.19
medtr2g019630.3	Phospho-N-acetylmuramoyl-pentapeptide-transferase	-1.15	-1.03
medtr3g082840.1	Metalloprotease	-1.17	-1.04
medtr5g006160.1	Receptor-like protein kinase	-1.23	-1.41
medtr8g030690.1	moderately similar to MtSYMRK	-1.25	-1.59
ac233669_4.1	Receptor-like protein kinase	-1.25	-1.88
medtr1g017940.1	E3 ubiquitin ligase. F-Box	-1.38	-1.52
medtr1g085300.1	nearly identical to At3g62010	-1.41	-2.00
medtr1g019740.1	E3 ubiquitin ligase. F-Box	-1.72	-2.31
medtr7g077780.1	Receptor-like protein kinase	-1.77	-1.19
medtr3g077030.1	weakly similar to At3g48240	-2.27	-2.17
medtr3g061110.1	Subtilisin protease	-2.65	-2.50
medtr5g032960.1	weakly similar to At3g26510	-3.14	-1.99
ac233661_3.1	Receptor-like protein kinase	-6.37	-3.66
Gene expression and RNA processing			
medtr2g099010.1	Constans-like zinc finger family	3.57	4.11
medtr3g095240.1	ribonuclease P	1.97	1.10
medtr3g103960.1	C3H zinc finger family	1.77	2.29
medtr7g118330.1	MYB-related transcription factor family	1.74	3.01
medtr2g089310.1	Constans-like zinc finger family	1.68	2.99
medtr5g021580.1	Constans-like zinc finger family	1.38	2.57
medtr4g081690.1	DOF zinc finger family	1.32	2.26
medtr7g093030.1	G2-like transcription factor family, GARP	1.19	2.53
medtr7g118260.1	Psudo ARR transcription factor family	1.19	2.36
medtr5g017980.1	G2-like transcription factor family, GARP	1.12	1.44
medtr3g092580.1	pre-mRNA-splicing factor SF2	1.11	1.39
medtr7g017320.1	Basic Helix-Loop-Helix family	1.07	1.28
medtr7g086780.1	DOF zinc finger family	-1.04	-1.18
medtr2g099490.1	CCAAT box binding factor family, HAP2	-1.06	-1.17
medtr5g041010.1	Ribonuclease III	-1.14	-2.56
medtr8g076470.1	FHA transcription factor	-1.24	-1.37
medtr3g080000.1	Ribonuclease III	-1.39	-1.48
medtr1g043050.1	MYB domain transcription factor family	-1.66	-2.22
medtr2g093740.1	ARF, Auxin Response Factor family	-1.83	-1.59
medtr7g028160.1	TCP transcription factor family	-2.13	-2.25
medtr5g040940.1	Ribonuclease I	-2.75	-7.40

Mt3.5 ID	Putative annotation	root +P/-P	shoot +P/-P
Transport and metal handling			
medtr1g084050.1	Nicotianamine synthase	5.50	3.78
medtr1g016120.1	Zinc/iron permease	3.25	3.10
medtr3g082050.2	Zinc/iron permease	2.98	1.25
medtr5g012290.1	NRT1.1; nitrate transmembrane transporter	2.10	2.47
medtr2g006870.1	Potassium channel AKT2/3	1.44	1.01
medtr3g110660.1	Amino acid permease	1.01	1.05
medtr4g014540.1	Ferritin	-1.04	-1.50
medtr1g074930.1	Inorganic phosphate transporter	-1.32	-1.33
medtr5g026640.1	Sodium/solute symporter	-1.50	-1.86
medtr1g043200.1	PHT1; inorganic phosphate transporter	-1.57	-1.12
medtr4g083960.1	Inorganic phosphate transporter	-1.59	-3.79
medtr2g081930.1	highly similar to AtOCT4	-1.76	-2.23
medtr8g030600.1	PHT4;4, Sodium-dependent phosphate transporter	-1.78	-1.81
medtr1g043290.1	PHT1; inorganic phosphate transporter	-2.39	-2.50
ac235757_49.1	Multidrug resistance protein	-3.06	-5.34
ac235669_8.1	Multi antimicrobial extrusion protein	-4.24	-3.05
Phosphatases			
medtr4g082940.1	Calcineurin-like phosphoesterase family protein	-1.05	-1.75
medtr4g103520.1	Acid phosphatase	-1.15	-2.62
medtr8g063080.2	Calcineurin-like phosphoesterase family protein	-1.67	-1.79
ac146550_1005.1	Acid phosphatase	-1.71	-3.37
ac235757_50.1	Pyridoxal phosphate phosphatase	-3.54	-6.30
medtr6g013050.1	Acid phosphatase	-4.17	-3.93
Nitrogen metabolism			
medtr3g073180.1	NIA1; nitrate reductase	3.12	2.73

Interestingly, a transcript encoding a constans-like zinc finger protein, *Medtr2g099010.1*, is highly induced (12-17 fold) by phosphate in roots and shoots compared to all other regulated TF encoding transcripts. Furthermore, this gene is downregulated in mycorrhizal shoots at low but not at high phosphate conditions (table 6).

Beside the phosphate transporters mentioned above two transcripts encoding for uncharacterized transporter proteins with homologies to a multi drug resistance and a multi antimicrobial extrusion protein, were strongly repressed in both organs. Moreover, a nicotianamine synthase and two zinc/iron permeases were highly induced (14-45 fold) in response to phosphate in shoots and roots of the plant, indicating an induced uptake of metal ions in response to phosphate. It is worth to mention, that another transcript encoding a nicotianamine synthase, *Medtr2g034240.1*, is specifically induced in mycorrhizal roots a high phosphate conditions (3 fold; LFC = 1.69) and is not detectable at low P_i or non-mycorrhizal conditions.

3.3. Identification of *Medicago truncatula* microRNAs involved in arbuscular mycorrhizal symbiosis

As described in the introduction, there are several indications that micro RNAs play a role during AM symbiosis formation. However, so far only conserved miRNA have been investigated, upon their regulation in plant shoots or roots during AM symbiosis. Specific, unknown miRNA might be involved the symbiosis process, therefore the goal of this part of the thesis, is to identify miRNA which are related to transcriptional reprogramming of plant cells during arbuscular mycorrhizal symbiosis.

3.3.1. Construction of small RNA cDNA libraries of colonized and non-colonized *M. truncatula* roots

High throughput sequencing with Illumina technology was used to detect and profile miRNAs of *M. truncatula* root tissue. Two small RNA libraries were prepared from either mycorrhizal (myc) or non-mycorrhizal (nm) roots of *M. truncatula* by purification and cloning a small RNA fraction of 15-30 nucleotides (nt) from total RNA. The quality of the RNA was confirmed via Bioanalyzer measurements (RIN = 1,6-1,7). The libraries were sequenced by using the SBS technique. In total more than 16 million reads were obtained and more than 97% of all reads were of the appropriate sizes, i.e. 15-31 nt. Within the small RNA libraries, the 21 nt and 24 nt molecules were the most abundant forms and the 24 nt small RNAs were more diverse than the 21 nt class (figure 30).

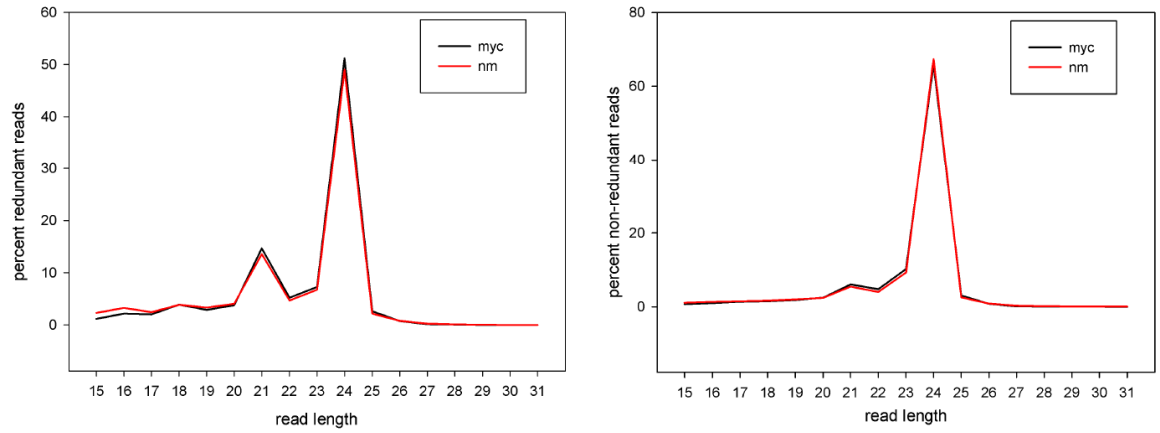

Figure 30: Read length distribution of the small RNA sequences obtained after deep sequencing. The distribution of redundant and non-redundant reads is comparable between mycorrhizal plant roots (black) and non-mycorrhizal plant roots (red).

3.3.2. High-throughput sequencing of the small RNA libraries

3.3.2.1. Mapping of small RNAs to the M. truncatula genome

The 15-31 nt small RNAs were trimmed and mapped to the *M. truncatula* genome version 2.0 (mt2.0); version 3.0 (mt3.0), other annotated *M. truncatula* sequences as well as to available *G. intraradices* sequences (The Glomus consortium, unpublished).

The mapping revealed that 69% of redundant sr-myc and 72% of the sr-nm could be mapped with 100% identity to the *M. truncatula* genome version mt3.0 (table 8). Of the sr-myc reads, 2.1% could be mapped with 100% identity to *G. intraradices* sequences. 63% of non-redundant reads were assigned to so far uncharacterized regions of the mt3.0 genome, supporting the assumption that most small RNAs originate from intergenic regions. An annotation of redundant and non-redundant small RNA reads is shown in figure 31.

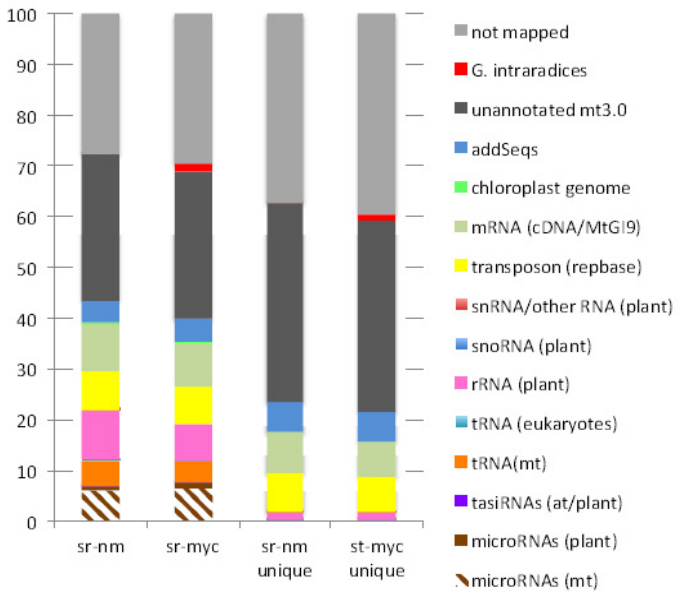

Figure 31: Annotation of redundant and non-redundant small RNA reads. Small RNA (sr) sequences mapped to relevant functional classes, which are distinct from bottom to top. AddSeqs: additional mt3 (Illumina) sequences. Figure published in (Devers *et al.*, 2011).

Table 8: Statistics of the Illumina sequencing of the two small RNA libraries. nm: non-mycorrhizal roots, myc: mycorrhizal roots. (Devers *et al.*, 2011)

	sr-nm	**sr-myc**
raw reads	8620161	8359230
reads of appropriate size	8350029	8187981
unique reads of appropriate size	3798457	3878418
% total reads mapping to *M. truncatula* mt3.0 (100% identity)	72.28	69.14
% total reads mapping to *G. intraradices* (100% identity)	0.05	1.57

3.3.2.2. Analysis of known miRNAs annotated at miRBase

In order to investigate the expression of known miRNAs in mycorrhizal and non-mycorrhizal roots, the small RNA libraries were scanned for annotated miRNAs. These miRNAs were identified by 100% matches of the read sequences to the mature sequences of the 375 *M. truncatula* miRNAs currently annotated at the miRBase (release 16) database (Griffiths-Jones *et al.*, 2008). Thereby, 162 mature miRNAs could be found (appendix table 10), representing 43.2% of the currently known *M. truncatula* miRNAs.

Next, it was analyzed if reads matching the annotated miRNA* or precursor could be found. Surprisingly, in some cases reads matching the miRBase-annotated precursor were found, but reads matching the annotated mature miRNA sequences with 100% identity were absent. This indicates that some miRNAs can occur as different isoforms or siblings (Vazquez *et al.*, 2008; Zhang *et al.*, 2010), i.e. miRNAs originating from the same primary transcript with distinct mature forms. MiRNA isoforms often contain a small sequence shift or additional nucleotides (Ebhardt *et al.*, 2010), whereas miRNA siblings are non-overlapping in comparison to the originally annotated mature or star miRNAs (Zhang *et al.*, 2010). 17 isoforms of miRNAs whose mature sequence was missing were detected (miR169e/h/I/n/o, miR393b, miR2594a/b, miR2611, miR2674, miR2678, miR2679c miR2680a-e, respectively). In addition, for two miRNAs, reads of the annotated star sequence but no reads matching the mature sequence were found (miR171f, miR398a). Taken this into account, in total 181 known miRNAs were either found as mature, star or isoform (isomiR) sequence in mycorrhizal and non-mycorrhizal *M. truncatula* roots (appendix table 10).

To investigate the specific abundance of annotated mature miRNAs, the corresponding miRNA* and found isomiRs, the read counts of the corresponding sequences in the small RNA libraries were calculated. Interestingly, for 11 miRNAs, the isoforms of the mature strand were found to have a higher abundance than the sequence annotated as mature miRNA sequence at miRBase (miR156, miR166b/c/f, miR1509a, miR1519b, miR2597, miR2610a/b,

miR2620, miR2645). In addition, miRNA* sequences of several legume specific miRNAs like miR1507*, miR2086*, miR2089* and miR2118* (Szittya *et al.*, 2008; Jagadeeswaran *et al.*, 2009) showed a high abundance. Additionally, the star strand for 8 miRNAs (miR160b/e, miR169d/l/m, miR369a, miR2089, miR2118) and a different isoform of 19 miRNA star strands (miR171c, miR2088a, miR2592a-g/i-j/o-s, miR2595, miR2612a, b) showed a higher abundance than the corresponding mature strand. 4 miRNAs showed a similar abundance between the mature and star strand (miR172, miR399c/j/k). Hence, 48% of all annotated *M. truncatula* miRNAs could be identified in the two small RNA libraries. Notably, a high proportion of these miRNA seemed to occur in different isoforms than the annotated mature miRNA sequence.

3.3.3. Prediction of novel *M. truncatula* miRNAs using the miRDeep prediction pipeline

In order to find novel *M. truncatula* miRNAs, the 15-31 nt reads of the small RNA libraries were subjected to a miRNA prediction pipeline developed by Dr. Patrick May (Pant *et al.*, 2009, Devers *et al.*, 2011). Candidate miRNAs were predicted with the miRDeep algorithm (Friedlaender *et al.*, 2008), which was adapted to plant miRNA-precursor sequences (Pant *et al.*, 2009; Devers *et al.*, 2011). Applying the plant miRDeep program to the small RNA datasets, revealed in the prediction of 515 novel miRNA candidates of 20-25 nt length.
To further validate these 515 miRNA candidates, criteria for plant miRNA annotation were included according to (Meyers *et al.*, 2008). All 515 predicted miRNA candidates are produced from a single-stranded stem-loop precursor, which is required for miRNA prediction within the miRDeep pipeline. For 69 candidate miRNAs the corresponding miRNA* sequence was present in the deep sequencing data, hence these candidates fulfill the primary criterion for miRNA annotation. Additional 369 out of 515 miRNA candidates satisfy at least one of the ancillary criteria including conservation amongst one or more plant species, clustering into miRNA families and confirmed target by degradome analysis (Devers *et al.*, 2011). However, criteria for miRNA annotation from deep sequencing data have been updated recently, and include now the requirement that high confident miRNAs have multiple cloned nucleotide reads with relatively fixed 5´ends at both arms of the precursor sequence and the possibility to identify the miRNA/miRNA* duplex pair (Berezikov *et al.*, 2010). Taking these criteria into account, 243 of the miRNA candidates were annotated as miRNAs

at miRBase (Griffiths-Jones *et al.*, 2008). All information about the novel miRBase annotated miRNAs and miRNA candidates found in this study are freely accessible on the following website (http://mirmyc.mpimp-golm.mpg.de).

Of the novel 234 miRNAs deposited at miRBase, 74 are novel conserved miRNAs (less than three mismatches to known family members) and 169 miRNAs belong to 95 novel plant miRNA families. Of the 169 novel miRNAs, 74 showed homologous sequences (less than three mismatches) in one the following organisms: *Arabidopsis thaliana*, *Zea mays*, *Lotus japonicus*, *Glycine max* or *Populus trichocarpa*, indicating that 44% of novel miRNAs are also conserved within other plants.

3.3.3.1. Expression profiling of miRNAs by read count analysis

In order to investigate a putative role of novel and conserved miRNAs in the mycorrhizal symbiosis, it was searched for miRNAs with induced or decreased expression in mycorrhizal roots when compared to non-mycorrhizal roots. To identify these differentially expressed miRNAs, the abundances of miRNAs were calculated by comparing the normalized numbers of reads in both libraries. Using a log2-fold cutoff of 0.7, 20 distinct miRNA sequences showed a differential abundance between mycorrhizal and non- mycorrhizal roots (table 9).

MiR5229a/b showed the strongest elevated abundance levels (log2-fold change 9.7) in mycorrhizal roots as compared to non-mycorrhizal roots. Interestingly, it was found that miRNA star sequences are regulated in mycorrhizal roots. MiR169d*/l*/m*/e.2* was more abundant as the annotated mature miRNA sequence, and in addition 4-fold higher abundant in mycorrhizal roots. This is of particular interest because the miR169d*/l*/m*/e.2* target identified by degradome analyses (Devers *et al.* 2011) is *MtBcp1*, which itself is specifically transcribed and located in arbuscule containing cells (Pumplin and Harrison, 2009). In addition miR160f* was not detected in non-mycorrhizal roots but was clearly abundant in mycorrhizal roots. In summary, 20 miRNA with significantly ($\chi 2$ test; $p \leq 0.05$) changed expression in mycorrhizal roots could be identified, indicating a role for these miRNA in mycorrhizal symbiosis. The secondary structures of the newly predicted precursor sequences are presented in the Appendix (figure 44).

Table 9: Differentially expressed miRNAs

miRNA identifier	sequence	length	rpm[a] myc	rpm[a] nm	LFC[b]	target gene family
miR5229a,b	TTAGCAGGAAGAGTGACTATG	21	98.9	0	9.7	Haem peroxidase[p]
						HSP20-like chaperon[p]
miR5206	ATGGGATCCTGTTGGTGGGTTAC	23	3.7	0.1	4.9	Hypothetical protein[c]
miR160f*	GCGTGAAGGGAGTCAAGCAGG	21	3.4	0	4.8	Hypothetical protein[p]
						Putative periplasmic lipoprotein[p]
miR5204	GCTGGAAGGTTTTGTAGGAAC	21	36.3	1.7	4.4	Heavy metal transport protein[p]
						Zinc finger transcription factor[p]
						Nucleotide-binding protein[p]
						RNA-binding protein[p]
						Protein kinase-like protein[p]
miR169d, l	AAGCCAAGGATGACTTGCCGG	21	6.4	0.4	4.1	CCAAT transcription factor[c,p]
						Hypothetical protein[c,p]
						MMS sensitivity-related protein[c,p]
miR169d*,e.2*,l*,m*	GGCAGGTCATCCTTCGGCTATA	22	20.9	1.3	4	Blue copper binding protein[c]
						Glycoside hydrolase[p]
						Serine/threonine protein kinase[p]
miR160c	TGCCTGGCTCCCTGAATGCCA	21	14.4	2.8	2.4	Auxin response factor[c,p]
						Hypothetical protein[c]
miR171h	CGAGCCGAATCAATATCACTC	21	345.6	153.9	1.1	Pentatricopeptide repeat protein[c,p]
						GRAS transcription factor [c,p]
						Nodulation-signaling pathway 2[c,p] protein
						E2 Ubiquitin-conjugating enzyme [p]
						Plant lipid transfer protein[p]
						Protein kinase[p]
miR167	TGAAGCTGCCAGCATGATCTA	21	869.5	401	1.1	Auxin response factors[c]
						WD40-like protein[c]
						Zinc finger transcription factor[p]
						Sodium/hydrogen exchanger[p]
						Protein kinase[p]
miR5244	TATCTCATGAAGATTGTTGGT	21	22.8	11.1	1	Leucine-rich repeat protein[p]
miR5232	TACATGTCGCTCTCACCTGAA	21	110.2	54.7	1	Glycoside hydrolase[c]
						Type IIB calcium ATPase[c,p]
						Protein kinase[p]
miR5281b-f	TCTTATAAATAGGACCGGAGGGAG	24	28.58	14.73	0.9	Alcohol dehydrogenase superfamily[p]
						TIR; Disease resistance protein [p]
						COG complex component[p]
						H+-transporting two-sector ATPase[p]
						Zinc finger transcription factor[p]
						Putative fructose-1,6-bisphosphatase[p]
						Cyclin-like F-box protein[p]
						Nodule-specific cysteine-rich peptide[p]
miR5250	TGAGAATGTTAGATACGGAAC	21	223	123.1	0.8	ATP binding protein[c]
						Glycosyl transferase[p]
miR2086	GACATGAATGCAGAACTGGAA	21	2167.9	1204	0.8	Biotin-binding site protein[c]
						Argonaute and Dicer protein[p]
						Antihaemostatic protein[p]
miR166b.2,c.2,f.2	TCTCGGACCAGGCTTCATTCC	21	5653.9	3158.8	0.8	HD-Zip transcription factor[c,p]
						Sugar transporter superfamily[p]
miR396b*	GTTCAATAAAGCTGTGGGAAG	21	124.08	73.64	0.8	FAD/NAD(P)-binding protein[p]
						Pentatricopeptide repeat protein[p]
						Leucine-rich repeat protein[p]
						DNA methylase[p]
miR5213	TACGTGTGTCTTCACCTCTGAA	22	1038.96	625.99	0.7	TIR; Disease resistance protein[c,p]
miR162	TCGATAAACCTCTGCATCCAG	21	59.72	36.05	0.7001	Argonaute and Dicer protein[c,p]
						FAD/NAD(P)-binding protein[p]
						Pentatricopeptide repeat protein[p]
						Ribonuclease[p]

miRNA identifier	sequence	length	rpm[a] myc	rpm[a] nm	LFC[b]	target gene family
miR4414a	AGCTGCTGACTCGTTGGTTCA	21	124.69	206.23	-0.8	Nuclear protein SET[p]
miR5285a-c	TGGGACTTTGGGTAGAATTAGGCG	24	12.09	25.03	-1.1	Zinc finger transcription factor[p]
						Sulfotransferase[p]
						Histone-like protein[p]
						XYPPX repeat protein[p]
						TIR; Disease resistance protein[p]
						Proteinase inhibitor[p]
						Beta-lactamase-like[p]
						reverse transcriptase-like protein[p]
						Methyltransferase[p]
						Bacteriophytochrome[p]
						Proteasome subunit[p]
						GTP-binding protein[p]

[a]reads per million

[b] p value ≤ 0.05; χ^2 test together with Benjamini-Hochberg P value correction

[c]target cleavage confirmed experimentally by degradome analysis (Devers *et al.*, 2011)

[p]psRNAtarget predicted target (Dai and Zhao, 2011), expectation range ≤ 3

3.3.4. Confirmation of the expression profile and localization of arbuscular mycorrhizal regulated miRNAs

3.3.4.1. Quantitative real time PCR analysis of miRNAs

To confirm the regulation of selected miRNAs, quantitative real time (qRT) PCR analysis was carried out. In addition to mycorrhizal roots, the mature miRNA abundance in nodulated roots fertilized with either 20 µM or 1 mM phosphate and in roots grown under full nutrition (1 mM phosphate and 5 mM nitrate) was measured. This allows first insight into the specificity of the miRNA regulation with regard to nodule symbiosis and nutrient availability. The mature miRNA abundance was measured by stem-loop qRT-PCR (Chen *et al.*, 2005) (figure 32).

For expression analysis, miR5229a/b and miR5204 was selected because of their strongly elevated levels in mycorrhizal roots. In addition, miR160f* was chosen for expression analysis, because this miRNA was undetectable in non-mycorrhizal roots. Also miR160c was selected due to the elevated levels of mature miRNAs in mycorrhizal roots and additionally because it belongs to the same family as the mycorrhizal root specific new miR160f*.

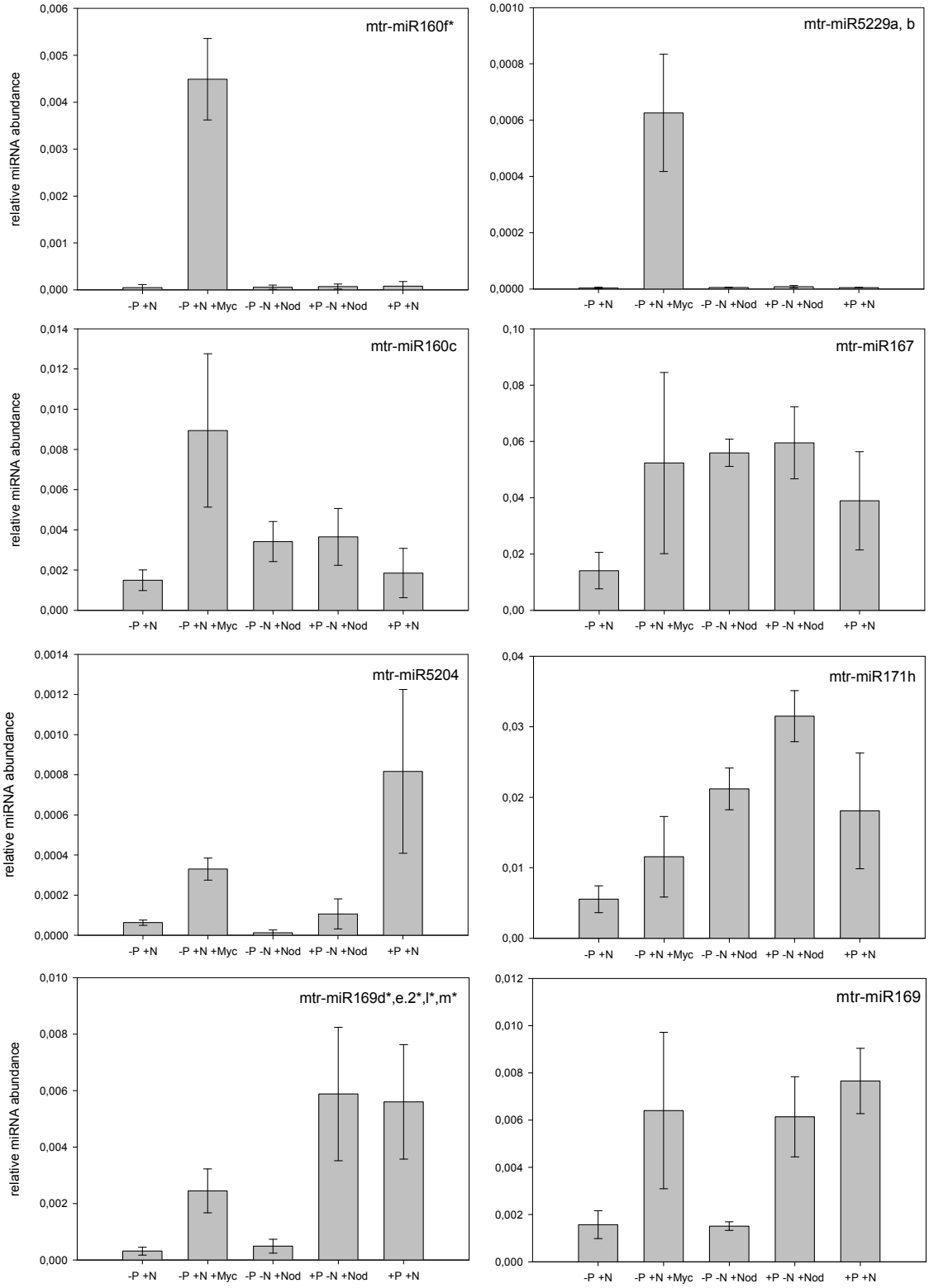

Figure 32: Relative abundance of AM symbiosis induced mature miRNAs. The following conditions were applied and roots were harvested after 3 wpi: -P: 20 µM phosphate fertilization; +P: 1 mM phosphate fertilization, -N: 0 µM nitrate, +N: 5 mM nitrate; myc: mycorrhizal roots; nod: nodulated by *Sinorhizobium meliloti*. If not indicated, plants were not inoculated with either symbiont. Normalization was carried out against a reference gene index (*MtPdf2*; *MtEf1-α*). Primers were designed to measure specific miRNAs, if possible (indicated by small letters). If primers bind to more than one mature or star miRNA sequence, small letters are absent (SD; n = 4). (Figure published in Devers *et al.*, 2011).

As expected, the qRT-PCR confirmed the induction in mycorrhizal roots as compared to non-mycorrhizal roots. Two of the measured miRNA candidates (miR160f* and miR5229a/b) were only detectable in mycorrhizal roots. MiR160c showed an increased abundance in mycorrhizal roots as compared to all other treatments measured.

MiR167 was induced in mycorrhizal roots as compared to non-mycorrhizal roots under low phosphate, but showed increased expression in nodulated roots and under full nutrition. The miR5204 highly accumulated in mycorrhizal roots according to the read count analysis, which could be confirmed by qRT-PCR. However, a further increased expression under full nutrition was found, indicating phosphate to be a positive regulator of miR5204. MiR171h exhibited strongest expression in nodulated roots. MiR169 and miR169d*/e.2*/l*/m* showed a clear positive response to increased phosphate nutrition. Comparable low expression levels of this miRNA in nodulated roots grown at high phosphate might be due to the root nodules as strong phosphate sinks.

In summary, the expression profiling showed miRNAs specifically accumulating in mycorrhizal roots as well as miRNAs induced in mycorrhizal roots but also regulated by other stimuli. The expression of miR5206 could not be confirmed by stem-loop qRT-PCR due to no detection of the miRNA.

3.3.4.2. Localization of mature and star miRNAs by *in situ* hybridization

In order to get information about the spatial accumulation of mature and star miRNAs in mycorrhizal roots, sequences which were proven to show elevated levels in mycorrhizal roots were analyzed by *in situ* hybridization. As negative control a DIG-labeled scramble probe was used, which is a random 21 nt locked nucleic acid (LNA) enhanced DNA oligonucleotide not binding to any known plant transcript.

After staining the hybridized root cross-sections witch NBT/BCIP, specific signals were observed for each of the six LNA probes (figure 33), whereas no signals were observed after hybridization to a scramble probe.

Mature miR5229a/b strongly accumulated in arbuscule containing cells in the root cortex. However, the signal strength varied between distinct arbuscule containing cells indicating that miR5229a/b is involved in specific stages of arbuscule development. The second mycorrhizal root specific miRNA, miR160f*, strongly accumulated in the central cylinder and also in arbuscule containing cells in the cortex of the root.

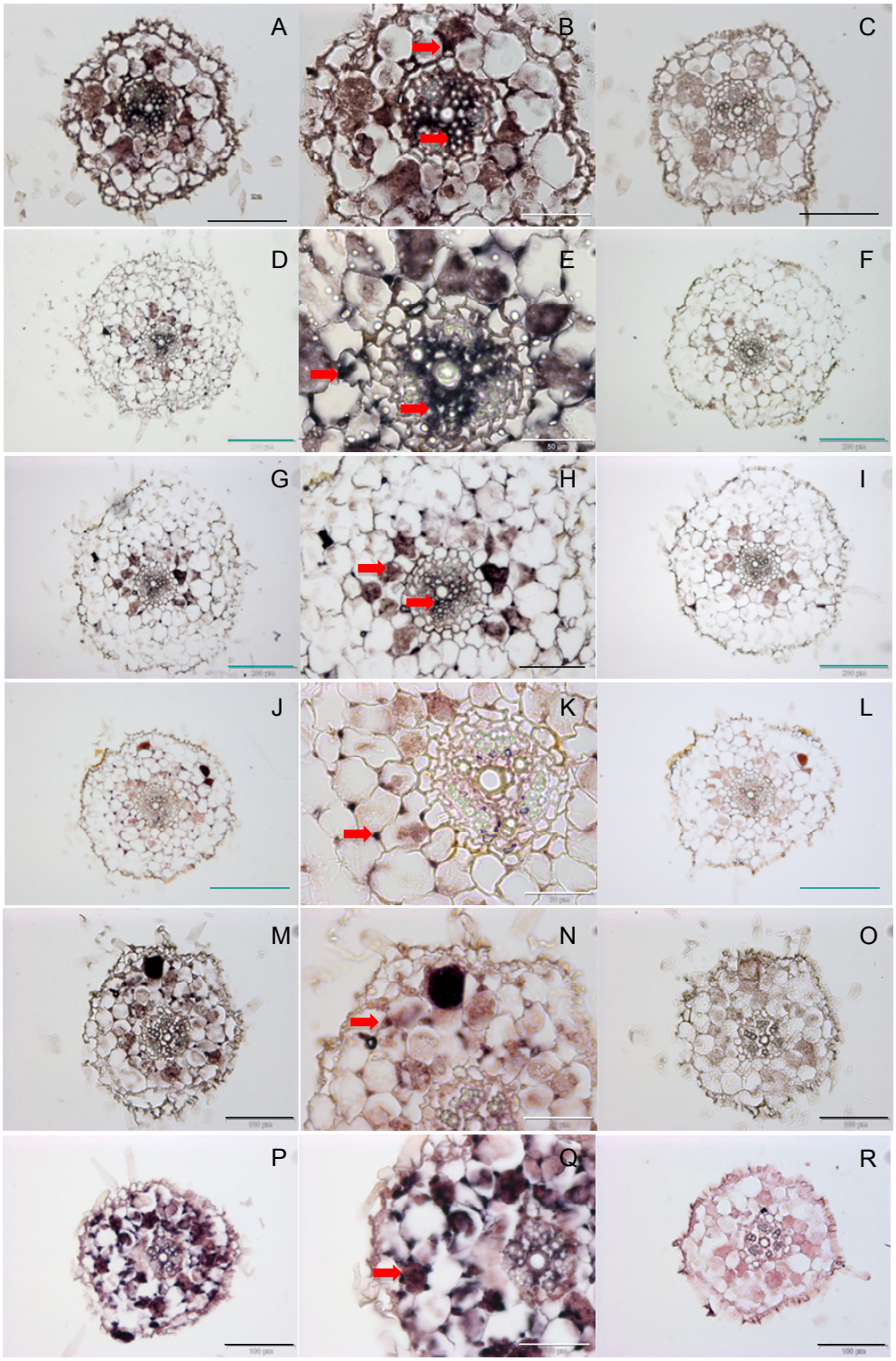

Figure 33: Tissue specific expression of miRNAs in mycorrhizal roots. Cross sections of mycorrhizal *M. truncatula* roots were hybridized to labeled locked nucleic acid (LNA) probes complementary to selected miRNA or miRNA*. For each LNA probe hybridization, adjacent sections were used for scramble probe hybridization. The following miRNA or miRNA* were analyzed: namely mtr-miR160c (A), detail in (B), scramble probe (C), mtr-miR160f* (D), detail in (E), scramble probe (F), mtr-miR169 (G), detail in (H), scramble probe (I), mtr-miR169d*/l*/m*/e.2* (J), detail in (K), scramble probe (L), mtr-miR5204 (M), detail in (N), scramble probe (O), mtr-miR5229a/b (P), detail in (Q), scramble probe (R). White scale bars represent 50 µm, black scale bars represent 100 µm, and cyan scale bars represent 200 µm. Red arrows represent examples of distinct signals indicating miRNA accumulation. (Figure published in Devers *et al.*, 2011).

A similar accumulation pattern was observed for miR160c, supporting the fact that both molecules belong to the same miRNA family. MiR5204, which was also regulated by phosphate, accumulated in arbuscule containing cells and also strongly around fungal hyphae, the latter visible as signals in the intracellular space surrounding cortex cells. Interestingly, not all arbuscule-containing cells showed accumulation of miR5204.

The miR169d*/l*/m*/e.2* probes revealed no signals in arbuscule containing cells but seemed to accumulate around intercellular fungal hyphae. As expected, the miR169 probe revealed a similar accumulation pattern. Strong hybridization signals were detected in the central cylinder and in addition around fungal hyphae in the intercellular space.

3.3.4.3. Sequence and expression analysis of the newly discovered miR171 family member miRNA171h

As mentioned above, miR171h exhibited strongest expression in nodulated roots (chapter 3.3.4.1.). Interestingly, the transcript of MtNsp2, encoding a GRAS transcription factor (TF) necessary for nodulation symbiosis signaling (Kalo *et al.*, 2005), was identified to be a target of this particular miRNA (Devers *et al.*, 2011). MiR171h is so far the only member of the miRNA 171 family which cleaves *MtNsp2*, together with another GRAS TF and a pentatricopeptide repeat protein (Devers *et al.*, 2011).

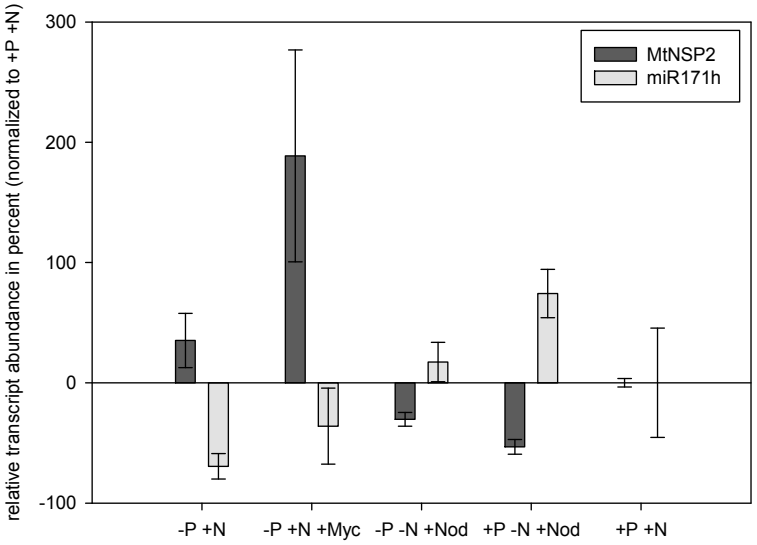

Figure 34: Comparison between the expression pattern of *MtNsp2* and mature miR171h. Relative transcript and miRNA abundance was measured via qRT-PCR, normalized to the full nutrition condition (+P +N) and is given in percent. Conditions are as described in figure 32 (SD; n = 4).

To investigate the correlation of *MtNsp2* and miR171h accumulation, the relative expression of *MtNsp2* was determined via qRT-PCR and compared with the relative abundance of mature miR171h (figure 34). This revealed that the miRNA and its target exhibit an antagonistic expression pattern in all tested conditions, suggesting that the transcript abundance of *MtNsp2* is regulated on a posttranscriptional level in the whole root tissue. However, during AM symbiosis the direct relationship is distorted towards a higher expression of *MtNsp2* indicating that transcription of this gene is induced in mycorrhizal root tissue. This was also observed by the analysis of the microarrays (chapter 3.2.2.1., table 3).

```
Majority        TGATTGAGCCGTGCCAATATCXXXX
                          10        20
mtr-miR171      TGATTGAGTCGTGCCAATATC
mtr-miR171b     TGATTGAGCCGCGTCAATATC
mtr-miR171c     TGATTGAGCCGTGCCAATATT
mtr-miR171d     TGATTGAGCCGTGCCAATATC
mtr-miR171e     AGATTGAGCCGCGCCAATATC
mtr-miR171f     - - - TTGAGCCGTGCCAATATCACG
mtr-miR171g     TGATTGAGCCGTGCCAATATC
mtr-miR171h     - - - - CGAGCCGAATCAATATCACTC
```

Figure 35: Alignment of all mature miRNA sequences from the miR171 family. Alignment was done using ClustalW.

To examine the cause of this target switch of miR171h, a sequence alignment of all known *M. truncatula* miR171 mature sequences was analyzed (figure 35). This showed that miR171a-e and miR171g posses nearly identical mature sequences with nucleotide exchanges in only three positions (nt 1, 12 and 21). Interestingly, miR171h displays a sequence shift of 4 nucleotides towards the 3' end of the miRNA in comparison to the above mentioned miRNAs, suggesting that this shift led to the target switch. Remarkably, target prediction with psRNATarget (Dai and Zhao, 2011) suggested that miR171f potentially inhibits *MtNsp2* on a translational level. MiR171f posses a 3 nt sequence shift, which allows the binding to *MtNsp2*. But this leads to a bulge in the target/miRNA pair, which possibly prevents target cleavage. However, the mature miR171f sequence was missing in the deep sequencing dataset, with only its star strand present at low abundance (table 10 appendix). Other miRNA 171 family members found were miR171a, b and e. From these three miRNAs, miR171a has the highest abundance. Surprisingly, MIR171e produces a miRNA* sibling, miR171e.2*, which predominantly accumulates in contrast to the mature sequence. Several targets can be predicted for miR171e.2*, the best score could be found for Medtr3g006060, which encodes a protein containing a NB-ARC domain. Contrary to miR171h, all other detected miRNA171 family members are not differentially expressed in myc and non-myc roots. These findings indicate a diverse precursor processing of this miRNA family.

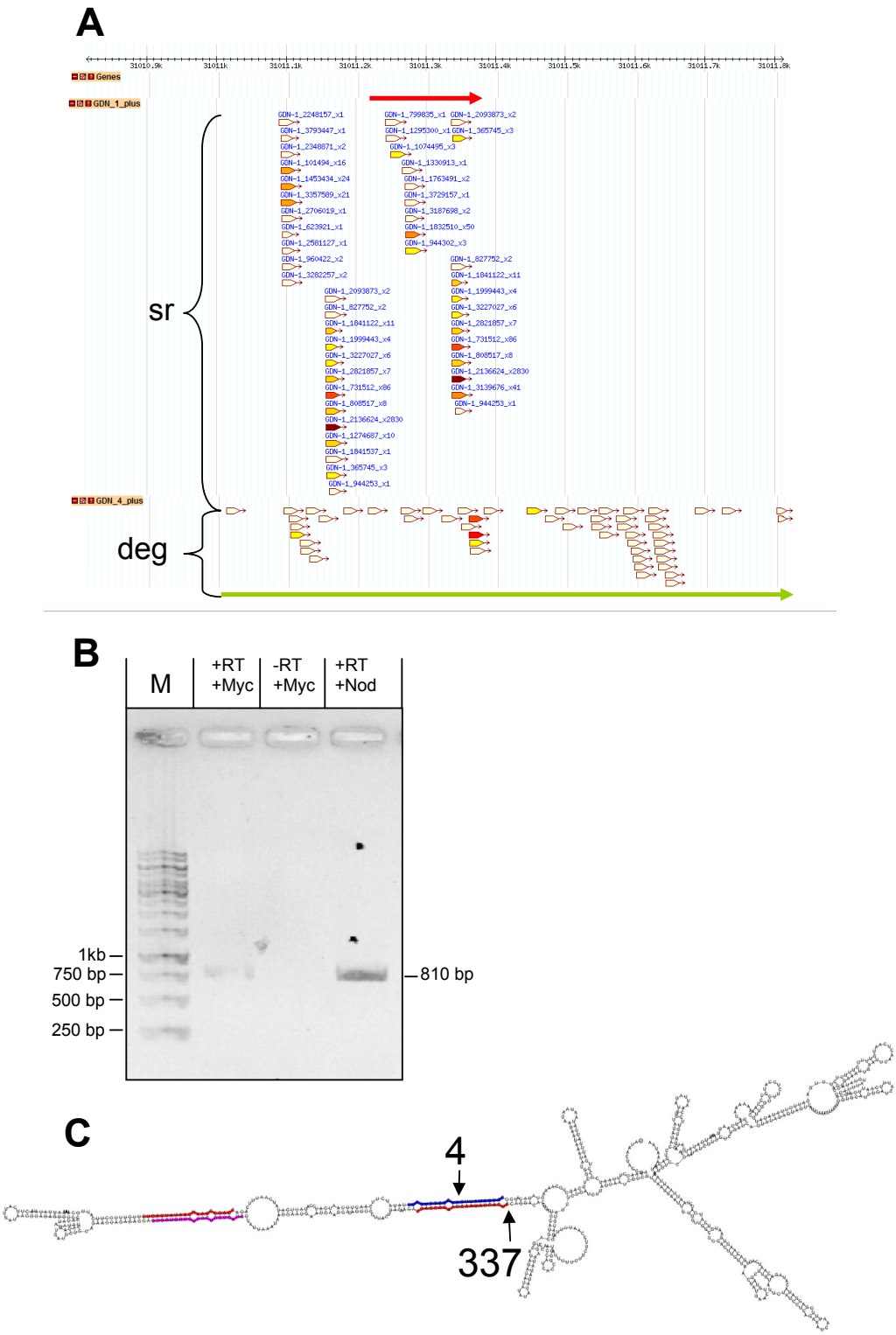

Figure 36: Analysis of the MIR171h genomic locus and primary transcript. A visualization of the genomic locus of MIR171h (+/- approx.400bp) using a genome browser of the Mt3.0 genome version. Upper short green arrow corresponds to length and position of pre-miR171h as predicted by miRDeep. Sr indicates all small RNAs of mycorrhizal roots which mapped in sense direction to this genomic region. Deg indicates transcripts (degradome tags) obtained from mycorrhizal roots which mapped in sense direction to the same genomic region. In both cases the abundance is indicated by a color gradient from light yellow (low abundant) to deep red (highly abundant). Lower long green arrow corresponds to the putative primary transcript of MIR171h. **B** Agarose gel analysis of RT-PCR products confirming the presence of a long primary transcript in mycorrhizal and nodulated roots. M = 1kb marker; –RT = control RT reaction without reverse transcriptase. **C** Secondary structure of the primary transcript of MIR171h depicting sites of miRNA generation (color) as well as Dicer and RISC cleavage sites (arrows with 337 tags and 4 tags, respectively). Red = miR171h (2830 reads); pink = miR171h.1* (50 reads); blue = miR171h.2* (24 reads).

In order to find the origin of the sequence shift of miR171h, the structure of the MIR171 gene was analyzed by mapping of small RNA reads and available degradome tags (Devers *et al.*, 2011) in sense direction to the genomic locus of the predicted precursor extended to 500 bp in both directions (figure 36 A). Interestingly, a second non-predicted miR171 locus with an identical mature sequence but different star sequence is located upstream of the predicted miR171h precursor. Mapping of the degradome tags to this genomic region reveals an approximately 800 bp long sequence which seems to be transcribed.

To confirm the presence of the long primary transcript an RT-PCR using cDNA from mycorrhizal and nodulated roots and primers flanking the degradome tagged region was carried out (figure 36 B). A specific band of the expected size using both cDNAs confirmed the presence of the long primary transcript and indicates that no introns are present in the 810 bp long region. The secondary structure of the miR171h primary transcript was predicted via RNAfold (http://srna-tools.cmp.uea.ac.uk/plant/cgi-bin/srna-tools.cgi) and is given in figure 36 C. The most abundant small RNA reads, miR171h, miR171h.1* and miR171h.2*, are annotated in the figure. The two miR171h loci are located in series on a long single stem-loop rather than two small stem-loops and a unique degradome tag with the highest abundance confirmed the canonical excision of the precursor from the primary transcript. Interestingly, another unique degradome tag confirmed the cleavage of the primary transcript at the miR171h.2* producing site between the 10^{th} and 11^{th} nucleotide of the corresponding mature miR171h, indicating a self regulation of the primary transcript abundance and miRNA biogenesis.

3.3.5. Functional analysis of miR5204 and miR5229a, b in *M. truncatula*

To get first insights into the function of the newly discovered miRNAs during AM symbiosis, two miRNAs, miR5204 and miR5229a, were chosen for further molecular analysis due to a high accumulation in mycorrhizal roots.

3.3.5.1. Molecular analysis of the mycorrhizal phenotype in miR5204 over-expressing roots

MiR5204 was overexpressed in transgenic *M. truncatula* roots by a 35S promoter-driven expression of the predicted precursor sequence, pre-miR5204, using the construct pKc1054oexD (see chapter 2.2.1.2.). As expression control pKmRFPD was used for root

transformation. Eight pKc1054oexD and four pKmRFPD root transformed plants were transferred to a sand/vermiculite mixture, inoculated with *G. intraradices* and grown at low P_i (20 µM) conditions.

After 21 dpi, whole roots were harvested and expression levels of the pre-miRNA, mature and star strand as well as molecular marker genes for AM symbiosis were analyzed by real time PCR. Seven plants showed a 23 to 548 fold increased expression of pre-miR5204 as

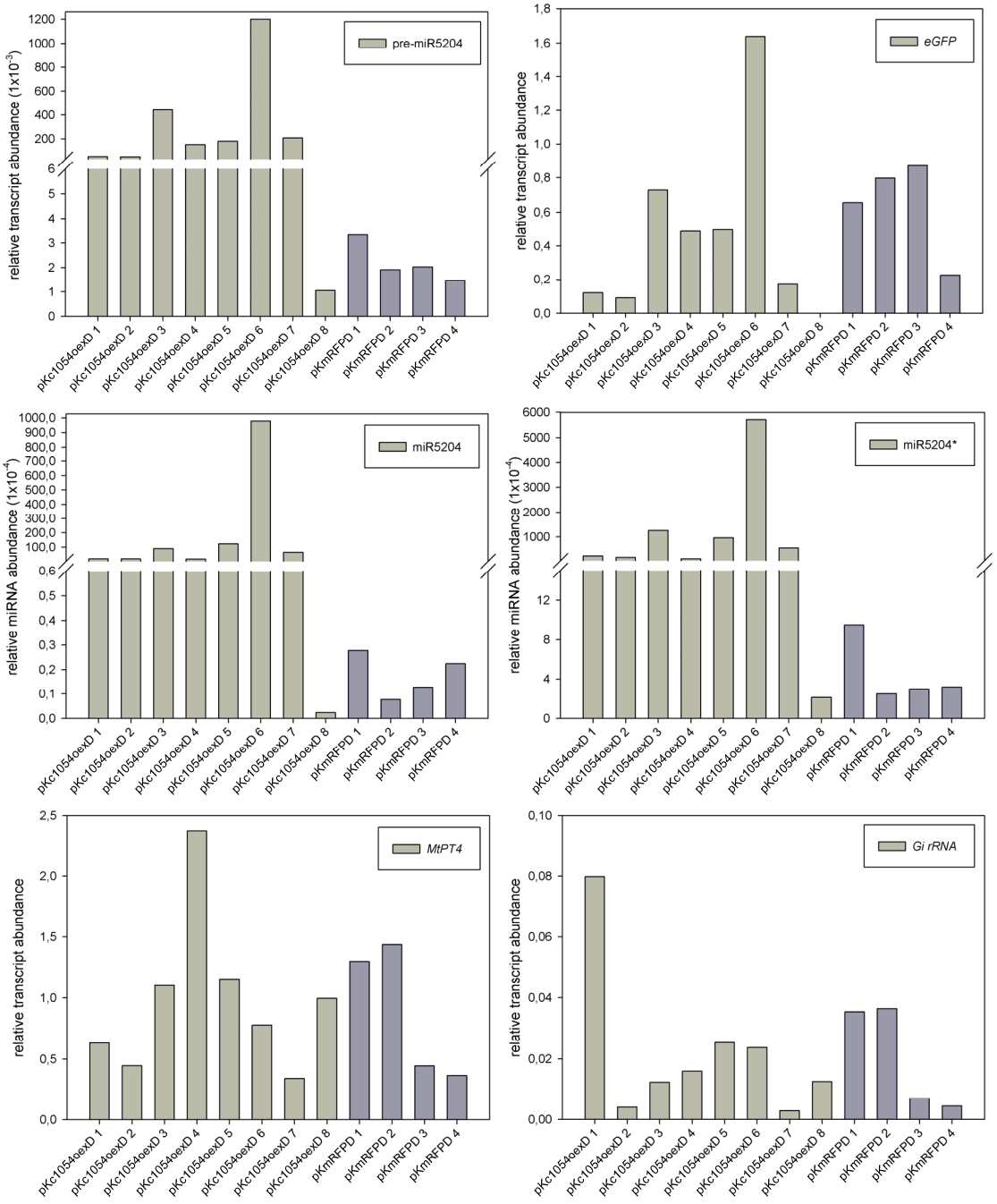

Figure 37: Overexpression of pre-miR5204 in *M. truncatula* via root transformation. Relative transcript abundance of the indicated genes or miRNAs (inset) measured by qRT-PCR using cDNA from individual root transformed plants. Rootsystems carrying the overexpression constructs are named pKc1054oexD 1-8 and vector control are named pKmRFPD 1-4. Expression of *eGFP* was measured as a transformation control.

compared to the mean of the vector control lines (figure 37). These plants were included in the statistical analysis. Overexpression of the precursor resulted strong (94 to 5544 fold) over-accumulation of mature miR5204, which highly correlated positively to the relative precursor abundance ($p \leq 0.001$) (figure 38). Interestingly, also miR5204* accumulation positively correlated to pre-miR5204 (figure 37 and figure 38), suggesting that miR5204* is not degraded after precursor processing by DCL. This result is contrary to the deep-sequencing data, which suggested a dominance of mature miR5204 due to a low read abundance of miR5204*. Stem-loop qRT-PCR of miR5204* in wild type plants using the same conditions as in chapter 3.3.4.1, confirmed the accumulation of the star strand to detectable levels with a comparable accumulation level as the mature strand (appendix figure 45).

These results indicate that pre-miR5204 is efficiently processed into the mature and star miRNA and that the star strand accumulates to detectable levels.

Analysis of the relative transcript abundance of *MtPt4* and *G. intraradices* rRNA revealed no difference in the expression of both marker genes in over-expressing roots comparing to the wild type roots (figure 37 and figure 38) indicating no change in arbuscule frequency and fungal colonization of the root system.

Degradome sequencing (Devers *et al.*, 2011) suggested a putative GRAS TF

Spearman Rank Order Correlation

Cell contents are given below gene name:
Correlation coefficient
p-value
Number of samples

	miR5204	**miR5204***	***MtPt4***	**Gi rRNA**
pre-miR5204	0.918	0.936	0.0636	-0.0636
	$2*10^{-7}$	$2*10^{-7}$	0.839	0.839
	11	11	11	11
miR5204		0.991	-0.0636	-0.0364
		$2*10^{-7}$	0.839	0.903
		11	11	11
miR5204*			-0.0727	-0.0636
			0.818	0.839
			11	11
MtPt4				0.673
				0.0209
				11

Figure 38: Spearman Rank order correlation analysis of the individual root transformed plants. All plants transformed with the overexpression construct pKc1054oexD and the control construct pKmRFPD were included in the analysis, except pKc1054oexD 8, which was excluded from the correlation analysis (see text).

(Medtr8g109760) to be a miR5204* target. The transcript of Medtr8g109760 is specifically accumulating in arbuscule-containing cells of mycorrhizal roots (Gaude *et al.*, submitted). To investigate the correlation of miR5204* and Medtr8g109760, the relative transcript abundance of *Medtr8g109760* was measured.

The roots over-expressing pre-miR5204 showed reduced transcript levels compared to the vector control lines, but transcript levels of *Medtr8g109760* vary greatly in mycorrhizal control roots (figure 39 A). This is even more pronounced when dividing the over-expressing roots into two groups for high and low miR5204/miR5204* expression (figure 39 B). Correlation analysis revealed a significant negative correlation ($r = -0.7$; $p \leq 0.05$) between miR5204/miR5204* and *Medtr8g109760*, confirming the negative regulation of *Medtr8g109760* by miR5204* (figure 40).

In wild type roots, *Medtr8g109760* and *MtPt4* transcript levels are positively correlated (r =

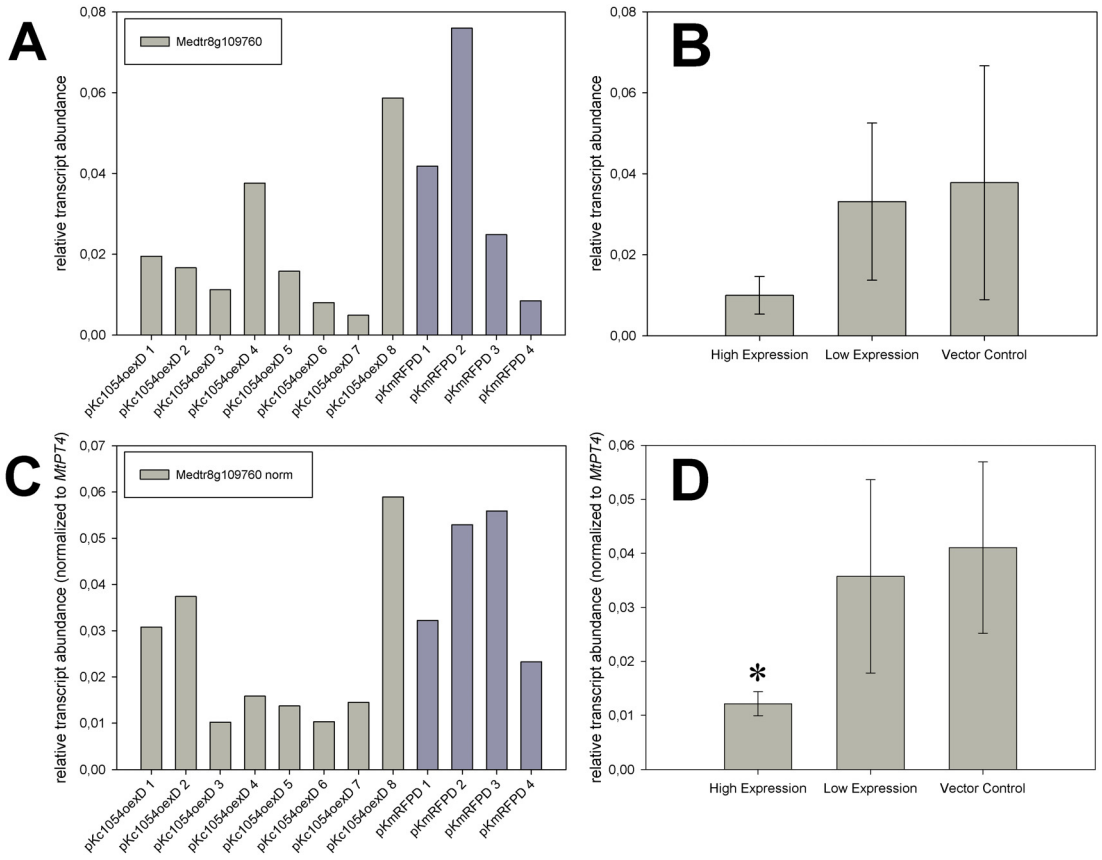

Figure 39: Relative expression abundances of the arbuscule specific putative GRAS transcription factor Medtr8g109760 in the pre-miR5204 over expressing plant roots. **A** Relative expression of *Medtr8g109760* in single root transformed plants (mean values of two technical replicates). **B** Mean expression values of *Medtr8g109760* in the plant roots with high expression of miR5204* (pKc1054oexD 3, 5,6 and 7) and low expression of miR5204* (pKc1054oexD 1, 2, 4, 8) compared to the vector controls (pKmRFPD 1-4). **C and D** Shows the same as A and B, but the relative transcript abundance of *Medtr8g109760* was normalized to the *MtPt4* expression in order to eliminate variation in transcript abundances due to different degrees of plant root colonization. Asterisk marks significant changes ($p \leq 0.05$; Student's t-test) compared to the vector controls.

0.7; $p \leq 0.05$), thus the high variation of *Medtr8g109760* transcript levels in control roots results from different colonization levels, mirrored by the different *MtPt4* transcript levels. Therefore, the relative transcript abundance of *Medtr8g109760* was normalized to *MtPt4* and statistically analyzed. Student's t-test revealed a statistically significant difference between highly over-expressing roots compared to control roots (figure 39 D) and correlation analysis resulted in extremely lower p-values (figure 40).
However, no correlation of *MtPt4*, as a marker for arbuscule abundance, and *Medtr8g109760* exists, due to an independent repression of *Medtr8g109760* transcript accumulation by miR5204* overexpression. This indicates, that transcription of *MtPt4* is not directly regulated by this GRAS TF.

3.3.5.2. Molecular analysis of the mycorrhizal phenotype in miR5229 over-expressing roots

Using the same conditions as mentioned above, overexpression of mature miR5229 was analyzed after root transformation with pKmiRAM09oexD which constitutively expresses pre-miR5229a (see chapter 2.2.1.2.). Similar to miR5204, over-expressing plants showed a

Spearman Rank Order correlation

Cell Contents are given below:
Correlation coefficient
p value
Number of samples

	Medtr8g109760	***MtPT4***	***Medtr8g109760*****norm**
pre-miR5204	-0.555	0.0636	-0.827
	0.0706	0.839	$2*10^{-7}$
	11	11	11
miR5204	-0.673	-0.0636	-0.845
	0.0209	0.839	$2*10^{-7}$
	11	11	11
miR5204*	-0.682	-0.0727	-0.864
	0.0186	0.818	$2*10^{-7}$
	11	11	11
Medtr8g109760		0.664	0.682
		0.0234	0.0186
		11	11

Figure 40: Spearman Rank order correlation analysis of the individual root transformed plants. All plants transformed with the overexpression construct pKc1054oexD and the control construct pKmRFPD were included in the analysis, except pKc1054oexD 8, which was excluded from the correlation analysis (see text).

high accumulation of pre-miR5229a compared to the vector control lines. However, *MtPt4* and *G. intraradices* rRNA transcript levels were not significantly changed in over-expressing roots as compared to the vector control lines. Furthermore, the predicted target Medtr1g078990 (table 9) showed no response to miR5229a/b overexpression.

4. DISCUSSION

4.1. *MtPho2* mutants of *Medicago truncatula* show increased AM fungal colonization at phases of progressive root colonization during symbiosis development

Identification of a functional AtPho2 orthologue in *M. truncatula*

The PHR1-miR399-PHO2 signaling pathway (Bari *et al.*, 2006; Chiou *et al.*, 2006) is conserved in all so far investigated flowering plants. Homologues of PHR1, PHO2 or At4/IPS1 were identified in common bean (Valdés-Lopéz *et al.*, 2008), Rice, *Populus trichocarpa* (Bari *et al.*, 2006) and more. Also, MIR399 genes are highly conserved in flowering plant species (see: miRBase v17).

Sequence comparisons indicated the presence of a PHO2 homologue sequence in the *M. truncatula* genome (Medtr2g013650.1) (Bari *et al.*, 2006). An additional PHO2-homologue (Medtr4g020620.2) with 90 % similarity to AtPho2 was identified in the *M. truncatula* genome (version 3.5). However, no transcript of this gene was found in *M. truncatula* roots. Since AtPho2 is transcribed and functional active in roots (Bari *et al.*, 2006; Chiou *et al.*, 2006), Medtr4g020620.2 cannot be regarded as a functional AtPho2 orthologue. In contrast, MtPho2 is not only transcribed, its transcripts are cleaved by miR399 (Branscheid *et al.*, 2010). Hence, in the current genome version of *M. truncatula* only one functional homologue, MtPho2, is present. Additionally, an expression perturbation experiment proved an AtPho2-like function of MtPho2 by over-accumulation of phosphate in the shoots, but not in the roots, when grown under phosphate replete conditions (Delhaize and Randall, 1995; Dong *et al.*, 1998).

Phosphite is able to suppress AM symbiosis

The structure analogue of phosphate, phosphite, is capable of repressing the PHR1-miR399-PHO2 signaling pathway in *A. thaliana* (Ticconi *et al.*, 2001; Stefanovic *et al.*, 2007; Ribot *et al.*, 2008). A suppression of AM symbiosis by Ph_i would indicate that components of the PHR1-miR399-PHO2 signaling pathway are also involved in this phenomenon. Results of the re-supply experiment clearly demonstrated that phosphate as well as phosphite is able to suppress the phosphate starvation inducible genes MtPlD, MtSPX and pri-miR399b (Branscheid *et al.*, 2010) and hence, the PHR1-miR399-PHO2 signaling pathway. All analyzed AM symbiosis-inducible genes showed significantly lower transcript levels when compared to plants under phosphate starvation indicating that phosphite is able to suppress the root colonization by *G. intraradices*. Hence, components of the PHR1-miR399-PHO2 signaling pathway are presumably involved in this process.

Loss of PHO2 function results in enhanced arbuscule development at stages of progressive root colonization by AM fungi

To further elucidate the involvement of the PHR1-miR399-PHO2 signaling pathway in AM regulation, expression perturbation experiments of individual pathway components were chosen. In this regard, a recently developed *Tnt1*-tagged mutant collection (Tadege *et al.*, 2008) has proven to be of high value for such reverse genetic approaches and is a useful alternative to the RNAi approach.

An identified *Tnt1* insertion mutant, *mtpho2*, was used to study the role of MtPHO2 in AM symbiosis development. The mutant line showed increased phosphate accumulation in leaves, although this phenotype was not as strong as observed in the RNAi experiment. A possible explanation for the different levels of P_i over-accumulation between the RNAi chimeric plants and the *Tnt1* mutants might be the different genetic background of both plants. For the RNAi-approach, *M. truncatula* Jemalong *cv* A17 was used, whereas the Tnt1-mutants were generated from Medicago *cv* R108 [i.e. *M. tricycla* (Medicago HapMap Project)]. Investigation of soluble phosphate concentration of both Medicago accessions revealed a clear decreased phosphorus use efficiency of Medicago R108 as compared to *M. truncatula* A17 (appendix figure 46). However, only 70 % of the *M. truncatula* genome is known to date. Therefore, it cannot be ruled out that yet unidentified PHO2 homologues are active at certain conditions and that the RNAi construct was able to repress different genes due to their high sequence similarity.

The *mtpho2* mutant plants were used to analyze the effect of PHO2 on systemic suppression of AM colonization by high P_i. Loss of MtPHO2 function leads to a constitutive triggering of a phosphate starvation response. Thus it might be anticipated that *mtpho2* mutants show increased AM colonization under high P_i conditions. However, *mtpho2* mutants showed, to a similar extent as wild type plants, reduced colonization levels under high P_i. This implies that additional PHO2-independent mechanisms are involved in this phenomenon. This goes in line with the fact that overexpression of MtPho2 in roots also did not change AM colonization.

In order to elucidate the role of PHO2 during the development of AM symbiosis, a time course experiment was carried out. Three time points, which represent three different stages of AM symbiosis development, were chosen: an early colonization stage (7 dpi), a stage of progressive root colonization (14 dpi) and a steady state level of colonization (21 dpi). Interestingly, *mtpho2* mutants showed significantly increased levels of *MtPt4* transcripts at 14 dpi, indicating a higher number of functional arbuscules at this stage as compared to wild type plants. Since *MtPt4* can be regarded as a diagnostic marker for functional arbuscule-containing cells, this implies that arbuscule development is enhanced in *mtpho2* mutants during the stage of progressive root colonization after initial colonization is finished.

Analysis of the shoot-to-root weight ratio and root length showed that *mtpho2* seedlings have longer primary roots after germination. This might be due to an altered P_i-storage allocation of *mtpho2* in contrast to the wild type. Analysis of mature plants will be carried out in future, in order to investigate if the observed mycorrhizal phenotype is conditioned by the longer primary roots of young seedlings.

Cross-talk of the Ph_i-sensitive and Ph_i-insensitive P_i-starvation signaling pathway

Interestingly, the P_i-starvation induced gene *Mt4* is not responding to phosphite. This indicates that *Mt4* expression is controlled by a Ph_i-insensitive P_i-starvation signaling pathway. This is in contrast to At4/IPS1 in *A. thaliana*, whose expression is Ph_i-sensitive (Ticconi *et al.*, 2001; Stefanovic *et al.*, 2007). As compared to wild type plants, *mtpho2* plants showed increased *Mt4* levels, indicating that MtPHO2, which belongs to the Ph_i-sensitive P_i-starvation signaling pathway, negatively regulates *Mt4* expression. This regulation could represent a cross-talk between both signaling pathways. Downregulation of *MtPho2* leads to increased *Mt4* expression which in turn results in reduced miR399 activity and thus resembles a negative feed-back cycle (figure 41).

Degradome analysis revealed a major facilitator superfamily (MFS) protein as a second miR399 target besides MtPho2 (Devers *et al.*, 2011). This MFS protein functions as an phosphate transporter specifically transcribed in arbuscule-containing cells (personal communication Maria J. Harrison; Anja Branscheid). Therefore, the observed mycorrhizal phenotype of *mtpho2* might be an indirect effect of the negative-feedback loop involving *Mt4* and miR399 and thus the miss-regulation of the AM symbiosis specific miR399-targets rather than a direct influence of MtPHO2 on AM symbiosis. As mentioned above, a functional loss of MtPHO2 leads to higher expression levels of *Mt4*. Hence, this would lead to a reduced miR399 activity and subsequent higher expression levels of the phosphate transporter. Presumably, this leads to a faster colonization during phases of progressive root colonization. An *mtpho2mt4* double mutant will be necessary to further elucidate the cross-talk of both pathways. Alternatively, overexpression of miR399 in the *mtpho2* background could be used to distinguish both possibilities.

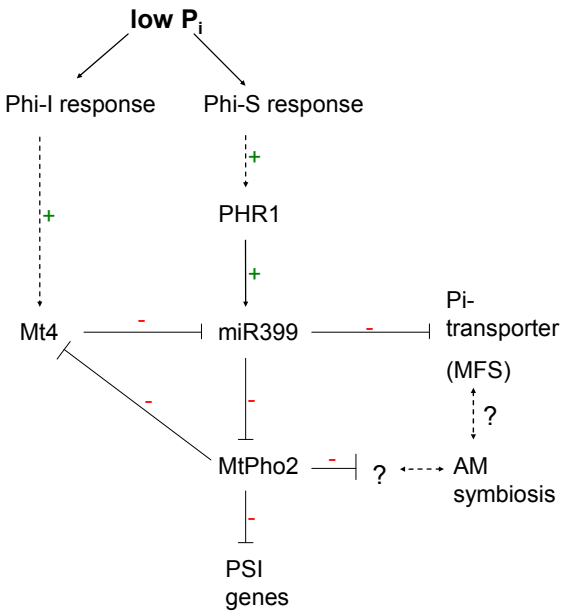

Figure 41: Model of a crosstalk between the Ph_i-insensitive (Phi-I) and Ph_i-sensitive (Phi-S) P_i-starvation signaling pathway. Mt4, miR399 and MtPho2 are part of a negative feed-back loop of MtPho2 expression. MFS = major facilitator superfamily; PSI = phosphate starvation induced.

4.2. Transcriptomic analysis of the systemic adaptation in *Medicago truncatula* shoots and roots to AM symbiosis and phosphate addition

Most studies of plant responses to phosphate have focused on transcriptional changes in response to phosphate starvation and on strategies to overcome P_i-limitation (Franco-Zorrilla *et al.*, 2004; Ticconi and Abel, 2004; Chiou and Lin, 2011). Plants in the environment constantly suffer P_i-limitation (Smith *et al.*, 2011). The beneficial association of plants with AM fungi improves their acquisition of phosphate as one strategy to cope with this condition (Harrison, 1999; Hause and Fester, 2005; Smith *et al.*, 2011). Interestingly, high P_i- levels

systemically suppress AM fungal colonization of plant roots (Sanders, 1975; Menge *et al.*, 1978; Breuillin *et al.*, 2010; Balzergue *et al.*, 2011). Hence, the extensive usage of P_i-fertilizers in agriculture limits the efficiency of functional AM symbioses in the field (He and Nara, 2007). Therefore, it is of great interest to investigate the molecular background of phosphate homeostasis and AM symbiosis correlation. The here presented work applied microarray hybridization to analyze this relationship.

Two recent studies in *Petunia hybrida* and *Pisum sativum* addressed the question whether strigolactones might be involved in mediating the systemic repression of root colonization by AM fungi at high phosphate conditions (Breuillin *et al.*, 2010; Balzergue *et al.*, 2011). Strigolactone is a recently discovered plant hormone (Akiyama and Hayashi, 2006), which was found to be an early signal in the pre-contact phase of AM symbiosis establishment and induces hyphal branching of sporulating AM fungi (Akiyama *et al.*, 2005; Besserer *et al.*, 2006; Besserer *et al.*, 2008). Because the amount of strigolactones released by the plant root system negatively correlates with P_i supply in red clover, sorghum (Yoneyama *et al.*, 2007a; Yoneyama *et al.*, 2007b) and tomato (Lopez-Raez *et al.*, 2008), it was speculated that reduced levels of strigolactone at high phosphate status of the plant might be responsible for the reduced AM symbiosis formation. Balzergue *et al.* indeed demonstrated that the amount of strigolactones is systemically reduced by P_i addition in a split-root system. But addition of a synthetic strigolactone is not sufficient to elevate fungal colonization levels at high P_i conditions, even though the number of hyphopodia formed by the AM fungi is restored to levels similar low P_i conditions. Similar results were obtained by Breullin *et al.*, where addition of a synthetic strigolactone to a strigolactone deficient petunia mutant, *dad1* (Snowden *et al.*, 2005), could not restore wild-type colonization levels. Additionally, the re-supply of phosphate and phosphite in this study was able to suppress an already established AM symbiosis. Hence, the repression of AM symbiosis by high P_i fertilization is not restricted to pre-symbiotic phases of interaction.

In the here presented study the formation of AM symbiosis at low (20 µM P_i) and high (2 mM P_i) conditions and the transcriptional response to AM of the root and shoot transcriptome of *M. truncatula* were analyzed using split-root systems to elucidate the systemic response to phosphate and mycorrhizal colonization. The split-root system represents an effective way to study systemic responses of AM symbiosis to high phosphate levels (Menge *et al.*, 1978; Rausch *et al.*, 2001; Breuillin *et al.*, 2010; Balzergue *et al.*, 2011). Soluble phosphate concentrations of roots and shoots demonstrated that phosphate predominantly accumulates in

the shoot and the split-root system allows the analysis of systemic responses without local P_i effects.

Colonization of the *M. truncatula* root system by *G. intraradices* leads to the expression of known AM symbiosis marker genes in roots of low and high phosphate treated plants

The analysis of the root transcriptome at low phosphate conditions confirmed the induction of many known genes in mycorrhizal roots. The transcriptional responses to mycorrhizal colonization at low P_i show only limited overlap as reported previously (Hohnjec *et al.*, 2005; Liu *et al.*, 2007).

The principal component analysis of the microarray data clearly separated all experimental conditions, indicating that mycorrhizal roots at high phosphate conditions posses a distinct transcriptome in contrast to all other conditions.

Breuillin *et al.* postulated several mechanisms, by which P_i might repress AM symbiosis. (1) P_i could limit the biosynthesis or secretion of strigolactone or other signals involved in pre-symbiotic interaction. (2) P_i could reduce the expression of components of the SYM pathway. (3) P_i could increase the defense status in the roots and would lead therefore to a rejection of the symbiont. (4) P_i influences the carbon allocation within the plant and might limit the delivery of essential nutrients to the symbiont and thereby slowing its growth. (5) P_i could downregulate essential components involved in downstream steps of root colonization and/or establishment of the symbiotic interface.

As discussed above, the first hypothesis can be ruled out as the sole factor of the repression of AM symbiosis by P_i. Additionally, the systemic response to high phosphate conditions did not alter the expression of known components of the SYM pathway (Parniske, 2008). In contrast, the expression of *MtNsp2*, a major component of the SYM pathway, was induced in response to AM symbiosis at low and high P_i levels. However, two genes with moderate homology to MtSYMRK/DMI2 (Catoira *et al.*, 2000) showed a reduced expression in roots and shoots in response to high phosphate conditions, but the expressions in the shoots indicate that this receptor-like kinase is not specifically involved in the root symbiosis. Therefore, it is unlikely that alterations in the root symbiosis signaling pathway in response to high shoot phosphate conditions are responsible for the repression of AM symbiosis.

Investigation of the regulated defense genes revealed that a subset of PR-proteins is induced in mycorrhizal roots at both phosphate conditions. No additional defense-related genes were induced in mycorrhizal roots at high P_i. In contrast, two PR-proteins were downregulated at high P_i conditions, but were distinct from low P_i myc induced PR-proteins. Hence, the

activation of defense response genes appears not to be involved in suppression of AM symbiosis and goes in line with results from *P. hybrida* (Breuillin *et al.*, 2010). Additionally, no alterations of genes involved in carbon metabolism were found in mycorrhizal roots at high phosphate conditions. However, a substantial number of genes encoding for transcription factors were specifically downregulated in mycorrhizal roots in a systemic response to high phosphate conditions and only one TF was found to be-upregulated. These TFs might be involved in downstream steps of root colonization and/or establishment of the symbiotic interface and could be interesting candidates for the adaptation of mycorrhizal roots to different phosphate conditions.

AM symbiosis leads to a systemic induction of genes involved in photosynthesis, amino acid metabolism and protein synthesis in the shoot of *M. truncatula*

Transcriptional responses in the shoot of mycorrhizal *M. truncatula* plants revealed evidence for a systemic induced resistance against pathogens in the shoot of mycorrhizal plant, because several PR-proteins were induced in mycorrhizal shoots (Liu *et al.*, 2007). This observation could be confirmed in this study. Moreover, the microarray data revealed a specific upregulation of a high number of transcripts involved in protein synthesis, mainly ribosomal protein encoding genes, as well as transcripts encoding proteins involved in the amino acid metabolism. The induction of these genes in the shoot of mycorrhizal plants is likely to account for the often observed increased growth of mycorrhizal plants. Additionally, several genes encoding proteins of the photosystems I and II as well as other photosynthesis related genes were induced in mycorrhizal shoots. AM symbiosis can enhance the CO_2 uptake rate of plants (Mathur and Vyas, 1995; Caravaca *et al.*, 2003; Boldt *et al.*, 2011) and the results obtained in this study indicate that this effect is due to an enhanced abundance and activity of RuBisCO and a higher turn-over rate of both photosystems.

All of these photosynthesis-related transcripts are specifically induced by AM symbiosis, because the regulation of these genes was not observed after addition of phosphate to non-mycorrhizal plants. Furthermore, AM symbiosis did not significantly increase the total phosphate concentration in the shoot of mycorrhizal plants. Hence, the results suggest a systemic root borne mycorrhizal-related signal independent of phosphate, which induces gene expression involved in photosynthesis and growth. The induced expression of numerous genes which encode transcription factors might be involved in mediating the response to the putative myc signal.

High phosphate treatment leads to a systemic repression of phosphate starvation and AM colonization induced genes in shoots of *M. truncatula*

Under high P_i conditions, a significantly lower number of transcripts are regulated in response to arbuscular mycorrhizal colonization. However, a number of transcripts showed stronger regulation levels in mycorrhizal shoots under high P_i as compared to low P_i condition. Most of the upregulated genes are involved in the secondary metabolism. A transcript encoding for a terpene synthase (Medtr7g010710.1) shows the highest induction in mycorrhizal shoots at high P_i conditions. However, the precise function of this gene is unknown. Terpene synthases are involved in producing volatile compounds. These compounds are involved in various processes, e.g. they can indirectly protect the plant by attracting herbivore predators (Kessler and Baldwin, 2001; Degenhardt *et al.*, 2009), they can actively protect the plant against pests, pathogens (Gershenzon, 2007; Gershenzon and Dudareva, 2007; Bednarek and Osbourn, 2009) and abiotic stress (Vickers *et al.*, 2009). Additionally, they can attract pollinators (Kessler *et al.*, 2008) and serve as signals between plants and within distal parts of the same plant (Baldwin *et al.*, 2006). The exact function of this terpene synthase with regard to the suppression of AM symbiosis at high P_i concentrations needs to be elucidated in future. Another interesting observation is the induction of an ethylene responsive transcription factor, which is repressed in mycorrhizal shoots at low P_i. Ethylene is a negative regulator of AM symbiosis (Penmetsa *et al.*, 2008), hence this TF might be important for the suppression of AM symbiosis.

The observed induction of genes involved in photosynthesis, protein synthesis and amino acid metabolism in mycorrhizal shoots at low P_i was not found in mycorrhizal shoots at high phosphate conditions. The principal component analysis indicated that the plant shoot transcriptome does not respond to AM symbiosis at high phosphate conditions. Moreover, in contrast to the induction of photosynthesis genes in shoots of mycorrhizal plants under low P_i, a transcript encoding a light harvesting center II subunit is downregulated in mycorrhizal plants at high P_i conditions as compared to non-mycorrhizal plants or low P_i conditions. Enhanced photosynthesis and carbon fixation in mycorrhizal shoots at low P_i would lead to an accumulation of sugars in the plant shoot (Wright *et al.*, 1998). However, Boldt *et al.* did not observe an increase in the sugar content in the leaves of tomato plants but found a significant increase in sucrose in the roots. They postulated a higher sucrose loading to the phloem and found two sucrose transporters induced in leaves. AM fungi receive carbohydrates from the plant host as the sole source for energy metabolism, maintenance and growth (Bago *et al.*, 2000). Additionally, sucrose synthase and invertase expressions are induced in mycorrhizal

roots (Hohnjec *et al.*, 2003; Garcia-Rodriguez *et al.*, 2005; Schaarschmidt *et al.*, 2006; Delano-Frier *et al.*, 2008). A recent study in *Solanum tuberosum* suggested that sucrose is involved in the regulation of AM symbiosis at high phosphate conditions (Gabriel-Neumann *et al.*, 2011). Overexpression of a phloem loading sucrose transporter, revealed an increased AM fungal colonization at high phosphate conditions as compared to wild type plants.

Additionally, sucrose itself discussed to be a systemic plant growth regulator and initiates acclimatory responses in roots to low P_i availability (reviewed in Hammond and White, 2011). During P_i limitation, sugars and starch accumulate in leaves and an increased loading of sucrose to the phloem functions to relocate carbon sources from source leaves to roots in order to increase root growth. Mycorrhizal roots represent a strong carbon sink (Wright *et al.*, 1998) and carbohydrates might be preferentially allocated to the place of fungal colonization.

Interestingly, there is evidence for a cross-talk between the PHR1-miR399-PHO2 P_i-starvation signaling pathway and photosynthates, as induction of miR399 is dependent on the presence of light at the onset of P_i-starvation (Liu *et al.*, 2010) and the authors speculate that most likely sucrose is mediating this response (Liu and Vance, 2010).

This suggests that the systemic response in suppressing AM symbiosis at high shoot phosphate concentrations is mainly due to a combined repression of both, the phosphate starvation responses, including the PHR1-miR399-PHO2 P_i-starvation signaling pathway, and the systemically AM symbiosis induced carbon fixation, including relocation of sucrose from shoot to root. And it is likely that both mechanisms, acting through long distance signaling via the phloem, are linked with each other.

4.3. Arbuscular mycorrhizal symbiosis leads to a differential expression of novel and conserved miRNAs in *Medicago truncatula*

The aim of this work was to identify miRNAs and miRNA targets related to arbuscular mycorrhizal symbiosis in *M. truncatula* roots. Therefore, small RNAs were isolated from mycorrhizal and non-mycorrhizal roots of *M. truncatula*, deep sequenced using Illumina technology and subsequently conserved and novel miRNAs were identified by homology or miRDeep predictions, respectively.

The genome-wide profiling carried out in this study revealed the identification of more than 500 novel miRNA candidates. Of these candidates, 243 are now annotated at miRBase as

novel *M. truncatula* miRNAs. The high number of miRNA candidates and annotated miRNAs expressed in *M. truncatula* roots indicates that miRNAs mediate a substantial part of the cellular regulation in plant roots.

Identification of novel miRNAs in *Medicago truncatula* roots

162 miRNAs, currently annotated at the miRBase database v.17, could be detected by small RNA sequencing being expressed in *M. truncatula* roots. In addition to these known miRNAs, deep sequencing coupled miRDeep predictions revealed 515 novel miRNA candidates of *M. truncatula* of 20-25 nt length. Although the majority of plant miRNAs reported so far is of 20-23 nt in lengths, there are reports of 24 nt miRNAs like ath-miR163 (Park *et al.*, 2002). In addition, the ath-miR156, ath-miR395 and ath-miR399, beside other miRNAs, can occur also as 23-25 nt variants (Vazquez *et al.*, 2008) and are then called long-miRNA. Such long-miRNAs are processed by DCL3 (Vazquez *et al.*, 2008). Unfortunately, DCL *M. truncatula* mutants are so far not available to test the DCL3 dependence of the 24-25 nt miRNA candidates. The 24-25 nt long miRNAs and miRNA candidates have a considerably lower conservation (22%) in contrast to the 20-23 nt long miRNAs (59%), supporting the assumption that these long miRNAs might be of younger evolutionary origin. This goes in line with the assumption that these "young" miRNAs derive from small inverted repeat loci in the genome (Vazquez *et al.*, 2008).

The criteria for the annotation of novel miRNA from high throughput sequencing data have been re-evaluated recently, since re-analysis of miRNA datasets of invertebrates and plants demonstrated a considerably high fraction of erroneously annotated miRNA (Rajagopalan *et al.*, 2006; Ruby *et al.*, 2006; Ruby *et al.*, 2007). With the availability of deep sequencing data it is now possible and essential to confidently determine the precise 5′ end of a mature miRNA (Chiang *et al.*, 2010; Berezikov *et al.*, 2011). In addition, reads matching the miRNA* should be present and have the potential to pair to the mature miRNA candidate with approximately 2 nt 3′ overhangs (Chiang *et al.*, 2010). Taken these two latter criteria into account, 243 novel miRNAs of *M. truncatula* were identified in this study and were deposited at miRBase.

Distinct miRNAs are upregulated in mycorrhizal roots

The read count analysis of the miRNA candidates showed that members of 20 miRNA families were regulated in mycorrhizal roots as compared to non-mycorrhizal roots. For 8 miRNAs of the most strongly regulated candidates (log2-fold >1), a significant differential

expression was proven by real time PCR analysis. The highest upregulation was observed for miR5229a/b (log2-fold 9.7), which is remarkably high taking into account that cellular differences in miRNA expression are hardly detectable, since whole root samples were used for library construction. MiR5229a/b was exclusively expressed in mycorrhizal roots and highly abundant in arbuscule-containing cells, suggesting a specific role during arbuscule development. So far, no target for this novel miRNA could be detected, but *in silico* predictions suggest a transcript, *Medtr1g078990*, encoding a haem peroxidase to be a target of this miRNA. Haem peroxidases have multiple tissue-specific functions, e.g. removal of hydrogen peroxide, oxidation of toxic compounds, cell wall biosynthesis, defense responses, auxin and ethylene metabolism (Welinder *et al.*, 1992). Hydrogen peroxide accumulates in mycorrhizal roots preferentially in degenerating arbuscules (Salzer *et al.*, 1999), and several haem peroxidases were found to be induced in mycorrhizal roots of petunia (Breuillin *et al.*, 2010). Thus it might be anticipated that the induction of miR5229a/b suppresses the haem peroxidase leading to locally increased hydrogen peroxide accumulation in cells with degenerating arbuscules. However, overexpression of pre-miR5229a, resulting in a high accumulation of mature miR5229, did not confirm post-transcriptional regulation of *Medtr1g078990* by miR5229 and did not show altered expression levels of AM symbiosis marker genes. MiR5229 is exclusively expressed during AM symbiosis at the tested conditions, therefore the abundance of miR5229 might have reached already saturating levels in mycorrhizal roots. Hence, it is necessary to downregulate their abundance for further analysis of their putative role during AM symbiosis development. An elegant way of controlling miRNA activity is the use of target mimicry constructs (Franco-Zorrilla *et al.*, 2007) to exploit the naturally occurring mechanism of sequestration of miR399 by IPS1 or At4 in Arabidopsis or Mt4 *M. truncatula*. Therefore, target mimicry constructs against miR5229 were generated and will be analyzed in future.

Interestingly, a clear induction in mycorrhizal roots was also found for miR169d/l. MiR169 targets the transcription factor *MtHAP2-1* and has been demonstrated to play an important role during nodule differentiation by spatial restriction of *MtHAP*2-1 expression to the nodule meristematic zone (Combier *et al.*, 2006). The increased expression of this miRNA in mycorrhizal roots together with the accumulation in the phloem and around fungal hyphae gives evidence that the miR169 family is also involved in the AM symbiosis. Moreover, miRNA* sequences of the miR169 family were also strongly induced in mycorrhizal roots and were shown to have a similar tissue specific accumulation as mature miR169. Remarkably, a transcript encoding MtBcp1 was identified to be a target of this miRNA* using

degradome sequencing (Devers *et al.*, 2011). *MtBcp*1 encodes a protein specifically accumulating in the periarbuscular membrane (Pumplin and Harrison, 2009) and it might be speculated that the miR169* restricts *MtBcp*1 expression to arbuscule containing cells. Interestingly, analysis of the microarray data showed a reduction of *MtBcp1* transcripts which might be an effect of the induced expression of miR169* at high phosphate levels rather than suppression of the AM symbiosis. A further miRNA, which was exclusively detectable in mycorrhizal roots, was miR160f*. This miRNA was primarily detected in the central cylinder. However, the function of this miRNA* is yet elusive, because no targets were found by degradome sequencing. The same situation is true for the miR5204. Nevertheless, several targets could be *in silico* predicted including a heavy metal transport protein and a zinc finger transcription factor. Notably, miR5204 appears to be a phosphate responsive miRNA and is located around individual arbuscules. It can be hypothesized that the presence of this miRNA correlates with the concentration of phosphate in distinct arbuscule-containing cells. Similar to miR160f*, the mycorrhizal induced miR160c was predominantly localized in the central cylinder, and targets several transcripts of the auxin response factor gene family. Moreover, different transcripts of auxin response factors are additionally targeted by miRNA167. Targets for both miRNAs were confirmed independently by Devers *et al.* (2011) and Jagadeeswaran *et al.* (2009). Auxin has been demonstrated to play a crucial role in AM symbiosis, probably in the presymbiotic phase of AM fungal development (Hanlon and Coenen, 2010), and the auxin content is elevated in mycorrhizal roots (Fitze *et al.*, 2005; Jentschel *et al.*, 2007). The fact that both miRNAs were significantly upregulated in mycorrhizal roots and target transcripts of the same gene family implies that miR160c and miR167 might be involved in the fine regulation of auxin responses in AM symbiosis. Future investigation will unravel the physiological relevance of the discussed miRNAs during AM symbiosis.

Regulation of symbiosis relevant transcripts by miRNAs

One example for the regulation of symbiosis relevant transcripts is miR169, which targets a CCAAT transcription factor important for root nodule development (Combier *et al.* 2006). In addition, miR169* mediates the cleavage of the arbuscule-specific protein MtBcp1 and is higher abundant than the mature miR169 in mycorrhizal roots (Devers et al,. 2011). Hence, it might be anticipated that the dominant form of this miRNA switches during the two endosymbioses and restricts the expression of different targets to distinct cell types. However, this needs to be further analyzed by strand specific expression using artificial miRNAs.

Besides *MtBcp*1, further transcripts strongly induced in mycorrhizal roots were found to be miRNA targets. A symbioses relevant gene regulated by miR171h is *MtNsp*2, a GRAS transcription factor essential for root nodule development (Oldroyd and Long, 2003). In addition, the *nsp*2-2 mutant shows decreased mycorrhizal colonization, which implies a role also during mycorrhizal signaling (Maillet *et al.*, 2011). MtNSP2 forms a dimer with MtNSP1 to bind to the early nodulin *MtEnod*11 promoter (Hirsch *et al.*, 2009). Surprisingly, significantly increased *MtNsp*2 transcript levels were found in mycorrhizal roots by microarray and qRT-PCR analysis and in addition to its inverse correlation to miR171h abundance, *MtNsp*2 transcripts are cleaved by miR171h (Devers *et al.*, 2011). This implies that *MtNsp*2 is both, transcriptionally regulated by myc and post-transcriptionally controlled by a miRNA. However, the role of these regulation steps in symbioses signaling remains to be elucidated. Another GRAS transcription factor (*Medtr8g109760*), strongly induced in arbuscule-containing cells (Gaude *et al.*, submitted), was found to be cleaved by miR5204* (Devers *et al.*, 2011), whose corresponding mature strand itself is highly upregulated in mycorrhizal roots (see above). Direct regulation of this GRAS TF by miR5204* could be confirmed by overexpression of pre-miR5204. This implies that the target is subjected to a strong spatial regulation by miR5204* in mycorrhizal roots. As the expression of miR5204* positively correlates with phosphate addition and is responsive to strong phosphate sinks, such as nodules, it can be hypothesized that this miR5204* functions as a mediating signal between the phosphate status of the plant and AM symbiosis formation. Therefore, overexpression of pre-miR5204 at low phosphate conditions should result in reduced colonization of the root system by AM fungi. Overexpression of pre-miR5204 resulted in high accumulation of mature miR5204 as well as miR5204* strands and negative regulation of Medtr8g109760 by this MIR gene expression product could be confirmed. However no effect on the expression of AM symbiosis marker genes could be detected. It is therefore hypothesized that this mycorrhiza induced GRAS TF acts down-stream of the established AM symbiosis. Further analysis will be carried out by using a target mimicry construct in analogy to miR5229.
In summary, the findings suggest that the establishment of a mycorrhizal symbiosis leads to a reprogramming of the miRNA-target network in roots including miRNA strand preferences.

MIR171h is transcribed as a long primary transcript which is comprised of a tandem of miR171h producing loci and is feed-back regulated by self-cleavage

Since miR171h exhibits a sequence shift compared to other miR171 family members, which allows targeting of MtNsp2, the genomic locus was further analyzed. It was observed that

MIR171 possesses two mature miRNA generating loci. Processing of these two loci could be confirmed by the presence of the two distinct miR171h* sequences. The presence of several degradome tags indicated that this MIR gene is transcribed as a long primary transcript of at least 800 bp what could be confirmed by RT-PCR. It is known that miRNA can be transcribed in tandem and this was already observed for the miR166 in *Medicago truncatula* (Boualem *et al.*, 2008). Additionally a recent study using deep sequencing of mRNAs and transcription start sites in *Vitis vinifera* additionally suggested that MIR genes are transcribed from TATA-box containing intergenic regions as ~1-1.2 kb long primary transcripts which can contain introns (Mica *et al.*, 2009).

Interestingly, the primary transcript of miR171h is cleaved by the mature miR171h in the miR171h.2* producing sequence, suggesting a self-regulation of its biogenesis as a feed-back mechanism. This mechanism could also be found for miR399c*/k* in *Medicago truncatula* (Devers *et al.*, 2011), where miR399c*/k* accumulation reaches a level comparable to the mature strand (appendix table 10). Cleavage of primary miRNA transcripts has already been observed in Arabidopsis and rice (German *et al.*, 2008; Zhou *et al.*, 2010), therefore self-regulation through a feedback-circuit between primary miRNA transcripts and corresponding miRNA/ miRNA* has been postulated by (Meng *et al.*, 2010). It was proposed that the overproduction of miRNA precursors results in an accumulation of miRNAs or miRNA*, which could in turn recognize their host precursors as the downstream targets.

These results further encourage the finding, that MIR genes in plants are generally transcribed as long primary transcripts which can contain several miRNA producing loci and can negatively regulate their biogenesis by self-cleavage.

miRNA* strands exhibit biological functions during AM symbiosis

In the case of *Medtr8g109760* and *MtBcp1*, this study and degradome sequencing (Devers *et al.*, 2011) provides evidence for miRNA*-mediated mRNA cleavage in *M. truncatula* roots. Moreover, often a notably high accumulation of miRNA* and for several miRNA* molecules even a higher abundance was found as compared to their mature miRNA. Interestingly, a recent study provided evidence that miR393b* is involved in the innate immunity of plants, by regulating the exocytosis of PR-proteins through silencing of the Golgi-localized SNARE gene, *MEMB12* (Zhang *et al.*, 2011). The regulatory role of miRNA* sequences has also been observed in animals (Jagadeeswaran *et al.*, 2010) and human, where miR-155* and miR-155 adjust the type I interferon production in an opposite manner through different targets (Zhou *et al.*, 2010). It is currently anticipated that one arm of the RNA duplex preferentially

accumulates and is then referred to as mature miRNA whereas the opposite strand is called miRNA*. Previous models suggested that the choice of the dominant miRNA arm encoding the mature miRNA depends on thermodynamic and structural properties of the duplex RNA molecule (Khvorova *et al.*, 2003; Schwarz *et al.*, 2003). Nevertheless it was recognized that many miRNA* species also accumulate to substantial levels and are able to downregulate target mRNAs (Okamura *et al.*, 2008; Yang *et al.*, 2011). Moreover, large-scale sequencing data have shown that the arm from which the dominant form is processed can switch in different tissues (Chiang *et al.*, 2010) and in different organisms (Griffiths-Jones *et al.*, 2011). Interestingly, the *in situ* hybridizations confirmed the accumulation of miR169d*/e.2*/l*/m*, and miR160f* in the intracellular space and central cylinder of the roots. Identical signal patterns were obtained for their corresponding mature strand or a mature strand of the same miRNA family, respectively. This goes in line with previous findings from Rapeseed, where beside other miRNA*, considerable levels of miR169* and miR160* were detected in the phloem sap (Buhtz *et al.*, 2008; Pant *et al.*, 2009). The fact that both, the mature miRNA and the corresponding miRNA*, were present in the phloem might indicate that phloem transported miRNAs, which act as long distance signals (Pant *et al.*, 2008) are transported as miRNA/miRNA* duplex, probably due to a higher stability of such a duplex molecule. However, double strand or single strand specific RNA nuclease assays did not prove the presence of RNA duplexes in the rapeseed phloem (Buhtz *et al.*, 2008). But it has been suggested that such duplex molecules are denaturized during RNA extraction and therefore difficult to detect (Buhtz *et al.*, 2008). In addition to the previously discussed miRNAs, also the highly conserved mature miR399 was proven to be phloem-transported from shoot to root (Pant *et al.*, 2008), which is also true for miR399* (Hsieh *et al.*, 2009). Remarkably, for the star strands of miR160f, miR5204, miR169d/e.2/l/m and miR396b elevated levels were found in mycorrhizal roots. In *Solanum lycopersicum*, miR169g* was found to be upregulated in leaves of mycorrhizal or high phosphate treated plants (Gu *et al.*, 2010).

Conclusively, these results further strengthens the assumption that miRNA* star strands can mediate biological relevant functions.

5. SUMMARY

AM symbiosis has a positive influence on plant P-nutrition and growth, but little is known about the molecular mechanism of the symbiosis adaptation to different phosphate conditions. The recently described induction of several pri-miR399 transcripts in mycorrhizal shoots and subsequent accumulation of mature miR399 in mycorrhizal roots indicates that local PHO2 expression must be controlled during symbiosis, presumably in order to sustain AM symbiosis development, in spite of locally increased P_i-concentration.

A reverse genetic approach used in this study demonstrated that PHO2 and thus the PHR1-miR399-PHO2 signaling pathway, is involved in certain stages of progressive root colonization. In addition, a transcriptomic approach using a split-root system provided a comprehensive insight into the systemic transcriptional changes in mycorrhizal roots and shoots of *M. truncatula* in response to high phosphate conditions. With regard to the transcriptional responses of the root system, the results indicate that, although the colonization is drastically reduced, AM symbiosis is still functional at high P_i concentrations and might still be beneficial to the plant. Additionally, the data suggest that a specific root-borne mycorrhizal signal systemically induces protein synthesis, amino acid metabolism and photosynthesis at low P_i conditions, which is abolished at high P_i conditions.

MiRNAs, such as miR399, are involved in long-distance signaling and are therefore potential systemic signals involved in AM symbiosis. A deep-sequencing approach identified 243 novel miRNAs in the root tissue of *M. truncatula*. Read-count analysis, qRT-PCR measurements and *in situ* hybridizations clearly indicated a regulation of miR5229a/b, miR5204, miR160f*, miR160c, miR169 and miR169d*/l*/m*/e.2* during arbuscular mycorrhizal symbiosis. Moreover, miR5204* represses a GRAS TF, which is specifically transcribed in mycorrhizal roots. Since miR5204* is induced by high P_i it might represent a further P_i status-mediating signal beside miR399. This study provides additional evidence that MtNsp2, a key regulator of symbiosis-signaling, is regulated and presumably spatially restricted by miR171h cleavage.

In summary, a repression of mycorrhizal root colonization at high phosphate status is most likely due to a repression of the phosphate starvation responses and the loss of beneficial responses in mycorrhizal shoots. These findings provide a new basis for investigating the regulatory network leading to cellular reprogramming during interaction between plants, arbuscular mycorrhizal fungi and different phosphate conditions.

6. REFERENCES

Akiyama K, Hayashi H (2006) Strigolactones: chemical signals for fungal symbionts and parasitic weeds in plant roots. Annals of Botany (Lond) **97:** 925-931

Akiyama K, Matsuzaki K, Hayashi H (2005) Plant sesquiterpenes induce hyphal branching in arbuscular mycorrhizal fungi. Nature **435:** 824-827

Aung K, Lin SI, Wu CC, Huang YT, Su CL, Chiou TJ (2006) pho2, a phosphate overaccumulator, is caused by a nonsense mutation in a microRNA399 target gene. Plant Physiology **141:** 1000-1011

Bago B, Pfeffer PE, Shachar-Hill Y (2000) Carbon metabolism and transport in arbuscular mycorrhizas. Plant Physiology **124:** 949-957

Baldwin IT, Halitschke R, Paschold A, von Dahl CC, Preston CA (2006) Volatile signaling in plant-plant interactions: "talking trees" in the genomics era. Science **311:** 812-815

Balzergue C, Puech-Pages V, Becard G, Rochange SF (2011) The regulation of arbuscular mycorrhizal symbiosis by phosphate in pea involves early and systemic signalling events. Journal of Experimental Botany **62:** 1049-1060

Bari R, Datt Pant B, Stitt M, Scheible WR (2006) PHO2, microRNA399, and PHR1 Define a Phosphate-Signaling Pathway in Plants. Plant Physiology **141:** 988-999

Barker DG, Pfaff T, Moreau D, Groves E, Ruffel S, Lepetit M, Whitehand S, Maillet F, Nair RM, Journet EP (2006) Growing *M. truncatula*: choice of substrates and growth conditions. *In Medicago truncatula* handbook version November 2006. http://www.noble.org/MedicagoHandbook/

Bartel DP (2004) MicroRNAs: genomics, biogenesis, mechanism, and function. Cell **116:** 281-297

Bartel DP (2009) MicroRNAs: target recognition and regulatory functions. Cell **136:** 215-233

Bednarek P, Osbourn A (2009) Plant-microbe interactions: chemical diversity in plant defense. Science **324:** 746-748

Benedito VA, Torres-Jerez I, Murray JD, Andriankaja A, Allen S, Kakar K, Wandrey M, Verdier J, Zuber H, Ott T, Moreau S, Niebel A, Frickey T, Weiller G, He J, Dai X, Zhao PX, Tang Y, Udvardi MK (2008) A gene expression atlas of the model legume Medicago truncatula. Plant Journal

Bennett EM, Carpenter SR, Caraco NF (2001) Human impact on erodable phosphorus and eutrophication: A global perspective. Bioscience **51:** 227-234

Berezikov E, Liu N, Flynt AS, Hodges E, Rooks M, Hannon GJ, Lai EC (2010) Evolutionary flux of canonical microRNAs and mirtrons in Drosophila. Nature Genetics **42:** 6-9

Berezikov E, Robine N, Samsonova A, Westholm JO, Naqvi A, Hung JH, Okamura K, Dai Q, Bortolamiol-Becet D, Martin R, Zhao Y, Zamore PD, Hannon GJ, Marra MA, Weng Z, Perrimon N, Lai EC (2011) Deep annotation of *Drosophila melanogaster* microRNAs yields insights into their processing, modification, and emergence. Genome Research **21:** 203-215

Besserer A, Becard G, Jauneau A, Roux C, Sejalon-Delmas N (2008) GR24, a synthetic analog of strigolactones, stimulates the mitosis and growth of the arbuscular mycorrhizal fungus *Gigaspora rosea* by boosting its energy metabolism. Plant Physiology **148:** 402-413

Besserer A, Puech-Pages V, Kiefer P, Gomez-Roldan V, Jauneau A, Roy S, Portais JC, Roux C, Becard G, Sejalon-Delmas N (2006) Strigolactones stimulate arbuscular mycorrhizal fungi by activating mitochondria. PLoS Biology **4:** e226

Bhat KKS, Nye PH (1973) Diffusion of phosphate to plant roots in soil. 1. Quantitative autoradiography of depletion zone. Plant and Soil **38:** 161

Bieleski RL (1973) Phosphate pools, phosphate transport, and phosphate availability. Annu Rev Plant Physiology Plant Molecular Biolology **24:** 225-252

Boisson-Dernier A, Chabaud M, Garcia F, Becard G, Rosenberg C, Barker DG (2001) *Agrobacterium rhizogenes*-transformed roots of *Medicago truncatula* for the study of nitrogen-fixing and endomycorrhizal symbiotic associations. Molecular Plant Microbe Interaction **14:** 695-700.

Boldt K, Pors Y, Haupt B, Bitterlich M, Kuhn C, Grimm B, Franken P (2011) Photochemical processes, carbon assimilation and RNA accumulation of sucrose transporter genes in tomato arbuscular mycorrhiza. Journal of Plant Physiology **168:** 1256-1263

Borsani O, Zhu J, Verslues PE, Sunkar R, Zhu JK (2005) Endogenous siRNAs derived from a pair of natural *cis*-antisense transcripts regulate salt tolerance in *Arabidopsis*. Cell **123:** 1279-1291

Boualem A, Laporte P, Jovanovic M, Laffont C, Plet J, Combier JP, Niebel A, Crespi M, Frugier F (2008) MicroRNA166 controls root and nodule development in *Medicago truncatula*. Plant Journal **54:** 876-887

Branscheid A, Sieh D, Pant BD, May P, Devers EA, Elkrog A, Schauser L, Scheible WR, Krajinski F (2010) Expression pattern suggests a role of MiR399 in the regulation of the cellular response to local Pi increase during arbuscular mycorrhizal symbiosis. Mol Plant Microbe Interact **23:** 915-926

Breuillin F, Schramm J, Hajirezaei M, Ahkami A, Favre P, Druege U, Hause B, Bucher M, Kretzschmar T, Bossolini E, Kuhlemeier C, Martinoia E, Franken P, Scholz U, Reinhardt D (2010) Phosphate systemically inhibits development of arbuscular mycorrhiza in *Petunia hybrida* and represses genes involved in mycorrhizal functioning. Plant Journal **64:** 1002-1017

Brodersen P, Sakvarelidze-Achard L, Bruun-Rasmussen M, Dunoyer P, Yamamoto YY, Sieburth L, Voinnet O (2008) Widespread translational inhibition by plant miRNAs and siRNAs. Science **320:** 1185-1190

Buhtz A, Springer F, Chappell L, Baulcombe DC, Kehr J (2008) Identification and characterization of small RNAs from the phloem of *Brassica napus*. Plant Journal **53:** 739-749

Burleigh SH, Harrison MJ (1997) A novel gene whose expression in Medicago truncatula roots is suppressed in response to colonization by vesicular-arbuscular mycorrhizal (VAM) fungi and to phosphate nutrition. Plant Molecular Biology **34:** 199-208

Cai X, Hagedorn CH, Cullen BR (2004) Human microRNAs are processed from capped, polyadenylated transcripts that can also function as mRNAs. Rna **10:** 1957-1966

Caravaca F, Diaz E, Barea JM, Azcon-Aguilar C, Roldan A (2003) Photosynthetic and transpiration rates of *Olea europaea* subsp *sylvestris* and *Rhamnus lycioides* as affected by water deficit and mycorrhiza. Biologia Plantarum **46:** 637-639

Carthew RW, Sontheimer EJ (2009) Origins and Mechanisms of miRNAs and siRNAs. Cell **136:** 642-655

Catoira R, Galera C, de Billy F, Penmetsa RV, Journet EP, Maillet F, Rosenberg C, Cook D, Gough C, Denarie J (2000) Four genes of Medicago truncatula controlling components of a nod factor transduction pathway. Plant Cell **12:** 1647-1666.

Chen C, Ridzon DA, Broomer AJ, Zhou Z, Lee DH, Nguyen JT, Barbisin M, Xu NL, Mahuvakar VR, Andersen MR, Lao KQ, Livak KJ, Guegler KJ (2005) Real-time quantification of microRNAs by stem-loop RT-PCR. Nucleic Acids Research **33:** e179

Chen X (2008) A silencing safeguard: links between RNA silencing and mRNA processing in Arabidopsis. Developmental Cell **14:** 811-812

Chiang HR, Schoenfeld LW, Ruby JG, Auyeung VC, Spies N, Baek D, Johnston WK, Russ C, Luo S, Babiarz JE, Blelloch R, Schroth GP, Nusbaum C, Bartel DP (2010) Mammalian microRNAs: experimental evaluation of novel and previously annotated genes. Genes & Development **24:** 992-1009

Chinnusamy V, Gong Z, Zhu JK (2008) Nuclear RNA export and its importance in abiotic stress responses of plants. Current Topics in Microbiology and Immunology **326:** 235-255

Chiou TJ, Aung K, Lin SI, Wu CC, Chiang SF, Su CL (2006) Regulation of Phosphate Homeostasis by MicroRNA in *Arabidopsis*. Plant Cell **18:** 412-421

Chiou TJ, Lin SI (2011) Signaling network in sensing phosphate availability in plants. Annual Review of Plant Biology **62:** 185-206

Combier JP, Frugier F, de Billy F, Boualem A, El-Yahyaoui F, Moreau S, Vernié T, Ott T, Gamas P, Crespi M, Niebel A (2006) MtHAP2-1 is a key transcriptional regulator of symbiotic nodule development regulated by microRNA169 in Medicago truncatula. Genes & Development **20:** 3084-3088

Dai X, Zhao PX (2011) psRNATarget: a plant small RNA target analysis server. Nucleic Acids Research **doi:10.1093/nar/gkr319**

Degenhardt J, Hiltpold I, Kollner TG, Frey M, Gierl A, Gershenzon J, Hibbard BE, Ellersieck MR, Turlings TC (2009) Restoring a maize root signal that attracts insect-killing nematodes to control a major pest. PNAS U S A **106:** 13213-13218

Delano-Frier JP, Tejeda-Sartorius M, de la Vega OM (2008) Jasmonic acid influences mycorrhizal colonization in tomato plants by modifying the expression of genes involved in carbohydrate partitioning. Physiologia Plantarum **133:** 339-353

Delhaize E, Randall PJ (1995) Characterization of a Phosphate-Accumulator Mutant of *Arabidopsis thaliana*. Plant Physiology **107:** 207-213

deMiranda JCC, Harris PJ (1994) Effects of soil phosphorus on spore germination and hyphal growth of arbuscular mycorrhizal fungi. New Phytologist **128:** 103-108

Devers EA, Branscheid A, May P, Krajinski F (2011) Stars and symbiosis: microRNA- and microRNA*-mediated transcript cleavage involved in arbuscular mycorrhizal symbiosis. Plant Physiology **doi:10.1104/pp.111.172627**

Doll J, Hause B, Demchenko K, Pawlowski K, Krajinski F (2003) A member of the germin-like protein family is a highly conserved mycorrhiza-specific induced gene. Plant Cell Physiology **44:** 1208-1214

Dong B, Rengel Z, Delhaize E (1998) Uptake and translocation of phosphate by pho2 mutant and wild-type seedlings of *Arabidopsis thaliana*. Planta **205:** 251-256

Dunoyer P, Himber C, Voinnet O (2006) Induction, suppression and requirement of RNA silencing pathways in virulent Agrobacterium tumefaciens infections. Nature Genetics **38:** 258-263

Ebhardt HA, Fedynak A, Fahlman RP (2010) Naturally occurring variations in sequence length creates microRNA isoforms that differ in argonaute effector complex specificity. Silence **1:** 12

Elbashir SM, Lendeckel W, Tuschl T (2001a) RNA interference is mediated by 21- and 22-nucleotide RNAs. Genes & Development **15:** 188-200

Elbashir SM, Martinez J, Patkaniowska A, Lendeckel W, Tuschl T (2001b) Functional anatomy of siRNAs for mediating efficient RNAi in *Drosophila melanogaster* embryo lysate. The EMBO Journal **20:** 6877-6888

Fahlgren N, Howell MD, Kasschau KD, Chapman EJ, Sullivan CM, Cumbie JS, Givan SA, Law TF, Grant SR, Dangl JL, Carrington JC (2007) High-throughput

sequencing of Arabidopsis microRNAs: evidence for frequent birth and death of MIRNA genes. PLoS ONE **2:** e219

Fiorilli V, Catoni M, Miozzi L, Novero M, Accotto GP, Lanfranco L (2009) Global and cell-type gene expression profiles in tomato plants colonized by an arbuscular mycorrhizal fungus. New Phytologist **184:** 975-987

Fitze D, Wiepning A, Kaldorf M, Ludwig-Muller J (2005) Auxins in the development of an arbuscular mycorrhizal symbiosis in maize. Journal of Plant Physiology **162:** 1210-1219

Franco-Zorrilla JM, Gonzalez E, Bustos R, Linhares F, Leyva A, Paz-Ares J (2004) The transcriptional control of plant responses to phosphate limitation. Journal of Experimental Botany **55:** 285-293

Franco-Zorrilla JM, Valli A, Todesco M, Mateos I, Puga MI, Rubio-Somoza I, Leyva A, Weigel D, Garcia JA, Paz-Ares J (2007) Target mimicry provides a new mechanism for regulation of microRNA activity. Nature Genetics **39:** 1033-1037

Frenzel A, Manthey K, Perlick AM, Meyer F, Puhler A, Kuster H, Krajinski F (2005) Combined transcriptome profiling reveals a novel family of arbuscular mycorrhizal-specific Medicago truncatula lectin genes. Molecular Plant Microbe Interactions **18:** 771-782

Friedlaender MR, Chen W, Adamidi C, Maaskola J, Einspanier R, Knespel S, Rajewsky N (2008) Discovering microRNAs from deep sequencing data using miRDeep. Nature Biotechnology **26:** 407-415

Gabriel-Neumann E, Neumann G, Leggewie G, George E (2011) Constitutive overexpression of the sucrose transporter *SoSUT1* in potato plants increases arbuscular mycorrhiza fungal root colonization under high, but not under low, soil phosphorus availability. Journal of Plant Physiology **168:** 911-919

Garcia-Rodriguez S, Pozo MJ, Azcon-Aguilar C, Ferrol N (2005) Expression of a tomato sugar transporter is increased in leaves of mycorrhizal or *Phytophthora parasitica*-infected plants. Mycorrhiza **15:** 489-496

German MA, Pillay M, Jeong DH, Hetawal A, Luo S, Janardhanan P, Kannan V, Rymarquis LA, Nobuta K, German R, De Paoli E, Lu C, Schroth G, Meyers BC, Green PJ (2008) Global identification of microRNA-target RNA pairs by parallel analysis of RNA ends. Nature Biotechnology **26:** 941-946

Gershenzon J (2007) Plant volatiles carry both public and private messages. PNAS U S A **104:** 5257-5258

Gershenzon J, Dudareva N (2007) The function of terpene natural products in the natural world. Nature Chemical Biology **3:** 408-414

Ghildiyal M, Zamore PD (2009) Small silencing RNAs: an expanding universe. Nature Reviews Genetics **10:** 94-108

Gomez SK, Javot H, Deewatthanawong P, Torres-Jerez I, Tang Y, Blancaflor EB, Udvardi MK, Harrison MJ (2009) Medicago truncatula and Glomus intraradices gene expression in cortical cells harboring arbuscules in the arbuscular mycorrhizal symbiosis. BMC Plant Biology **9:** 10

Griffiths-Jones S, Hui JH, Marco A, Ronshaugen M (2011) MicroRNA evolution by arm switching. EMBO Reports **12:** 172-177

Griffiths-Jones S, Saini HK, van Dongen S, Enright AJ (2008) miRBase: tools for microRNA genomics. Nucleic Acids Research **36:** D154-158

Gu M, Xu K, Chen AQ, Zhu YY, Tang GL, Xu GH (2010) Expression analysis suggests potential roles of microRNAs for phosphate and arbuscular mycorrhizal signaling in *Solanum lycopersicum*. Physiologia Plantarum **138:** 226-237

Hammond JP, White PJ (2011) Sugar signalling in root responses to low P availability. Plant Physiology

Hanlon MT, Coenen C (2010) Genetic evidence for auxin involvement in arbuscular mycorrhiza initiation. New Phytologist

Harrison MJ (1999) Molecular and Cellular Aspects of the Arbuscular Mycorrhizal Symbiosis. Annual Reviews of Plant Physiology Plant Molecular Biology **50:** 361-389

Harrison MJ, Dewbre GR, Liu J (2002) A Phosphate Transporter from *Medicago truncatula* Involved in the Acquisition of Phosphate Released by Arbuscular Mycorrhizal Fungi. Plant Cell **14:** 2413-2429

Hause B, Fester T (2005) Molecular and cell biology of arbuscular mycorrhizal symbiosis. Planta **221:** 184-196

He L, Hannon GJ (2004) MicroRNAs: small RNAs with a big role in gene regulation. Nature Reviews Genetics **5:** 522-531

He X, Nara K (2007) Element biofortification: can mycorrhizas potentially offer a more effective and sustainable pathway to curb human malnutrition? Trends in Plant Science **12:** 331-333

Hernandez G, Ramirez M, Valdes-Lopez O, Tesfaye M, Graham MA, Czechowski T, Schlereth A, Wandrey M, Erban A, Cheung F, Wu HC, Lara M, Town CD, Kopka J, Udvardi MK, Vance CP (2007) Phosphorus stress in common bean: Root transcript and metabolic responses. Plant Physiology **144:** 752-767

Hirsch S, Kim J, Munoz A, Heckmann AB, Downie JA, Oldroyd GE (2009) GRAS proteins form a DNA binding complex to induce gene expression during nodulation signaling in *Medicago truncatula*. Plant Cell **21:** 545-557

Hoagland DR, Arnon DI (1950) The water-culture method of growing plants without soil. Calif. Agr. Expt. Sta. Circ **347**

Hohnjec N, Perlick AM, Puhler A, Kuster H (2003) The *Medicago truncatula* sucrose synthase gene MtSucS1 is activated both in the infected region of root nodules and in the cortex of roots colonized by arbuscular mycorrhizal fungi. Molecular Plant-Microbe Interactions **16:** 903-915

Hohnjec N, Vieweg MF, Puhler A, Becker A, Kuster H (2005) Overlaps in the transcriptional profiles of Medicago truncatula roots inoculated with two different Glomus fungi provide insights into the genetic program activated during arbuscular mycorrhiza. Plant Physiology **137:** 1283-1301

Hsieh LC, Lin SI, Shih ACC, Chen JW, Lin WY, Tseng CY, Li WH, Chiou TJ (2009) Uncovering Small RNA-Mediated Responses to Phosphate Deficiency in Arabidopsis by Deep Sequencing. Plant Physiology **151:** 2120-2132

Isayenkov S, Fester T, Hause B (2004) Rapid determination of fungal colonization and arbuscule formation in roots of Medicago truncatula using real-time (RT) PCR. Journal of Plant Physiology **161:** 1379-1383

Itaya K, Ui M (1966) A new micromethod for the colorimetric determination of inorganic phosphate. Clinica Chimica Acta **14:** 361-366

Jagadeeswaran G, Zheng Y, Li YF, Shukla LI, Matts J, Hoyt P, Macmil SL, Wiley GB, Roe BA, Zhang W, Sunkar R (2009) Cloning and characterization of small RNAs from Medicago truncatula reveals four novel legume-specific microRNA families. New Phytologist **184:** 85-98

Jagadeeswaran G, Zheng Y, Sumathipala N, Jiang HB, Arrese EL, Soulages JL, Zhang WX, Sunkar R (2010) Deep sequencing of small RNA libraries reveals dynamic regulation of conserved and novel microRNAs and microRNA-stars during silkworm development. Bmc Genomics **11:** -

Javot H, Pumplin N, Harrison MJ (2007) Phosphate in the arbuscular mycorrhizal symbiosis: transport properties and regulatory roles. Plant, Cell & Environment **30:** 310-322

Jentschel K, Thiel D, Rehn F, Ludwig-Muller J (2007) Arbuscular mycorrhiza enhances auxin levels and alters auxin biosynthesis in *Tropaeolum majus* during early stages of colonization. Physiologia Plantarum **129:** 320-333

Kalo P, Gleason C, Edwards A, Marsh J, Mitra RM, Hirsch S, Jakab J, Sims S, Long SR, Rogers J, Kiss GB, Downie JA, Oldroyd GE (2005) Nodulation signaling in legumes requires NSP2, a member of the GRAS family of transcriptional regulators. Science **308:** 1786-1789

Karimi M, Inze D, Depicker A (2002) GATEWAY vectors for Agrobacterium-mediated plant transformation. Trends in Plant Science **7:** 193-195

Kessler A, Baldwin IT (2001) Defensive function of herbivore-induced plant volatile emissions in nature. Science **291:** 2141-2144

Kessler D, Gase K, Baldwin IT (2008) Field experiments with transformed plants reveal the sense of floral scents. Science **321:** 1200-1202

Khvorova A, Reynolds A, Jayasena SD (2003) Functional siRNAs and miRNAs exhibit strand bias. Cell **115:** 209-216

Kidner CA, Martienssen RA (2005) The developmental role of microRNA in plants. Current Opinions in Plant Biology **8:** 38-44

Kosuta S, Chabaud M, Lougnon G, Gough C, Denarie J, Barker DG, Becard G (2003) A diffusible factor from arbuscular mycorrhizal fungi induces symbiosis-specific MtENOD11 expression in roots of Medicago truncatula. Plant Physiology **131:** 952-962

Kosuta S, Hazledine S, Sun J, Miwa H, Morris RJ, Downie JA, Oldroyd GE (2008) Differential and chaotic calcium signatures in the symbiosis signaling pathway of legumes. PNAS U S A **105:** 9823-9828

Krajinski F, Frenzel A (2007) Towards the elucidation of AM-specific transcription in Medicago truncatula. Phytochemistry **68:** 75-81

Krajinski F, Hause B, Gianinazzi-Pearson V, Franken P (2002) Mtha1, a plasma membrane H^+-ATPase gene from *Medicago truncatula*, shows arbuscule-specific induced expression in mycorrhizal tissue. Plant Biology **4:** 754-761

Laporte P, Merchan F, Amor BB, Wirth S, Crespi M (2007) Riboregulators in plant development. Biochemical Society Transactions **35:** 1638-1642

Lee Y, Kim M, Han J, Yeom KH, Lee S, Baek SH, Kim VN (2004) MicroRNA genes are transcribed by RNA polymerase II. The EMBO Journal **23:** 4051-4060

Lelandais-Briere C, Naya L, Sallet E, Calenge F, Frugier F, Hartmann C, Gouzy J, Crespi M (2009) Genome-wide Medicago truncatula small RNA analysis revealed novel microRNAs and isoforms differentially regulated in roots and nodules. Plant Cell **21:** 2780-2796

Lin SI, Chiang SF, Lin WY, Chen JW, Tseng CY, Wu PC, Chiou TJ (2008) Regulatory Network of MicroRNA399 and *PHO2* by Systemic Signaling. Plant Physiology **147:** 732-746

Liu J, Blaylock LA, Endre G, Cho J, Town CD, VandenBosch KA, Harrison MJ (2003) Transcript profiling coupled with spatial expression analyses reveals genes involved in distinct developmental stages of an arbuscular mycorrhizal symbiosis. Plant Cell **15:** 2106-2123

Liu J, Carmell MA, Rivas FV, Marsden CG, Thomson JM, Song JJ, Hammond SM, Joshua-Tor L, Hannon GJ (2004) Argonaute2 is the catalytic engine of mammalian RNAi. Science **305:** 1437-1441

Liu J, Maldonado-Mendoza I, Lopez-Meyer M, Cheung F, Town CD, Harrison MJ (2007) Arbuscular mycorrhizal symbiosis is accompanied by local and systemic alterations in gene expression and an increase in disease resistance in the shoots. Plant Journal **50:** 529-544

Liu J, Vance CP (2010) Crucial roles of sucrose and microRNA399 in systemic signaling of P deficiency: A tale of two team players? Plant Signaling & Behavior **5**

Liu JQ, Allan DL, Vance CP (2010) Systemic signaling and local sensing of phosphate in common bean: cross-talk between photosynthate and microRNA399. Molecular Plant **3:** 428-437

Liu PP, Montgomery TA, Fahlgren N, Kasschau KD, Nonogaki H, Carrington JC (2007) Repression of AUXIN RESPONSE FACTOR10 by microRNA160 is critical for seed germination and post-germination stages. Plant Journal **52:** 133-146

Lohse M, Nunes-Nesi A, Kruger P, Nagel A, Hannemann J, Giorgi FM, Childs L, Osorio S, Walther D, Selbig J, Sreenivasulu N, Stitt M, Fernie AR, Usadel B (2010) Robin: An Intuitive Wizard Application for R-Based Expression Microarray Quality Assessment and Analysis. Plant Physiology **153:** 642-651

Lopez-Raez JA, Charnikhova T, Gomez-Roldan V, Matusova R, Kohlen W, De Vos R, Verstappen F, Puech-Pages V, Becard G, Mulder P, Bouwmeester H (2008) Tomato strigolactones are derived from carotenoids and their biosynthesis is promoted by phosphate starvation. New Phytologist **178:** 863-874

Lu C, Jeong DH, Kulkarni K, Pillay M, Nobuta K, German R, Thatcher SR, Maher C, Zhang L, Ware D, Liu B, Cao X, Meyers BC, Green PJ (2008) Genome-wide analysis for discovery of rice microRNAs reveals natural antisense microRNAs (nat-miRNAs). PNAS U S A **105:** 4951-4956

Lu XY, Huang XL (2008) Plant miRNAs and abiotic stress responses. Biochemical and Biophysical Research Communications **368:** 458-462

Maillet F, Poinsot V, Andre O, Puech-Pages V, Haouy A, Gueunier M, Cromer L, Giraudet D, Formey D, Niebel A, Martinez EA, Driguez H, Becard G, Denarie J (2011) Fungal lipochitooligosaccharide symbiotic signals in arbuscular mycorrhiza. Nature **469:** 58-U1501

Marschner H (1995) Mineral nutrition of higher plants, Ed 2. Academic Press, London

Mathur N, Vyas A (1995) Influence of VA mycorrhizae on net photosynthesis and transpiration of *Ziziphus mauritiana*. Journal of Plant Physiology **147:** 328-330

Meister G, Landthaler M, Patkaniowska A, Dorsett Y, Teng G, Tuschl T (2004) Human Argonaute2 mediates RNA cleavage targeted by miRNAs and siRNAs. Molecular Cell **15:** 185-197

Meng Y, Gou L, Chen D, Wu P, Chen M (2010) High-throughput degradome sequencing can be used to gain insights into microRNA precursor metabolism. Journal of Experimental Botany **61:** 3833-3837

Menge JA, Steirle D, Bagyaraj DJ, Johnson ELV, Leonard RT (1978) Phosphorus concentrations in plants responsible for inhibition of mycorrhizal infection. New Phytologist **80:** 575-578

Mengel K (1997) Agronomic measures for better utilization of soil and fertilizer phosphates. European Journal of Agronomy **7:** 221-233

Meyers BC, Axtell MJ, Bartel B, Bartel DP, Baulcombe D, Bowman JL, Cao X, Carrington JC, Chen X, Green PJ, Griffiths-Jones S, Jacobsen SE, Mallory AC, Martienssen RA, Poethig RS, Qi Y, Vaucheret H, Voinnet O, Watanabe Y, Weigel D, Zhu JK (2008) Criteria for annotation of plant MicroRNAs. Plant Cell **20:** 3186-3190

Mica E, Piccolo V, Delledonne M, Ferrarini A, Pezzotti M, Casati C, Del Fabbro C, Valle G, Policriti A, Morgante M, Pesole G, Pè ME, Horner DS (2009) High throughput approaches reveal splicing of primary microRNA transcripts and tissue specific expression of mature microRNAs in *Vitis vinifera*. BMC Genomics **10:** 558

Misson J, Raghothama KG, Jain A, Jouhet J, Block MA, Bligny R, Ortet P, Creff A, Somerville S, Rolland N, Doumas P, Nacry P, Herrerra-Estrella L, Nussaume L,

Thibaud MC (2005) A genome-wide transcriptional analysis using *Arabidopsis thaliana* Affymetrix gene chips determined plant responses to phosphate deprivation. PNAS USA **102:** 11934-11939

Morcuende R, Bari R, Gibon Y, Zheng WM, Pant BD, Blasing O, Usadel B, Czechowski T, Udvardi MK, Stitt M, Scheible WR (2007) Genome-wide reprogramming of metabolism and regulatory networks of Arabidopsis in response to phosphorus. Plant Cell and Environment **30:** 85-112

Nagahashi G, Doud DDJ, Abney GD (1996) Phosphorous amendment inhibit hyphal branching of the VAM fungus Gigaspora margarita directly and indirectly through its effect on root exudation. Mycorrhiza **6:** 403-408

Navarro L, Dunoyer P, Jay F, Arnold B, Dharmasiri N, Estelle M, Voinnet O, Jones JD (2006) A plant miRNA contributes to antibacterial resistance by repressing auxin signaling. Science **312:** 436-439

Navarro L, Jay F, Nomura K, He SY, Voinnet O (2008) Suppression of the microRNA pathway by bacterial effector proteins. Science **321:** 964-967

Nogueira FT, Sarkar AK, Chitwood DH, Timmermans MC (2006) Organ polarity in plants is specified through the opposing activity of two distinct small regulatory RNAs. Cold Spring Harbor Symposia on Quantitative Biology **71:** 157-164

Nuovo GJ (2010) In situ detection of microRNAs in paraffin embedded, formalin fixed tissues and the co-localization of their putative targets. Methods **52:** 307-315

Okamura K, Phillips MD, Tyler DM, Duan H, Chou YT, Lai EC (2008) The regulatory activity of microRNA* species has substantial influence on microRNA and 3' UTR evolution. Nature Structural Molecular Biology **15:** 354-363

Oldroyd GE, Long SR (2003) Identification and characterization of nodulation-signaling pathway 2, a gene of *Medicago truncatula* involved in Nod actor signaling. Plant Physiology **131:** 1027-1032

Ozanne PG (1980) Phosphate nutrition in plants - a general treatise. *In* FE Khasawneh, EC Sample, EJ Kamprath, eds, The Role of Phosphorus in Agriculture. American Society of Agronomy, Madison, pp 559-589

Pant BD, Buhtz A, Kehr J, Scheible WR (2008) MicroRNA399 is a long-distance signal for the regulation of plant phosphate homeostasis. Plant Journal **53:** 731-738

Pant BD, Musialak-Lange M, Nuc P, May P, Buhtz A, Kehr J, Walther D, Scheible WR (2009) Identification of Nutrient-Responsive Arabidopsis and Rapeseed MicroRNAs by Comprehensive Real-Time Polymerase Chain Reaction Profiling and Small RNA Sequencing. Plant Physiology **150:** 1541-1555

Papp I, Mette MF, Aufsatz W, Daxinger L, Schauer SE, Ray A, van der Winden J, Matzke M, Matzke AJ (2003) Evidence for nuclear processing of plant micro RNA and short interfering RNA precursors. Plant Physiology **132:** 1382-1390

Park MY, Wu G, Gonzalez-Sulser A, Vaucheret H, Poethig RS (2005) Nuclear processing and export of microRNAs in Arabidopsis. PNAS U S A **102:** 3691-3696

Park W, Li J, Song R, Messing J, Chen X (2002) CARPEL FACTORY, a Dicer homolog, and HEN1, a novel protein, act in microRNA metabolism in Arabidopsis thaliana. Current Biology **12:** 1484-1495

Parniske M (2008) Arbuscular mycorrhiza: the mother of plant root endosymbioses. Nature Reviews Microbiology **6:** 763-775

Pena JT, Sohn-Lee C, Rouhanifard SH, Ludwig J, Hafner M, Mihailovic A, Lim C, Holoch D, Berninger P, Zavolan M, Tuschl T (2009) miRNA in situ hybridization in formaldehyde and EDC-fixed tissues. Nature Methods **6:** 139-141

Penmetsa RV, Uribe P, Anderson J, Lichtenzveig J, Gish JC, Nam YW, Engstrom E, Xu K, Sckisel G, Pereira M, Baek JM, Lopez-Meyer M, Long SR, Harrison MJ, Singh KB, Kiss GB, Cook DR (2008) The *Medicago truncatula* ortholog of

Arabidopsis EIN2, sickle, is a negative regulator of symbiotic and pathogenic microbial associations. Plant Journal **55:** 580-595

Phillips JR, Dalmay T, Bartels D (2007) The role of small RNAs in abiotic stress. FEBS Letter **581:** 3592-3597

Poirier Y, Bucher M (2002) Phosphate transport and homeostasis in Arabidopsis. *In* CR Somerville, EM Meyerowitz, eds, The Arabidopsis Book. American Society of Plant Biologists, p doi/10.1199/tab.0024

Pumplin N, Harrison MJ (2009) Live-cell imaging reveals periarbuscular membrane domains and organelle location in *Medicago truncatula* roots during arbuscular mycorrhizal symbiosis. Plant Physiology

Quandt HJ, Puehler A, I. B (1993) Transgenic root nodules of *Vicia hirsuta*: A fast and efficient system for the study of gene expression in indeterminate-type nodules. Molecular Plant-Microbe interactions **6:** 699-706

Raghothama KG (2000) Phosphate transport and signaling. Curr Opin Plant Biol **3:** 182-187

Rajagopalan R, Vaucheret H, Trejo J, Bartel DP (2006) A diverse and evolutionarily fluid set of microRNAs in *Arabidopsis thaliana*. Genes & Development **20:** 3407-3425

Ramakers C, Ruijter JM, Deprez RH, Moorman AF (2003) Assumption-free analysis of quantitative real-time polymerase chain reaction (PCR) data. Neuroscience Letters **339:** 62-66

Rausch C, Daram P, Brunner S, Jansa J, Laloi M, Leggewie G, Amrhein N, Bucher M (2001) A phosphate transporter expressed in arbuscule-containing cells in potato. Nature **414:** 462-470

Rhoades MW, Reinhart BJ, Lim LP, Burge CB, Bartel B, Bartel DP (2002) Prediction of plant microRNA targets. Cell **110:** 513-520

Rhodes LH, Gerdemann JW (1975) Phosphate uptake zones of mycorrhizal and non-mycorrhizal onions. New Phytologist **75:** 555

Ribot C, Wang Y, Poirier Y (2008) Expression analyses of three members of the *AtPHO1* family reveal differential interactions between signaling pathways involved in phosphate deficiency and the responses to auxin, cytokinin, and abscisic acid. Planta **227:** 1025-1036

Ruby JG, Jan C, Player C, Axtell MJ, Lee W, Nusbaum C, Ge H, Bartel DP (2006) Large-scale sequencing reveals 21U-RNAs and additional microRNAs and endogenous siRNAs in *C. elegans*. Cell **127:** 1193-1207

Ruby JG, Stark A, Johnston WK, Kellis M, Bartel DP, Lai EC (2007) Evolution, biogenesis, expression, and target predictions of a substantially expanded set of Drosophila microRNAs. Genome Research **17:** 1850-1864

Salzer P, Corbière H, Boller T (1999) Hydrogen peroxide accumulation in *Medicago truncatula* roots colonized by the arbuscular mycorrhiza-forming fungus *Glomus intraradices*. Planta **208:** 319-325

Sambrook J, Russell DW (2001) Molecular cloning: a laboratory manual, Ed 3. CSHL press, New York

Sanders FE (1975) The effect of foliar-applied phosphate on the mycorrhizal infections of onion roots. *In* FE Sanders, B Mosse, PB Tinker, eds, *Endomycorrhizas*. Academic Press, London, pp 261-276

Sanders IR, Croll D (2010) Arbuscular mycorrhiza: the challenge to understand the genetics of the fungal partner. Annual Review of Genetics **44:** 271-292

Schaarschmidt S, Hause B, Roitsch T (2006) Arbuscular mycorrhiza induces gene expression of the apoplastic invertase LIN6 in tomato (*Lycopersicon esculentum*) roots. Journal of Experimental Botany **57:** 4015-4023

Schwarz DS, Hutvágner G, Du T, Xu Z, Aronin N, Zamore PD (2003) Asymmetry in the assembly of the RNAi enzyme complex. Cell **115:** 199-208

Smit P, Raedts J, Portyanko V, Debelle F, Gough C, Bisseling T, Geurts R (2005) NSP1 of the GRAS protein family is essential for rhizobial Nod factor-induced transcription. Science **308:** 1789-1791

Smith SE, Jakobsen I, Groenlund M, Smith FA (2011) Roles of arbuscular mycorrhizas in plant phosphorus (P) nutrition: interactions between pathways of P uptake in arbuscular mycorrhizal (AM) roots have important implications for understanding and manipulating plant P acquisition. Plant Physiology

Smith SE, Read DJ (1997) Mycorrhizal symbiosis, Ed 2. Academic Press, San Diego and London

Smith SE, Read DJ (2008) Mycorrhizal Symbiosis, Ed 3. Elsevier, New York, London, Burlington and San Diego

Smyth GK (2005) Limma: linear models for microarray data. *In* R Gentleman, V Carey, S Dudoit, R Irizarry, W Huber, eds, Bioinformatics and Computational Biology Solutions using R and Bioconductor. Springer, New York, pp 397-420

Snowden KC, Simkin AJ, Janssen BJ, Templeton KR, Loucas HM, Simons JL, Karunairetnam S, Gleave AP, Clark DG, Klee HJ (2005) The Decreased apical dominance1/*Petunia hybrida* CAROTENOID CLEAVAGE DIOXYGENASE8 gene affects branch production and plays a role in leaf senescence, root growth, and flower development. Plant Cell **17:** 746-759

Stefanovic A, Ribot C, Rouached H, Wang Y, Chong J, Belbahri L, Delessert S, Poirier Y (2007) Members of the *PHO1* gene family show limited functional redundancy in phosphate transfer to the shoot, and are regulated by phosphate deficiency via distinct pathways. Plant Journal **50:** 982-994

Subramanian S, Fu Y, Sunkar R, Barbazuk WB, Zhu JK, Yu O (2008) Novel and nodulation-regulated microRNAs in soybean roots. BMC Genomics **9:** 160

Sunkar R, Chinnusamy V, Zhu J, Zhu JK (2007) Small RNAs as big players in plant abiotic stress responses and nutrient deprivation. Trends in Plant Science **12:** 301-309

Szittya G, Moxon S, Santos DM, Jing R, Fevereiro MP, Moulton V, Dalmay T (2008) High-throughput sequencing of *Medicago truncatula* short RNAs identifies eight new miRNA families. BMC Genomics **9:** 593

Tadege M, Wen J, He J, Tu H, Kwak Y, Eschstruth A, Cayrel A, Endre G, Zhao PX, Chabaud M, Ratet P, Mysore KS (2008) Large-scale insertional mutagenesis using the *Tnt1* retrotransposon in the model legume *Medicago truncatula*. Plant Journal **54:** 335-347

Thimm O, Blasing O, Gibon Y, Nagel A, Meyer S, Kruger P, Selbig J, Muller LA, Rhee SY, Stitt M (2004) MAPMAN: a user-driven tool to display genomics data sets onto diagrams of metabolic pathways and other biological processes. Plant Journal **37:** 914-939

Ticconi CA, Abel S (2004) Short on phosphate: plant surveillance and countermeasures. Trends in Plant Science **9:** 548-555

Ticconi CA, Delatorre CA, Abel S (2001) Attenuation of Phosphate Starvation Responses by Phosphite in Arabidopsis. Plant Physiology **127:** 963-972

Tiessen H (2008) Phosphorus in the global environment. *In* PJ White, JP Hammond, eds, The Ecophysiology of Plant-Phosphorus Interactions, Vol 7. Springer, New York, pp 1-7

Valdés-Lopéz O, Arenas-Huertero C, Ramírez M, Girard L, Sánchez F, Vance CP, Luis Reyes J, Hernández G (2008) Essential role of MYB transcription factor: PvPHR1 and microRNA: PvmiR399 in phosphorus-deficiency signalling in common bean roots. Plant, Cell & Environment **31:** 1834-1843

Vaucheret H, Vazquez F, Crete P, Bartel DP (2004) The action of ARGONAUTE1 in the miRNA pathway and its regulation by the miRNA pathway are crucial for plant development. Genes & Development **18:** 1187-1197

Vazquez F, Blevins T, Ailhas J, Boller T, Meins F, Jr. (2008) Evolution of Arabidopsis MIR genes generates novel microRNA classes. Nucleic Acids Research **36:** 6429-6438

Vazquez F, Gasciolli V, Crete P, Vaucheret H (2004) The nuclear dsRNA binding protein HYL1 is required for microRNA accumulation and plant development, but not posttranscriptional transgene silencing. Current Biology **14:** 346-351

Vickers CE, Gershenzon J, Lerdau MT, Loreto F (2009) A unified mechanism of action for volatile isoprenoids in plant abiotic stress. Nature Chemical Biology **5:** 283-291

Voinnet O (2008) Post-transcriptional RNA silencing in plant-microbe interactions: a touch of robustness and versatility. Current Opinions in Plant Biology **11:** 464-470

Voinnet O (2009) Origin, biogenesis, and activity of plant microRNAs. Cell **136:** 669-687

Walter MH, Hans J, Strack D (2002) Two distantly related genes encoding 1-deoxy-D-xylulose 5-phosphate synthases: differential regulation in shoots and apocarotenoid-accumulating mycorrhizal roots. Plant Journal **31:** 243-254

Wang CY, Chen YQ, Liu Q (2011) Sculpting the meristem: The roles of miRNAs in plant stem cells. Biochemical and Biophysical Research Communications **doi:10.1016/j.bbrc.2011.04.123**

Wang Y, Juranek S, Li H, Sheng G, Tuschl T, Patel DJ (2008a) Structure of an argonaute silencing complex with a seed-containing guide DNA and target RNA duplex. Nature **456:** 921-926

Wang Y, Sheng G, Juranek S, Tuschl T, Patel DJ (2008b) Structure of the guide-strand-containing argonaute silencing complex. Nature **456:** 209-213

Wasaki J, Yonetani R, Kuroda S, Shinano T, Yazaki J, Fujii F, Shimbo K, Yamamoto K, Sakata K, Sasaki T, Kishimoto N, Kikuchi S, Yamagishi M, Osaki M (2003) Transcriptomic analysis of metabolic changes by phosphorus stress in rice plant roots. Plant Cell and Environment **26:** 1515-1523

Welinder KG, Mauro JM, Norskov-Lauritsen L (1992) Structure of plant and fungal peroxidases. Biochemical Society Transactions **20:** 337-340

Willmann MR, Poethig RS (2007) Conservation and evolution of miRNA regulatory programs in plant development. Current Opinions in Plant Biology **10:** 503-511

Wright DP, Read DJ, Scholes JD (1998a) Mycorrhizal sink strength influences whole plant carbon balance of *Trifolium repens* L. Plant, Cell & Environment **21:** 881-891

Wright DP, Scholes JD, Read DJ (1998b) Effects of VA mycorrhizal colonization on photosynthesis and biomass production of *Trifolium repens* L. Plant, Cell & Environment **21:** 209-216

Wulf A, Manthey K, Doll J, Perlick AM, Linke B, Bekel T, Meyer F, Franken P, Küster H, Krajinski F (2003) Transcriptional changes in response to arbuscular mycorrhiza development in the model plant Medicago truncatula. Molecular Plant Microbe Interactions **16:** 306-314

Xie Z, Johansen LK, Gustafson AM, Kasschau KD, Lellis AD, Zilberman D, Jacobsen SE, Carrington JC (2004) Genetic and functional diversification of small RNA pathways in plants. PLoS Biology **2:** E104

Xie Z, Kasschau KD, Carrington JC (2003) Negative feedback regulation of Dicer-Like1 in *Arabidopsis* by microRNA-guided mRNA degradation. Current Biology **13:** 784-789

Yang JH, Li JH, Shao P, Zhou H, Chen YQ, Qu LH (2011) starBase: a database for exploring microRNA-mRNA interaction maps from Argonaute CLIP-Seq and Degradome-Seq data. Nucleic Acids Research

Yang Z, Ebright YW, Yu B, Chen X (2006) HEN1 recognizes 21-24 nt small RNA duplexes and deposits a methyl group onto the 2' OH of the 3' terminal nucleotide. Nucleic Acids Research **34:** 667-675

Yoneyama K, Xie X, Kusumoto D, Sekimoto H, Sugimoto Y, Takeuchi Y, Yoneyama K (2007) Nitrogen deficiency as well as phosphorus deficiency in sorghum promotes the production and exudation of 5-deoxystrigol, the host recognition signal for arbuscular mycorrhizal fungi and root parasites. Planta

Yoneyama K, Yoneyama K, Takeuchi Y, Sekimoto H (2007) Phosphorus deficiency in red clover promotes exudation of orobanchol, the signal for mycorrhizal symbionts and germination stimulant for root parasites. Planta **225:** 1031-1038

Yu B, Yang Z, Li J, Minakhina S, Yang M, Padgett RW, Steward R, Chen X (2005) Methylation as a crucial step in plant microRNA biogenesis. Science **307:** 932-935

Zhang WX, Gao S, Zhou XF, Xia J, Chellappan P, Zhou XA, Zhang XM, Jin HL (2010) Multiple distinct small RNAs originate from the same microRNA precursors. Genome Biology **11:** -

Zhang XM, Zhao HW, Gao S, Wang WC, Katiyar-Agarwal S, Huang HD, Raikhel N, Jin HL (2011) Arabidopsis Argonaute 2 Regulates Innate Immunity via miRNA393*-Mediated Silencing of a Golgi-Localized SNARE Gene, MEMB12. Molecular Cell **42:** 356-366

Zhao B, Ge L, Liang R, Li W, Ruan K, Lin H, Jin Y (2009) Members of miR-169 family are induced by high salinity and transiently inhibit the NF-YA transcription factor. BMC Molecular Biology **10:** 29

Zhou H, Huang X, Cui H, Luo X, Tang Y, Chen S, Wu L, Shen N (2010) miR-155 and its star-form partner miR-155* cooperatively regulate type I interferon production by human plasmacytoid dendritic cells. Blood

Zhou M, Gu L, Li P, Song X, Wei L, Chen Z, Cao X (2010) Degradome sequencing reveals endogenous small RNA targets in rice (Oryza sativa L. ssp. indica). Frontiers in Biology **1:** 67-90

Zhou X, Wang G, Zhang W (2007) UV-B responsive microRNA genes in *Arabidopsis thaliana*. Molecular Systems Biology **3:** 103

7. APPENDIX

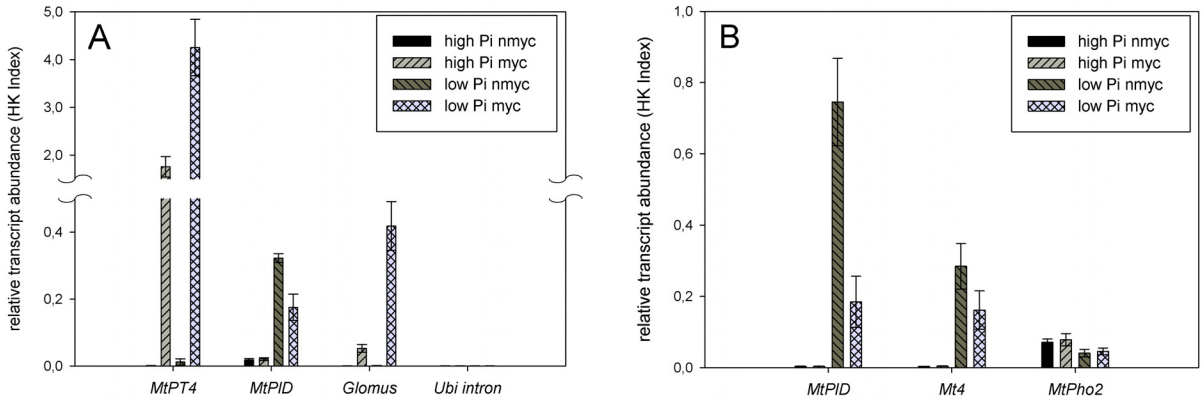

Figure 42: Relative expression levels of *MtPt4*, Glomus rRNA, *MtPlD*, *Mt4* and *MtPho2* as diagnostic markers for mycorrhizal colonization and P_i-stress responses prior to microarray hybridization. Quantitative RT-PCR measurements to analyze the expression of known mycorrhizal and phosphate starvation marker genes using cDNA from plant roots (A) and shoots (B). The cDNA was generated from RNA used for microarray hybridization. Ubi intron expression from plant roots is shown exemplary, and was measured in roots and shoots to check for genomic DNA contamination. (SD; n = 4 distinct biological replicates each consisting of pools of 4 individual plant roots or shoots).

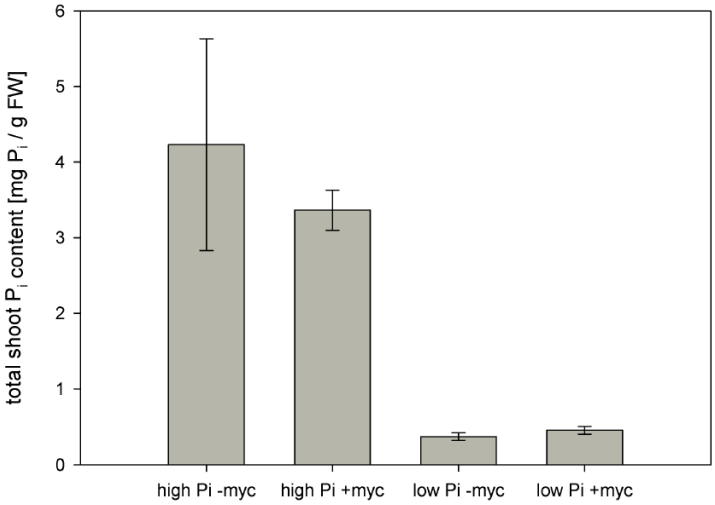

Figure 43: Total P_i concentrations in plant shoots of the split-root experiment whose RNA was used for microarray hybridization (SD; n = 4 independent pools of 4 plant shoots per conditions).

Table 10: Previously annotated miRNAs from *M. truncatula* identified by homology searches, and their most abundant isoform (isomiR)

miRNA	Sequence	Size	total reads				IsomiR	Sequence	Size	mature	
			mature		star						
		(nt)	myc	nm	myc	nm			(nt)	myc	nm
MIR156	TGACAGAAGAGAGAGAGCACA	21	2	0	0	0	156.2	TGACAGAAGAGAGAGAGCAC	20	178	191
MIR156b	TGACAGAAGAGAGTGAGCAC	20	77825	77075	9	15					
MIR156c	TGACAGAAGAGAGTGAGCAC	20	77825	77075	23	19					
MIR156d	TGACAGAAGAGAGTGAGCAC	20	77825	77075	0	0					

miRNA	Sequence	Size	total reads				IsomiR	Sequence	Size		
			mature		star					mature	
		(nt)	myc	nm	myc	nm			(nt)	myc	nm
MIR156e	**TTGACAGAAGATAGAGAGCAC**	21	**25080**	**15506**	0	0					
MIR156f	**TTGACAGAAGATAGAGAGCAC**	21	**25080**	**15506**	0	0					
MIR156g	TTGACAGAAGATAGAGGGCAC	21	35597	30752	4	4					
MIR156h	**TTGACAGAAGATAGAGAGCAC**	21	**25080**	**15506**	0	0					
MIR156i	TGACAGAAGAGAGTGAGCAC	20	77825	77075	8	5					
MIR159a	TTTGGATTGAAGGGAGCTCTA	21	2260	2021	1	4					
MIR160	TGCCTGGCTCCCTGTATGCCA	21	214	258	18	28					
MIR160b	TGCCTGGCTCCCTGTATGCCA	21	214	258	609	548					
MIR160c	**TGCCTGGCTCCCTGAATGCCA**	21	**118**	**23**	9	5					
MIR160d	TGCCTGGCTCCCTGTATGCCA	21	214	258	19	35					
MIR160e	TGCCTGGCTCCCTGTATGCCA	21	214	258	609	548					
MIR162	**TCGATAAACCTCTGCATCCAG**	21	**489**	**301**	44	62					
MIR164a	**TGGAGAAGCAGGGCACGTGCA**	21	**5219**	**8412**	1	0					
MIR164b	**TGGAGAAGCAGGGCACGTGCA**	21	**5219**	**8412**	1	1					
MIR164c	**TGGAGAAGCAGGGCACGTGCA**	21	**5219**	**8412**	3	1					
MIR164d	TGGAGAAGCAGGGCACATGCT	21	9	25	0	0					
MIR166	TCGGACCAGGCTTCATTCCCC	21	172542	180891	3	8					
MIR166b	TCGGACCAGGCTTCATTCCTA	21	44219	36842	129	109	**166b.2**	**TCTCGGACCAGGCTTCATTCC**	21	**46294**	**26376**
MIR166c	TCGGACCAGGCTTCATTCCTC	21	1122	972	0	0	**166c.2**	**TCTCGGACCAGGCTTCATTCC**	21	**46294**	**26376**
MIR166d	TCGGGCCAGGCTTCATCCCCC	21	0	1	0	0					
MIR166e	TCGGACCAGGCTTCATTCCCC	21	172542	180891	1111	1041					
MIR166f	TCGGACCAGGCTTCATTCCTC	21	1122	972	0	0	**166f.2**	**TCTCGGACCAGGCTTCATTCC**	21	**46294**	**26376**
MIR166g	TCGGACCAGGCTTCATTCCCC	21	172542	180891	2029	1935					
MIR166h	TCGGACCAGGCTTCATTCCCC	21	172542	180891	3	8					
MIR167	**TGAAGCTGCCAGCATGATCTA**	21	**7119**	**3348**	0	0					
MIR169a	CAGCCAAGGATGACTTGCCGA	21	6	4	0	1					
MIR169b	CAGCCAAGGATGACTTGCCGA	21	6	4	0	0					
MIR169c	CAGCCAAGGGTGATTTGCCGG	21	9	5	0	0					
MIR169d	**AAGCCAAGGATGACTTGCCGG**	21	**52**	**3**	**171**	**11**					
MIR169e	GGAGCCAAGGATGACTTGCCG	21	0	0	0	0	**169e.2***	**GGCAGGTCATCCTTCGGCTATA**	22	**171**	**11**
MIR169g	CAGCCAAGGATGACTTGCCGG	21	18	7	0	0					
MIR169h	GAGCCAAAGATGACTTGCCGG	21	0	0	0	0	169h.2	TGAGCCAAAGATGACTTGCCGG	22	17	2
MIR169i	TGAGCCAAAGATGACTTGCCG	21	0	0	0	0	169i.2	TGAGCCAAAGATGACTTGCCGG	22	17	2
MIR169j	CAGCCAAGGATGACTTGCCGG	21	18	7	0	0					
MIR169k	CAGCCAAGGGTGATTTGCCGG	21	9	5	0	0					
MIR169l	**AAGCCAAGGATGACTTGCCGG**	21	**52**	**3**	**171**	**11**					
MIR169m	**GAGCCAAGGATGACTTGCCGG**	21	7	2	**171**	**11**					
MIR169n	TGAGCCAAAGATGACTTGCCG	21	0	0	0	0	169n.2	TGAGCCAAAGATGACTTGCCGG	22	17	2
MIR169o	TGAGCCAAAGATGACTTGCCG	21	0	0	0	0	1690.2	TGAGCCAAAGATGACTTGCCGG	22	17	2
MIR169q	TGAGCCAGGATGACTTGCCGG	21	13	1	na	na					
MIR171	TGATTGAGTCGTGCCAATATC	21	43	57	1	0					
MIR171b	TGATTGAGCCGCGTCAATATC	21	29	8	4	1					
MIR171e	AGATTGAGCCGCGCCAATATC	21	0	1	0	0	171e.2*	CGATGTTGGTGAGGTTCAATC	21	79	89
MIR171f	TTGAGCCGTGCCAATATCACG	21	0	0	13	11					
MIR172	AGAATCCTGATGATGCTGCAG	21	145	103	66	43					
MIR319	TTGGACTGAAGGGAGCTCCC	20	0	6	0	2					
MIR319b	TTGGACTGAAGGGAGCTCCC	20	0	6	0	0					
MIR390	**AAGCTCAGGAGGGATAGCGCC**	21	**506**	**750**	10	8					
MIR393b	TCCAAAGGGATCGCATTGATC	21	0	0	0	0	393b.2*	ATCATGCTATCCCTTTGGATT	21	27	30
MIR396a	TTCCACAGCTTTCTTGAACTT	21	93	76	2542	2593					
MIR396b	**TTCCACAGCTTTCTTGAACTG**	21	1162	1123	**1016**	**603**					
MIR398a	TGTGTTCTCAGGTCACCCCTT	21	0	0	23	18					

miRNA	Sequence	Size	total reads				IsomiR	Sequence	Size	mature	
			mature		star						
		(nt)	myc	nm	myc	nm			(nt)	myc	nm
MIR398b	TGTGTTCTCAGGTCGCCCCTG	21	1	1	1	0					
MIR398c	TGTGTTCTCAGGTCGCCCCTG	21	1	1	0	0					
MIR399a	TGCCAAAGGAGATTTGCCCAG	21	297	265	9	23					
MIR399b	TGCCAAAGGAGAGCTGCCCTG	21	225	236	2	4					
MIR399c	TGCCAAAGGAGATTTGCCCTG	21	53	60	21	26					
MIR399d	TGCCAAAGGAGAGCTGCCCTA	21	408	416	18	32					
MIR399e	TGCCAAAGGAGATTTGCCCAG	21	297	265	9	23					
MIR399f	TGCCAAAGGAGATTTGCCCAG	21	297	265	9	23					
MIR399g	TGCCAAAGGAGATTTGCCCAG	21	297	265	2	2					
MIR399h	TGCCAAAGGAGATTTGCCCTG	21	53	60	8	6					
MIR399i	TGCCAAAGGAGATTTGCCCTG	21	53	60	0	0					
MIR399j	CGCCAAAGAAGATTTGCCCCG	21	55	65	16	30					
MIR399k	TGCCAAAGAAGATTTGCCCTG	21	122	116	71	108					
MIR399l	TGCCAAAGGAGAGTTGCCCTG	21	131	148	0	0					
MIR399m	TGCCAAAGGAGAGCTGCCCTA	21	408	416	18	32					
MIR399n	TGCCAAAGGAGAGCTGCCCTA	21	408	416	18	32					
MIR399o	TGCCAAAGGAGAGCTGCCCTG	21	225	236	18	32					
MIR399p	TGCCAAAGGAGAGTTGCCCTG	21	131	148	0	0					
MIR399q	TGCCAAAGGAGAGCTGCTCTT	21	110	89	na	na					
MIR1507	**CCTCGTTCCATACATCATCTAG**	22	**4008**	**2975**	870	723					
MIR1509a	TTAATCTAGGAAAATACGGTG	21	32	26	2	0	1509.2	TTAATCTAGGAAAATACGGTGG	22	2308	2067
MIR1509b	TTAATCTAGGAAATTACACTCG	22	4	0	na	na					
MIR1510a	**CGGAGGATTAGGTAAAACAAC**	21	**1397**	**947**	2	3					
MIR1510b	ACATGGTCGGTATCCCTGGAA	21	284	215	3	0	1510b.2	TGGAATGGAGGATCAGGTAAA	21	11392	8785
MIR2086	**GACATGAATGCAGAACTGGAA**	21	**17751**	**10053**	69	67					
MIR2087	GAAGTAAAGAACCGGCTGCAG	21	19	23	1	1					
MIR2088a	AGGCCTAGATTACATTGGAC	20	5	6	5	3	**2088.2***	**TCCAATGTAATCTAGGTCTAC**	21	**1197**	**855**
MIR2088b	**TCCAATGTAATCTAGGTCTAC**	21	**1197**	**855**	na	na					
MIR2089	**TTACCTATTCCACCAATTCCAT**	22	65	41	**1322**	**1023**					
MIR2111a	TAATCTGCATCCTGAGGTTTA	21	379	265	na	na					
MIR2111b	TAATCTGCATCCTGAGGTTTA	21	379	265	na	na					
MIR2111c	TAATCTGCATCCTGAGGTTTA	21	379	265	na	na					
MIR2111d	TAATCTGCATCCTGAGGTTTA	21	379	265	na	na					
MIR2111e	TAATCTGCATCCTGAGGTTTA	21	379	265	na	na					
MIR2111f	TAATCTGCATCCTGAGGTTTA	21	379	265	na	na					
MIR2111g	AGCCTCGGAGTGCGGATTATC	21	107	48	na	na					
MIR2111h	TAATCTGCATCCTGAGGTTTA	21	379	265	na	na					
MIR2111i	TAATCTGCATCCTGAGGTTTA	21	379	265	na	na					
MIR2111j	TAATCTGCATCCTGAGGTTTA	21	379	265	na	na					
MIR2111k	TAATCTGCATCCTGAGGTTTA	21	379	265	na	na					
MIR2111l	TAATCTGCATCCTGAGGTTTA	21	379	265	na	na					
MIR2111m	TAATCTGCATCCTGAGGTTTA	21	379	265	na	na					
MIR2111n	TAATCTGCATCCTGAGGTTTA	21	379	265	na	na					
MIR2111o	TAATCTGCATCCTGAGGTTTA	21	379	265	na	na					
MIR2111p	TAATCTGCATCCTGAGGTTTA	21	379	265	na	na					
MIR2111q	TAATCTGCATCCTGAGGTTTA	21	379	265	na	na					
MIR2111r	TAATCTGCATCCTGAGGTTTA	21	379	265	na	na					
MIR2111s	TAATCTGCATCCTGAGGTTTA	21	379	265	na	na					
MIR2118	**TTACCGATTCCACCCATTCCTA**	22	238	309	**512**	**747**					
MIR2119	TCAAAGGGAGGTGTGGAGTAG	21	27	14	0	0					
MIR2199	TGATACACTAGCACGGATCAC	21	6206	6416	1	2					
MIR2592a	AAATGCTTGAGTCCTGTTGTT	21	21	25	na	na	2592a*	GAAAAACATGAATGTCGAGCG	21	49	38

miRNA	Sequence	Size	total reads				IsomiR	Sequence	Size		
			mature		star					mature	
		(nt)	myc	nm	myc	nm			(nt)	myc	nm
MIR2592b	AAATGCTTGAGTCCTGTTGTT	21	21	25	na	na	2592b*	CAACAGGACTCAAGCATTTCGC	22	155	121
MIR2592c	AAATGCTTGAGTCCTGTTGTT	21	21	25	na	na	2592c*	CAACAGGACTCAAGCATTTCGC	22	155	121
MIR2592d	AAATGCTTGAGTCCTGTTGTT	21	21	25	na	na	2592d*	CAACAGGACTCAAGCATTTCGC	22	155	121
MIR2592e	AAATGCTTGAGTCCTGTTGTT	21	21	25	na	na	2592e*	CAACAGGACTCAAGCATTTCGC	22	155	121
MIR2592f	AAATGCTTGAGTCCTGTTGTT	21	21	25	na	na	2592f*	CAACAGGACTCAAGCATTTCGC	22	155	121
MIR2592g	AAATGCTTGAGTCCTGTTGTT	21	21	25	na	na	2592g*	AACAGGACTCAAGCATTTCGC	21	77	60
MIR2592h	AAATGCTTGAGTCCTGTTGTT	21	21	25	na	na					
MIR2592i	AAATGCTTGAGTCCTGTTGTT	21	21	25	na	na	2592i*	CAACAGGACTCAAGCATTTCGC	22	155	121
MIR2592j	AAATGCTTGAGTCCTGTTGTT	21	21	25	na	na	2592j*	CAACAGGACTCAAGCATTTCGC	22	155	121
MIR2592k	AAATGCTTGAGTCCTGTTGTT	21	21	25	na	na					
MIR2592l	AAATGCTTGAGTCCTGTTGTT	21	21	25	na	na					
MIR2592m	AAATGCTTGAGTCCTGTTGTT	21	21	25	na	na					
MIR2592n	AAATGCTTGAGTCCTGTTGTT	21	21	25	na	na					
MIR2592o	AAATGCTTGAGTCCTGTTGTT	21	21	25	na	na	2592o*	CAACAGGACTCAAGCATTTCGC	22	155	121
MIR2592p	AAATGCTTGAGTCCTGTTGTT	21	21	25	na	na	2592p*	CAACAGGACTCAAGCATTTCGC	22	155	121
MIR2592q	AAATGCTTGAGTCCTGTTGTT	21	21	25	na	na	2592q*	CAACAGGACTCAAGCATTTCGC	22	155	121
MIR2592r	AAATGCTTGAGTCCTGTTGTT	21	21	25	na	na	2592r*	CAACAGGACTCAAGCATTTCGC	22	155	121
MIR2592s	AAATGCTTGAGTCATGTTGTT	21	0	1	na	na	2592s*	CAACAGGACTCAAGCATTTCGC	22	155	121
MIR2594a	CCATGGCCAAGGATGCCAGAG	21	0	0	na	na	2594a*	GCTGCTGTAGTTCCTTCGGCGA	22	33	40
MIR2594b	CCATGGCCAAGGATGCCAGAG	21	0	0	na	na	2594b*	GCTGCTGTAGTTCCTTCGGCGA	22	33	40
MIR2595	TACATTTTCTTCTTTATGTCT	21	0	1	na	na	2595*	TATAGAGATGAGAATGTTACA	21	11	1
MIR2597	TTTGGTACTTCGTCGATTTGA	21	12	31	na	na	2597.2	TTTGGTACTTCGTCGATTTGAT	22	612	692
MIR2610a	AGATTGAGACTTGTATGGCTT	21	8	8	na	na	2610a.2	AGACTTGTATGGCTTCGTTGAA	22	25	26
MIR2610b	AGATTGAGACTTGTATGGCTT	21	8	8	na	na	2610b.2	AGACTTGTATGGCTTCGTTGAA	22	25	26
MIR2611	TATTTGTCAGTGTTTGATGAA	21	0	0	na	na	2611-3p	TACTGGGAAGATTGCACGCTGG	22	33	26
MIR2612a	TGATAGTGTCAACTAGTACAG	21	1	1	na	na	2612a*	TAGTAGTTGACATTATCAAAT	21	8	2
MIR2612b	TGATAGTGTCAACTAGTACAG	21	1	1	na	na	2612b*	TAGTAGTTGACATTATCAAAT	21	8	2
MIR2620	TTCTGATAGACACCGGCTCTGC	22	1	0	na	na	2620.2	TGTTCTGATAGACACCGGCTC	21	77	59
MIR2630a	TGGTTTTGGTCCTTGGTATTT	21	7	8	na	na					
MIR2630b	TGGTTTTGGTCCTTGGTATTT	21	7	8	na	na					
MIR2630c	TGGTTTTGGTCCTTGGTATTT	21	7	8	na	na					
MIR2630d	TGGTTTTGGTCCTTGGTATTT	21	7	8	na	na					
MIR2630e	TGGTTTTGGTCCTTGGTATTT	21	7	8	na	na					
MIR2630f	TGGTTTTGGTCCTTGGTATTT	21	7	8	na	na					
MIR2630g	TGGTTTTGGTCCTTGGTATTT	21	7	8	na	na					
MIR2630h	TGGTTTTGGTCCTTGGTATTT	21	7	8	na	na					
MIR2630i	TGGTTTTGGTCCTTGGTATTT	21	7	8	na	na					
MIR2630j	TGGTTTTGGTCCTTGGTATTT	21	7	8	na	na					
MIR2630k	TGGTTTTGGTCCTTGGTATTT	21	7	8	na	na					
MIR2630l	TGGTTTTGGTCCTTGGTATTT	21	7	8	na	na					
MIR2630m	TGGTTTTGGTCCTTGGTATTT	21	7	8	na	na					
MIR2630n	TGGTTTTGGTCCTTGGTATTT	21	7	8	na	na					
MIR2630o	TGGTTTTGGTCCTTGGTATTT	21	7	8	na	na					
MIR2630p	TGGTTTTGGTCCTTGGTATTT	21	7	8	na	na					
MIR2630q	TGGTTTTGGTCCTTGGTATTT	21	7	8	na	na					
MIR2630r	TGGTTTTGGTCCTTGGTATTT	21	7	8	na	na					
MIR2630s	TGGTTTTGGTCCTTGGTATTT	21	7	8	na	na					
MIR2630t	TGGTTTTGGTCCTTGGTATTT	21	7	8	na	na					
MIR2630u	TGGTTTTGGTCCTTGGTATTT	21	7	8	na	na					
MIR2630v	TGGTTTTGGTCCTTGGTATTT	21	7	8	na	na					
MIR2630w	TGGTTTTGGTCCTTGGTATTT	21	7	8	na	na					
MIR2630x	TGGTTTTGGTCCTTGGTATTT	21	7	8	na	na					

miRNA	Sequence	Size	total reads				IsomiR	Sequence	Size	mature	
			mature		star						
		(nt)	myc	nm	myc	nm			(nt)	myc	nm
MIR2630y	TGGTTTTGGTCCTTGGTATTT	21	7	8	na	na					
MIR2633	TGACATTTTGCTCCAGATTCA	21	111	86	na	na					
MIR2636	TTTGGTTAGTGTGCTGAATAT	21	0	1	na	na					
MIR2643	TTTGGGATCAGAAATTAGAGA	21	123	99	na	na					
MIR2645	TTTCTAGAGATGAGCATATAT	21	0	1	na	na	2654.2	TCTAGAGATGAGCATATATTG	21	1	4
MIR2648	TAGCCAATGGGAATAACAGAT	21	10	4	na	na					
MIR2651	TTTGATTGGTATGCCTGCATT	21	55	63	na	na					
MIR2661	TAGGTTTGAGAAAATGGGCAG	21	757	686	na	na					
MIR2666	CGAAAGTGAGGATATCAAGGA	21	44	65	na	na					
MIR2670a	CAAGAAGGTTGCTCACTATTT	21	1	1	na	na					
MIR2670b	CAAGAAGGTTGCTCACTATTT	21	1	1	na	na					
MIR2670c	CAAGAAGGTTGCTCACTATTT	21	1	1	na	na					
MIR2670d	CAAGAAGGTTGCTCACTATTT	21	1	1	na	na					
MIR2674	CACTCGCTTTGGAAGTCATGG	21	0	0	na	na	2674-5p	CTCGGGACAAAAGGTTGCTAA	21	4	6
MIR2678	TGAAATTGTTGCGAGTGTCTT	21	0	0	na	na	2678-5p	TCAGAAGGATCAACATCATAG	21	7	8
MIR2679c	CTTTTCACTTTCGAACGGGTG	21	0	0	na	na	2679c-3p	GAGGTTGAATTGTTACGGCTC	21	7	11
MIR2680a	TCCTCGGTACCTATGTTGAT	20	0	0	na	na	2680a-5p	CTAGACCTGGCATATCTTCATA	22	12	6
MIR2680b	TCCTCGGTACCTATGTTGAT	20	0	0	na	na	2680b-5p	CTAGACCTGGCATATCTTCATA	22	12	6
MIR2680c	TCCTCGGTACCTATGTTGAT	20	0	0	na	na	2680c-5p	CTAGACCTGGCATATCTTCATA	22	12	6
MIR2680d	TCCTCGGTACCTATGTTGAT	20	0	0	na	na	2680d-5p	CTAGACCTGGCATATCTTCATA	22	12	6
MIR2680e	TCCTCGGTACCTATGTTGAT	20	0	0	na	na	2680e-5p	CTAGACCTGGCATATCTTCATA	22	12	6

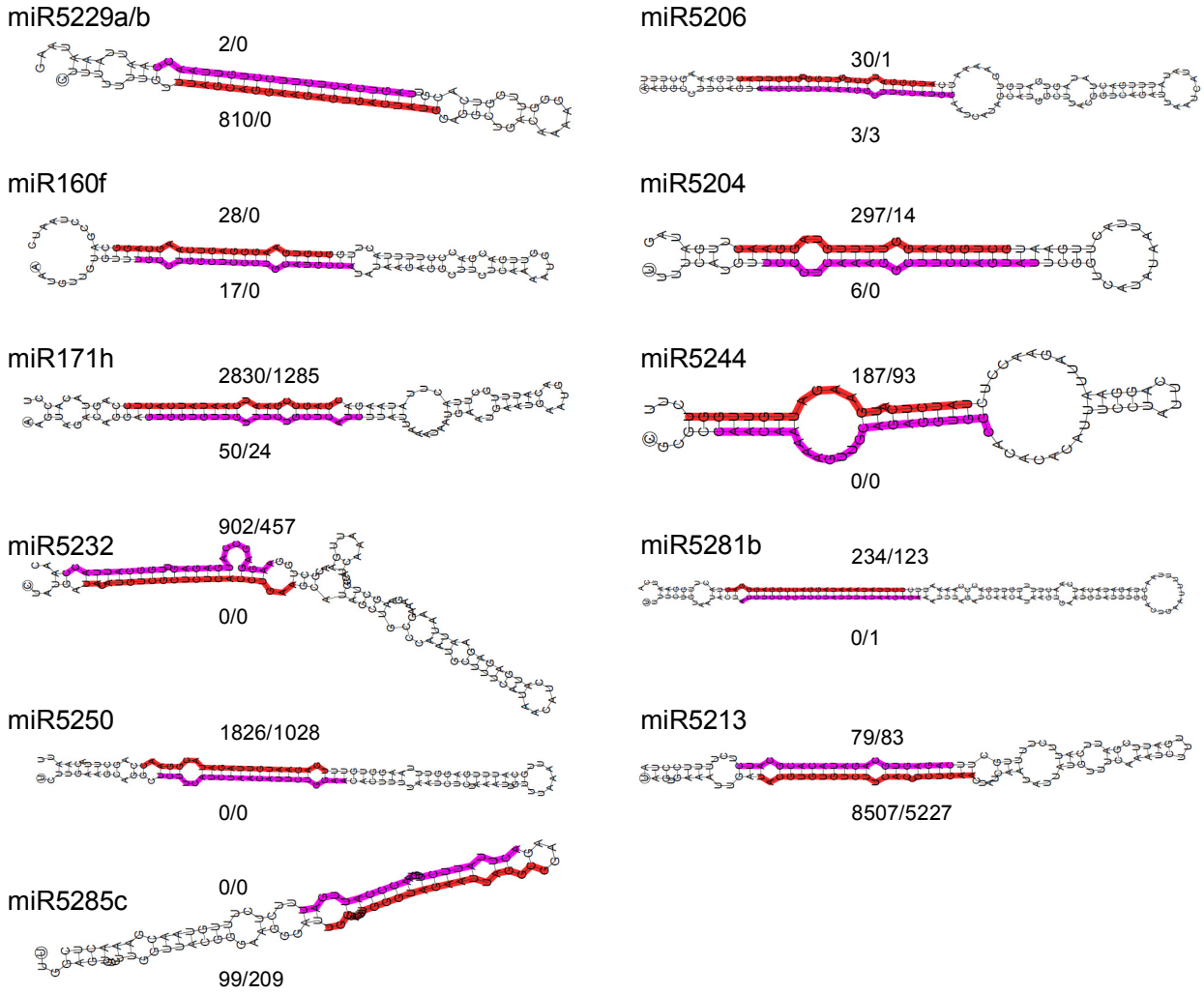

Figure 44: Precursor fold-back structures of the miRDeep predicted differentially expressed miRNAs. Predicted mature sequences are marked in red and predicted star sequence in pink. Numbers next to the respective arm of the precursor indicate the abundance of the sequenced reads at this position (myc/nm). The 5'-phosphate of the RNA is marked by a circle around the first nucleotide. For miRNA families, where the duplex produces identical mature miRNA sequences, the precursor with the highest expression based on the overall abundance of reads mapping 100% to the predicted precursor is presented. Fold back-structures with annotations are created using the UEA sRNA toolkit (http://srna-tools.cmp.uea.ac.uk/plant/).

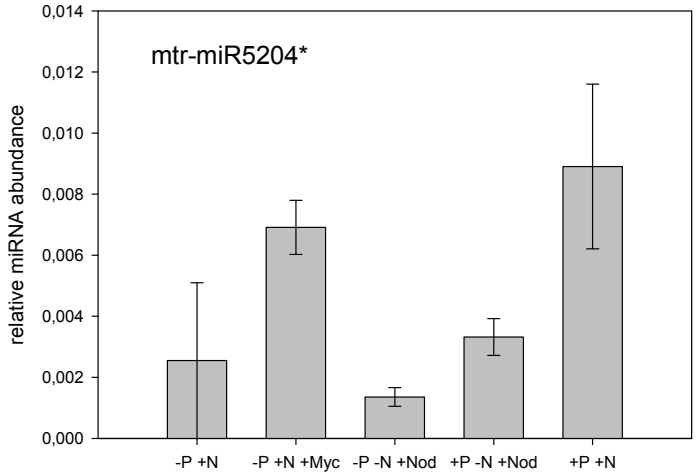

Figure 45: Expression levels of mtr-miR5204*. Same conditions were used as in figure 32.

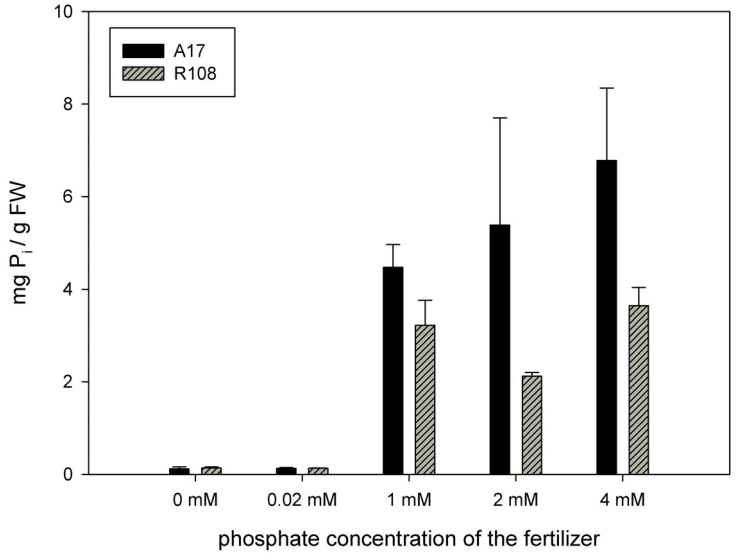

Figure 46: Soluble phosphate concentrations in the shoot of Medicago *cv* A17 and R108 fertilized with different phosphate concentrations.

8. ACKNOWLEDGEMENTS

First, I would like to give thanks to Prof. Dr. Franziska Krajinski for giving me the opportunity to work on my PhD thesis in her group and especially for her supervision, mentoring, great support and trust in my work.
I would also like to express my gratitude to my evaluation committee members Prof. Dr. Mark Stitt, Dr. Wolf-Rüdiger Scheible and Dr. Dirk Hincha for their helpful positive and negative criticism, suggestions and valuable comments to my PhD work.
My thanks go to Prof. Dr. Steffen Abel, Prof. Dr. Martin Crespi and Prof. Dr. Mark Stitt for the willingness to review this thesis and to Prof. Dr. Lothar Willmitzer for supervision.
Special thanks go to my colleague Anja Branscheid for her friendship, tremendous support, motivation, very fruitful (sometimes endless ☺) discussions and ideas from the beginning of our studies in biochemistry until our sharing PhD-time and I hold her in high esteem.
I thank Dr. Patrick May for the great cooperation on the miRNA project. Without his bioinformatic expertise I would have been drowning in millions and millions of sequences, still trying to trim them manually.
I want to thank Prof. Dr. Martin Crespi for giving me the opportunity to speak of my work to an international audience at the small RNA workshop during the ICLGG 2011 in Asilomar. It was a great experience for me and very helpful for my PhD work.
I am thankful to Dr. Daniela Sieh and Dr. Nicole Gaude for their critical proof-reading of my thesis and I want to thank all former and present members of AG Krajinski for the nice working atmosphere, their help and support.
I would like to thank all of my friends for their big support and encouragement, especially Christian Sack for his effort in proof-reading this thesis and for definitively being my soul mate (Sonata Arctica, Warhammer 40.000 and philosophical discussions until the end of time! ☺).

Last but not least and most important, I want to give thanks to my Family – my father Andreas Devers, my mother Ursula Devers and my sister Simone Devers (or should I say Dr. Devers) – for their unconditional love and support! Without them I would not have been able to complete my studies and I want to dedicate this thesis to them.

Thank you very much!

Eidesstattliche Erklärung

Ich versichere hiermit, die vorliegende Arbeit selbstständig angefertigt und keine anderen als die angegebenen Quellen und Hilfsmittel verwendet zu haben. Ich versichere ebenfalls, dass die Arbeit an keiner anderen Hochschule als der Universität Potsdam eingereicht wurde.

Potsdam, den 27.06.2011

Emanuel Devers